UNIVERSITEIT GENT

FACULTEIT WETENSCHAPPEN

The geometrical Bohr-Mottelson model: Analytic solutions and an algebraic Cartan-Weyl perspective.

Stijn De Baerdemacker

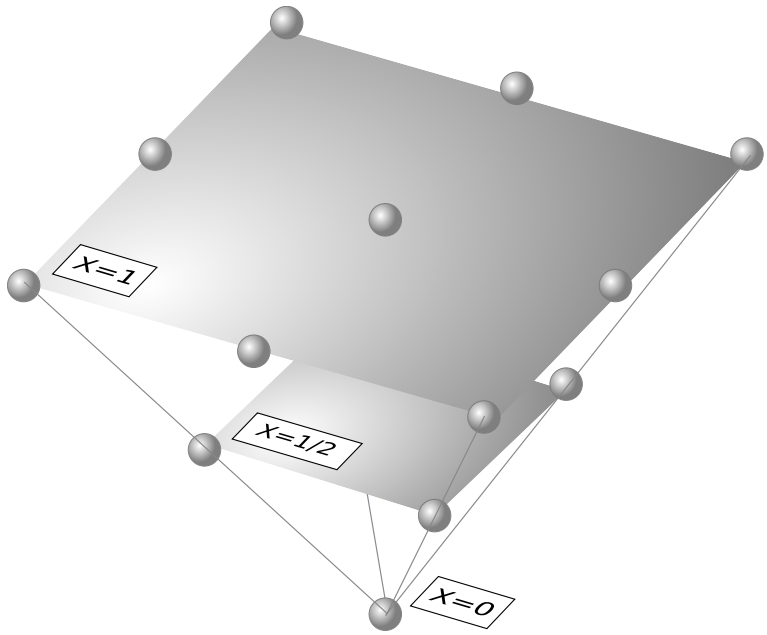

Faculty of Sciences

Proefschrift tot het bekomen van de graad van
Doctor in Wetenschappen: Natuurkunde
Academiejaar 2007-2008

Promotor: Prof. dr. Kris Heyde

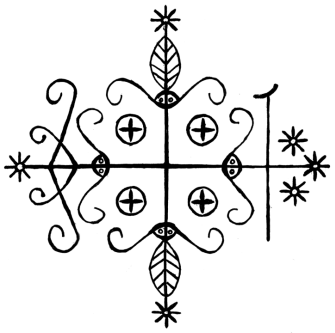

voor veve

You only require two things in life: your sanity and your wife.

Tony Blair

ACKNOWLEDGMENTS

Ask a little boy what he wants to be as a grown up, and you are very likely to end up with a future professional soccer player or a courageous fireman. If you would have addressed this question to me -I was a little boy once too-, chances are high that I would have stumbled a mute 'idunno'. I was not really the goal-getter type on the playground, and fire was considered to me a very fascinating 'phenomenon', though not in quite the same spirit as half of my class [1], who were already discussing who would deserve the cross of honour first.

Almost 20 years later, I'm able to answer the question. It was my fascination for 'phenomena' that drove me into the exact sciences, my interest in models that made me decide to step into physics and my fondness towards mathematical methods that directed me towards the field of theoretical physics. The result of this lies here right before you: the dissertation with the title 'The geometrical Bohr-Mottelson model: Analytic solutions and an algebraic Cartan-Weyl perspective'. However, I would not be able to call myself a physicist, without the invaluable help and support of a number people for which the next couple of words are intended.

Short after the 3th workshop on shape phase transitions and critical point phenomena in nuclei in Athens, I had a short conversation with David Rowe and Piet Van Isacker on the metro rushing towards the acropolis. We were discussing the comparison of the scientific community with a society of families in which knowledge and tradition are handed over generation by generation. It is in this spirit that I would like to thank my 'scientific father' Kris Heyde. It was under his guidance that I could explore the immense world of scientific research. At any time, he let me the freedom to determine my own directions, however not

[1] the other half were girls, determined to either save all pets from illness or be saved by an enormous squad of firemen

without keeping an eye in the background. Discussing physics with Kris was always a major experience and I hope that I have somehow acquired some of his enthusiasm and deep insight in the subject from these sessions. Kris, I consider it a great honour that I could call you the 'chief'.

Discussing scientific families in the Athens metro felt a little peculiar since Piet and I are rooted in the same 'Ghent' tradition. However, I'd also like to consider Piet as my 'French scientific father'. I'm thinking about the many hours spent in his office, in which I enjoyed very much his uncommitted views on physics and encyclopedic knowledge concerning group theoretical methods, and I'm positively certain that this thesis would have been written in a slightly different 'language' if he wouldn't have taught me the vocabulary.

Talking about languages, I am automatically redirected towards Ruben Fossion, my 'scientific brother'. It was only by guiding undergraduate students myself, that I was able to appreciate how much patience he had with me during my training year as a 'thesis slaafje'. As he already mentioned in the acknowledgments of his thesis, the spirit in our office was always animated, and meeting him now somewhere abroad on a conference (or somewhere else), is always something to look forward to. I will cherish the best memories about my other office mate and colleague Lorenzo Fortunato. It was he who introduced me with titanic enthusiasm into the collective model, the Italian way of living and Belgian beers, so everytime I pull a bottle of Trappist, I hail a toast to 'SPQR'.

'Meneer' wishes to express his feelings of thanks towards the dynamical atmosphere at the department of subatomic and radiation physics ('tiejenwee'). Whether it was during a coffee break (thanks Peter), a computer break(down) (thanks Klaas), just a night out (thanks Peter, Klaas, Arne, Arne, Bino, Kris, Lode,...) or a quick afternoon pita & pizza (thanks Peter, Klaas, Arne, Arne, Jelle, Bino, Kris, Lode, Freija, Tiko, Gunar, Tamara, Christophe, Annelies, Bart, Wim, Simon, Pieter, Arne, Pascal, Tim, Christina, and the unknown soldier I might have forgotten), I always enjoyed your company and I hope you enjoyed mine, at least to some extent. How Daniella and Linda always kept their calm when I was entering their office is a plain mystery to me, but I presume I owe them one for the many times they saved me from administrational disaster. Also I would like to thank Rudi for helping me out with the copies of this manuscript.

I realise that these copies would never have been produced without financial support. Therefore, my BOF scholarship at the University of Ghent and a Marie Curie

Fellowship to sustain my stay at GANIL are greatly acknowledged.

All work and no play makes Jack a dull boy. I'm grateful to my friends for putting me back into the real world when I was once again found to be trapped into a high excitation energy isomeric state, and also for understanding that sometimes one needs to tunnel through a deadline barrier to be a free particle again. Marleen and Jan, your support during all these years was very well appreciated.

To my parents, saying that I'm grateful for their support and sympathising is an understatement. They always let me free in my choices, giving care and advice whenever needed, somehow trusting that in the end, I will land on my feet. I think the mere copy of this thesis proves them right.

A special word of thanks is devoted to Veerle. In the traditional Haitian voodoo culture, a *veve* is a drawing, made by the priestess with powder on the ground. These drawings are made prior to a ritual in which the gods are invoked to bring their blessing to the people. It is considered a great art to draw a veve as it is full of details and it is said that only a drawing of the perfect veve can bring total blessing. However, it is not mentioned in the oral tradition that one can also simply find one.

stijn,
Gent 2007

CONTENTS

Gruppenpest!

Wolfgang Pauli

1 NUCLEAR STRUCTURE AND SYMMETRIES

ABSTRACT

In this introductory chapter, a brief overview is given on nuclear structure physics and how symmetry principles can enhance insight in the solutions of the Schrödinger equation. A pairing Hamiltonian is discussed as an example of the power of Lie algebras, and extended towards the Interacting Boson Model (IBM). Via a mean field approach, the connection between the IBM and geometric collective models is shown and the topic of quantum shape phase transitions is introduced.

Section 1.1 Different levels of nuclear structure

'The atomic nucleus is like a huge soccer team: although the actions are set by the individual players, in the end, it is the team that wins the game'.
The physical meaning of this metaphor is that all the interactions between the players in the field (protons and neutrons) contribute to the final structure of the team. Nevertheless, no matter how tempting, one cannot extend the metaphor over the whole line. In contrast to the popular sport discipline, the interactions between the particles are not fully known nor understood. This is partly due to the fact that the protons and neutrons are not elementary particles, rather composite particles in the sense that they are also built from other constituent parts, which means that one is forced to start from the underlying quark degrees of freedom if a fundamental nucleon-nucleon interaction is desired. Another problem is that the atomic nucleus is a typical example of a *many-body* system. One could

start from the bottom up and describe the A number of nucleons from a microscopic nucleon-nucleon interaction (containing n-body forces), the so-called *ab-initio* calculations [Car98] (see figure 1.1(a)), but such calculations are restricted to very light nuclei (typically $A \sim 10$) as the Hilbertspace quickly becomes intractably expanded. From the other side, the number of particles in the nuclear many-body system is way too low to successfully apply statistical methods. As a consequence, we need to settle with nuclear structure models when studying the structure of atomic nuclei. Fortunately, there are a number of different complementary approaches, either based on microscopic or macroscopic assumptions.

The *Hartree-Fock* (HF) method is a typical example of the microscopic approach. Starting from two-body nucleon-nucleon (density-dependent) interactions, the Hartree-Fock approach generates a mean field in which the individual nucleons move like independent particles in a one-body potential, created in an iterative self-consistent way [Fet71].
Along a similar line, the *nuclear shell model* can also be regarded as a microscopic model [Hey94]. It starts from the observation that nuclei with particular number of protons- and neutrons (The so called *magic* numbers 8, 20, 28, 50, etc.) are more strongly bound than predicted by macroscopic liquid-drop models. A similar phenomenon was already observed in the shell structure of electrons in an atom, which led to the idea that the protons and neutrons can also be organised in shells. However, contrary to the electronic shell model, no external central-force field is present to generate the shell structure. Legimitation for the use of such a field, can be derived from HF-theory, which shows that the single nucleons can be approximated very well as moving in a mean field, evoked by the interactions of the other particles (see figure 1.1(b)). Rather than using a HF alike technique, one quite often uses a phenomenological and solvable potential (such as the three-dimensional (3D) harmonic oscillator potential) and corrects for residual interactions, not incorporated in this potential.

Historically the first nuclear model is the macroscopic *liquid-drop* model [Wei35, Bet36]. Since binding energies (or masses) were among the first observables one was able to measure in atomic nuclei, there was need for an intuitive model to describe these experimental data. Starting from the assumption that atomic nuclei are made up from constituent particles, we can compare it to a charged liquid drop (see figure 1.1(c)). This resulted in the Bethe-Weizsäcker formula that was able to describe the binding energies of atomic nuclei in an empirical way.
Nevertheless, the systematic deviations of this binding energy formula with the experimental data around the magic numbers instigated the development of the

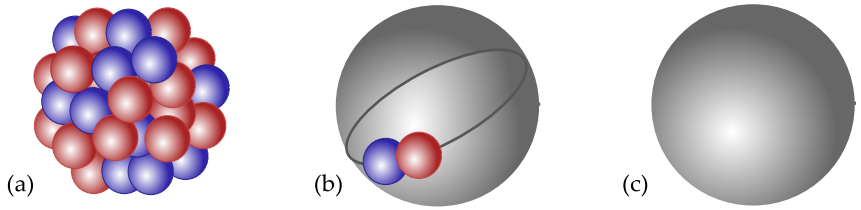

Figure 1.1: The different levels of nuclear structure. In (a) the nucleus is seen as a bunch of particles that interact with one another, the starting point for ab-initio calculations. Figure (b) schematically shows that the interactions of all particles can be substituted by means of a mean field in which the particles can move. In (c), all microscopic substructure has been replaced by a macroscopic charged liquid drop.

nuclear shell model, and the macroscopic interpretation was driven to the background. Until it became clear that the observed large quadrupole moments could not be explained by the shell model [Rai50] at the time of speaking[1]. To cure for the problem, it was suggested that all nucleons cooperate in a *collective* way to the deformation of the nucleus. The idea was to recover the liquid-drop approach, and extend it to a dynamical picture in which a single nucleon can be coupled to the excitations of the atomic surface [Boh52, Boh53]. The Bohr-Mottelson collective model was conceived, giving rise to a macroscopic picture of nuclear structure, complementary to microscopic models, such as the nuclear shell model.

These different models can give rise to an intuitive physical insight in the structure of atomic nuclei. However still, since it is a quantum mechanical system, we cannot fully trust our intuition and need to rely on the technical side of the models, i.e. solving the (Schrödinger) equations. To do so, many methods have been introduced into the literature since the dawn of quantum mechanics, such as the theory of special functions [Arf01], diagrammatic perturbation theory [Fet71] and many others. One among them is based on symmetry principles, a concept which has already proven to be very useful when handling quantum mechanical problems. This will be demonstrated in the following section.

[1] It should be noted that, with the advent of large-scale shell-model calculations, collectivity can be accessed by means of the microscopic shell model, as long as large-scale model spaces are used.

Section 1.2 Symmetries

1.2.1 Why do we rely on symmetries?

The answer to this question is simple though cryptic at the same time: the concept of symmetry is strongly intertwined with quantum mechanics. The main goal of a quantum physicist is to find the equation of state of a quantum system, better known as the *Schrödinger equation*, and solve it

$$\hat{H}|\psi\rangle = E|\psi\rangle. \tag{1.1}$$

Knowledge of the symmetries of a system leads to an enhanced insight in the construction of the Hamiltonian, and furthermore in finding its solutions. The question, however, remains: how to track the symmetry in a system and exploit it? If we start from nothing but the raw experimental data, the occurrence of degeneracy in spectral data is a clear smoking gun for the presence of symmetry. Suppose e.g. that there are n independent solutions $|\psi_n\rangle$ of the Schrödinger equation (1.1) with the same eigen value E_n, and that there exists a set of transformations $\{\hat{P}_\theta\}$ that leaves the system invariant. The action of a transformation on the Schrödinger equation (1.1) gives

$$\hat{P}_\theta \hat{H} \hat{P}_\theta^{-1} \hat{P}_\theta |\psi_n\rangle = E_n \hat{P}_\theta |\psi_n\rangle. \tag{1.2}$$

This is identical to the original equation if

$$[\hat{H}, \hat{P}_\theta] = 0, \qquad \hat{P}_\theta |\psi_n\rangle = \sum_m D_{nm}(\theta)|\psi_m\rangle. \tag{1.3}$$

The set $\mathcal{G} = \{\hat{P}_\theta\}$ is said to form a *group* under combination, since it fulfils the four defining criteria [McW02, Ham64]

1. the set comprises the identity,
2. the inverse of every element is also present in the set,
3. the combination of two elements is also a member of the set,
4. the combination is associative.

From group theory, we learn that the matrix $D(\theta)$ forms a matrix representation of the group with the solutions $|\psi_n\rangle$ as associated basis functions. Therefore, if we know the representations of a group that leaves a Schrödinger equation invariant, we immediately obtain the solutions of the equation for free. So, tracking

the symmetry in a quantum mechanical system is equivalent to solving the associated equations of state.

Unfortunately, life is not allways that straightforward, especially in nuclear structure physics. Apart from the degeneracy stemming from the rotational symmetry, no other degeneracies are observed in experimental spectra. Therefore, it is difficult to pinpoint the actual symmetries in the system and construct Hamiltonians from this perspective. So one is obliged to start from a model, where, thanks to the theory of *Lie groups*, symmetries can still be used to grasp an understanding of the model and the physics it is aiming to describe.
Lie groups are also known under the name of *continuous* groups, which means that the group elements can be expressed in terms of a continuous parameter (θ), such as e.g. the orthogonal group $O(3)$, which incorporates all rotations in the 3D Euclidian space. Every Lie-group element in general can be expressed in an exponential form

$$\hat{P}_\theta = e^{i\theta\cdot\hat{G}}. \tag{1.4}$$

This has the consequence that we can reduce our study of the infinite set (θ is a *continuous* parameter) of group elements to a discrete set of *generators* $\hat{G}$. This set of generators is said to form a *Lie algebra*, associated to the Lie group. The most eye-catching feature of a Lie algebra, is the fact that the elements close under commutation [Wyb74]

$$[\hat{G}_i, \hat{G}_j] = \sum_k c_{ij}^k \hat{G}_k. \tag{1.5}$$

The coefficients c_{ij}^k are called the structure constants, and act more or less[2] as the fingerprints of a given Lie algebra. Moreover, if we calculate the commutation relations of the operators making up a model Hamiltonian, and we find out that they close similarly to (1.5), we can associate the same Lie algebra to this set of model operators, independent from the specific realisation (whether the operators are expressed in terms of differential operators, or in the framework of second quantization, etc.). The set of operators is then said to span a Lie algebra, associated with a Lie group. This has a major consequence: at this point, we can revert to Lie group theory which teaches us how the generators act on the basis functions of the Lie group. In other terms, Lie group theory offers a suitable basis in which the model Hamiltonian can be diagonalized.
The next subsection will demonstrate these ideas using a simple pairing problem.

[2]Caution is necessary here: the structure constants are determined up to a rotation, as will be shown in chapter 3

1.2.2 A simple pairing problem

In the nuclear shell model, protons and neutrons are allowed to fill up orbitals generated by a mean field potential created by the other particles in the medium [Hey94]. A particle, occupying a given orbital, is characterised by a complete set of quantum numbers $|njlm\rangle$ and the associated single particle energies ε_{njl}. However, even though the larger part of the nucleon-nucleon interactions can be absorbed in the one-body potential, there are of course remaining residual two-body interactions to be taken care of when treating nuclei with a number of nucleons outside the closed-shell core. So we can construct a Hamiltonian for an A-body system within a shell-model approximation as follows[3]

$$\hat{H} = \hat{H}_{\text{sp}} + \hat{H}_{\text{2b}} \tag{1.6}$$

$$= \sum_{\alpha} \varepsilon_a a^{\dagger}_{\alpha} a_{\alpha} + \tfrac{1}{4} \sum_{\alpha\beta\gamma\delta} \langle \alpha\beta | V | \gamma\delta \rangle_{\text{nas}} a^{\dagger}_{\alpha} a^{\dagger}_{\beta} a_{\delta} a_{\gamma}, \tag{1.7}$$

Taking a look at experimental spectra, we notice a degeneracy in the magnetic quantum number of the total spin, which means that we can expand the Hamiltonian into total spin (J) invariant components. [Bru77]

$$\hat{H}_{\text{sp}} = \sum_{a} \varepsilon_a \sqrt{2j_a + 1} [a^{\dagger}_{j_a} \tilde{a}_{j_a}]^0 = \sum_{a} \epsilon_a \hat{n}_a, \tag{1.8}$$

$$\hat{H}_{\text{2b}} = -\tfrac{1}{4} \sum_{J} \sum_{abcd} \sqrt{(1+\delta_{ab})(1+\delta_{cd})} \langle ab, JM | V | cd, JM \rangle \sqrt{2J+1} [[a^{\dagger}_{j_a} a^{\dagger}_{j_b}]^J [\tilde{a}_{j_c} \tilde{a}_{j_d}]^J]^0 \tag{1.9}$$

with $\tilde{a}_{j,m} \equiv (-)^{j+m} a_{j,-m}$. Considering the case that the particles can only occupy a single orbital ($a = b = c = d$), and interact with a short-range interaction typical for nuclear systems (e.g. a δ-force), then it can be shown [Bri05] that the extra binding energy contributions in the two-particle configuration decrease with increasing spin J. If we restrict the sum over J to the $J = 0$ part only (the lowest-order term), we obtain the well known *pairing* Hamiltonian

$$\hat{H}_{\text{pair}} = \varepsilon_j \hat{n}_j + g(a^{\dagger}_j \cdot a^{\dagger}_j)(\tilde{a}_j \cdot \tilde{a}_j) \tag{1.10}$$

[3] A note on the notation: α denotes the full set of quantum numbers $\alpha \equiv (n_a, l_a, j_a, m_a)$, whereas with a the full set excluding the magnetic quantum number is addressed $a \equiv (n_a, l_a, j_a)$. The notation 'nas' is an abbreviation of 'normalised antisymmetric'.

This Hamiltonian can now easily be diagonalized making use of Lie algebras. If we define the following operators

$$\hat{S}_j^0 = \tfrac{1}{2}\hat{n}_j - \tfrac{1}{4}\Omega_j, \tag{1.11}$$

$$\hat{S}_j^\dagger = \tfrac{1}{2}(a_j^\dagger \cdot a_j^\dagger), \tag{1.12}$$

$$\hat{S}_j = \tfrac{1}{2}(\tilde{a}_j \cdot \tilde{a}_j), \tag{1.13}$$

(with $\Omega_j \equiv 2j+1$ the degeneracy in the j-shell), we notice that these operators close according to the $SU(2)$ commutation relations [Wyb74]

$$[\hat{S}_j^\dagger, \hat{S}_j] = 2\hat{S}_j^0, \quad [\hat{S}_j^0, \hat{S}_j^\dagger] = \hat{S}_j^\dagger, \quad [\hat{S}_j^0, \hat{S}_j] = -\hat{S}_j. \tag{1.14}$$

The quadratic Casimir (or invariant) operator for $SU(2)$ is given by

$$\hat{\mathcal{C}}_{2SU(2)_j} = (\hat{S}_j^0)^2 + \tfrac{1}{2}(\hat{S}_j^\dagger \hat{S}_j + \hat{S}_j \hat{S}_j^\dagger). \tag{1.15}$$

Since the Casimir operator commutes with any generator of the Lie algebra by definition, we have a basis $|SM_S\rangle$ at our disposal, defined by

$$\hat{\mathcal{C}}_{2SU(2)_j}|S_jM_{Sj}\rangle = S_j(S_j+1)|S_jM_{Sj}\rangle, \tag{1.16}$$

$$\hat{S}_j^0|S_jM_{Sj}\rangle = M_{Sj}|S_jM_{Sj}\rangle, \tag{1.17}$$

(with $M_{S_j} = -S_j, \ldots, S_j$). We are now in the position to diagonalize the pairing Hamiltonian (1.10). Rewriting the Hamiltonian using the generators of $SU(2)$ leads to the result

$$\hat{H}_{\text{pair}} = \varepsilon_j(2\hat{S}_j^0 + \tfrac{1}{2}\Omega_j) + 4g(\hat{\mathcal{C}}_{2SU(2)_j} - \hat{S}_j^0(\hat{S}_j^0 - 1)). \tag{1.18}$$

This Hamiltonian is completely diagonal in the basis $|S_jM_{Sj}\rangle$, with the eigenvalues

$$E_{pair} = \varepsilon_j(2M_{S_j} + \tfrac{1}{2}\Omega_j) + 4g(S_j(S_j+1) - M_{Sj}(M_{Sj}-1)). \tag{1.19}$$

A typical spectrum for a pairing system for a single $j = \frac{11}{2}$ shell is given in figure (1.2)

It is noteworthy that, although $SU(2)$ is not a symmetry for the pairing Hamiltonian, the Hamiltonian is still diagonal in the $SU(2)$ basis. This is due to the particular structure of the Hamiltonian, as it can be expressed entirely in terms of Casimir operators of the group reduction chain of $SU(2)$[4]. Therefore, $SU(2)$ is

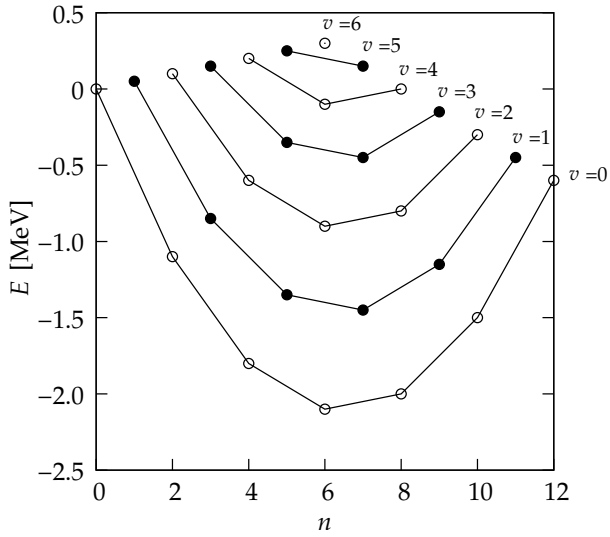

Figure 1.2: Spectrum of a pairing Hamiltonian (1.10) in one $j = \frac{11}{2}$ shell with ε_j=50 keV and g=-50 keV. The open dots are for n even states and the filled dots are for n odd nuclei. The seniority v is given for every S_j multiplet.

not a symmetry but a *dynamical* symmetry of the system [Iac93, Iac99, Fra94].

Making use of Lie algebras does not only have technical advantages, we can also extract physical information from them, e.g. for the quantum numbers. The connection of the quantum number M_{Sj} with the number of particles n_j is obvious from the definition of the generators (eq. (1.11)). However, also the Casimir quantum number S_j has a most interesting physical meaning. Acting with the pair lowering operator $\hat{S}_j$ on a lowest-weight state $|S_j, M_{Sj} = -S_j\rangle$ renders identically zero. Thus, no particles pairwise coupled to zero are present in the lowest weight states. Acting with the pair creation operator $\hat{S}_j^\dagger$ alters the number of particles, but not the Casimir quantum number so the number of particles not coupled to zero, called the *seniority* v [Tal93], stays constant within an S_j multiplet. All S_j multiplets in figure (1.2) are denoted by full lines and labeled by the seniority v. The connection of the $SU(2)$ quantum numbers with the physically

[4] In this case of $SU(2)$, the sub-group is $O(2)$ with only operator and thus Casimir operator $\hat{S}_j^0$.

relevant quantum numbers is given by the following relations

$$S_j = \tfrac{1}{4}\Omega_j - \tfrac{1}{2}v_j, \tag{1.20}$$

$$M_{Sj} = \tfrac{1}{2}n_j - \tfrac{1}{4}\Omega_j. \tag{1.21}$$

This particular example of a simple pairing problem has demonstrated the power of symmetries and Lie algebras in the treatment of quantum mechanical systems. In the following chapters, similar approaches will be used to handle collective model Hamiltonians in all of its facets.

1.2.3 The Interacting Boson Model (IBM), a truncated shell-model approach

The previous subsection already pointed out that, in a single j shell system, the $J = 0$ coupled pair states correspond to the strongest binding energy configurations, relative to the unperturbed single-particle energy. This holds more generally when the model space is expanded to encompass many j-shells. In this case, it will turn out that it suffices to consider the $J = 0$ and $J = 2$ components to cover most of the important low-lying modes in atomic nuclei, especially for medium and heavy mass nuclei (excluding the double closed-shell nuclei). However, completing a full shell-model calculation based on expansion (1.8-1.9) is a tremendous task, since the model space increases extremely fast with increasing particle number, and computational demands quickly become infeasible. Fortunately, the IBM comes to help. If we take e.g. the $J = 0$ pair creation and annihilation operators, and recover the commutation relation (1.14)

$$[\hat{S}_j, \hat{S}_j^\dagger] = -\hat{n}_j + \tfrac{1}{2}\Omega_j, \tag{1.22}$$

we can justify an approximation in the regime of large degenerate shells. Whenever the number of particles n_j remains reasonably small compared to the degeneracy Ω, and we redefine the generators as

$$\hat{s} = \frac{\sqrt{2}}{\sqrt{\Omega_j}}\hat{S}_j, \qquad \hat{s}^\dagger = \frac{\sqrt{2}}{\sqrt{\Omega_j}}\hat{S}_j^\dagger, \tag{1.23}$$

we obtain the fundamental boson commutation relation (for $\hat{s}$ and $\hat{s}^\dagger$) to a good approximation

$$[\hat{s}, \hat{s}^\dagger] \approx 1. \tag{1.24}$$

The same procedure can now be used for the $J = 2$ coupled pair states, which gives rise to the d-boson. The combination of the 5 spin projection components of

the d_μ-boson with the single s-boson can be regarded as the 6 vector components in the 6D unitary space. Or, in other words, the s- and d_μ-bosons form the fundamental representation of $U(6)$, which is the fundamental group of the Interacting Boson Model (IBM) [Iac87].

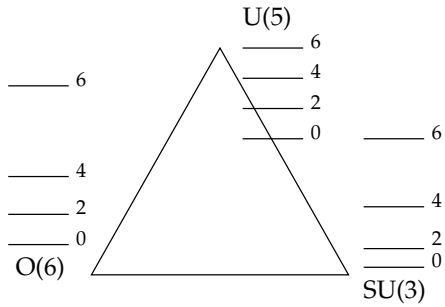

Figure 1.3: The Casten triangle with the limits of the IBM. A typical spectrum of the ground band with its spins is given with every limit.

The linear Casimir operator $\hat{N} = \hat{s}^\dagger \hat{s} + \hat{d}^\dagger \cdot \hat{\tilde{d}}$ of $U(6)$ counts the number of bosons, or equivalently half the number of fermions outside a closed-shell core. Within the framework of a regular shell-model calculation (without particle-hole excitations across the closed shell), this number is kept as a constant, so the Hamiltonian must commute with the linear Casimir operator of $U(6)$. This is guaranteed if the Hamiltonian is built from the generators of $U(6)$. A common way to represent the Hamiltonian, is the consistent-Q formalism, where it appears in the following form [War82]

$$\hat{H}_{CQ} = \varepsilon \hat{n}_d + \kappa \hat{Q}(\chi) \cdot \hat{Q}(\chi), \tag{1.25}$$

with

$$\hat{n}_d = d^\dagger \cdot \tilde{d}, \tag{1.26}$$

$$\hat{Q}(\chi)_\mu = s d^\dagger_\mu + s^\dagger \tilde{d}_\mu + \chi [d^\dagger \tilde{d}]^2_\mu. \tag{1.27}$$

This representation generates a simple though rich structure, depending on the choice of the parameter set $(\varepsilon, \kappa, \chi)$. First of all, the consistent-Q formalism contains the 3 limiting cases of the model, each single one corresponding to a reduction chain of $U(6)$ preserving the rotational symmetry $O(3)$.

1. $U(5)$: for $\kappa = 0$, the Hamiltonian (1.25) reduces to one single term $\hat{n}_d$ which is the Casimir operator of the $U(5)$ group. This limit is able to describe vibrational-like structures.

2. $SU(3)$: for $\varepsilon = 0$, and $\chi = \pm\sqrt{7}/2$, the dynamical symmetry of the system is lowered from $U(6)$ to $SU(3)$, which enables a description of rotational structures.

3. $O(6)$: for $\varepsilon = 0$, and $\chi = 0$, the dynamical symmetry becomes $O(6)$. This symmetry corresponds to a γ-soft rotational structure, as is known from the coherent-state IBM (see next section).

Secondly, the consistent-Q Hamiltonian is not limited to these particular symmetries, but can also be used to describe intermediate cases where none of the three groups form dynamical symmetries for the Hamiltonian. This is also the reason why the IBM has proven to be successful in the description of nuclear structure phenomena in medium-heavy and heavy nuclei at low excitation energy. In regions of the nuclear chart where shell-model calculations are far beyond computational reach, the IBM can be applied. On the one hand because it is able to describe a large variety of different structures, and on the other hand since it is still firmly rooted in the microscopy of the nuclear shell model [Cas93].

Section 1.3 Quantum shape phase transitions

In the previous section, it was shown that the IBM can be connected to the nuclear shell-model. However, it is also possible to make a link with the geometrical collective model. This can be performed using a coherent-state formalism [Gin80, Die80, Boh80]. Within this formalism, the standard IBM bosons are replaced by a Γ boson, which couples the s and d bosons to a deformation field α.

$$(s^\dagger, d^\dagger_\mu) \rightarrow \Gamma^\dagger(\alpha) = \frac{1}{\sqrt{1+\alpha\cdot\alpha}}(s^\dagger + \alpha \cdot d^\dagger). \tag{1.28}$$

Γ is again a boson, so we can build a normalised trial wave function to study the IBM Hamiltonian in a variational way. The free parameters α can be related to the collective quadrupole deformation parameters (see equation (2.2)), so we can rotate them to the intrinsic frame of the ellipsoid. The total energy surface then

becomes, using the consistent-Q Hamiltonian (1.25)

$$E(\beta,\gamma;\varepsilon,\kappa,\chi) = \frac{1}{N!}\langle 0|(\Gamma)^N \hat{H}_{CQ}(\Gamma^\dagger)^N|0\rangle \tag{1.29}$$

$$= \varepsilon N \frac{\beta^2}{1+\beta^2} + \kappa \left[\frac{N[5+(1+\chi^2)\beta^2]}{1+\beta^2} + \frac{N(N-1)}{(1+\beta^2)^2}\left(\frac{2}{7}\chi^2\beta^4 - 4\sqrt{\frac{2}{7}}\chi\beta^3\cos 3\gamma + 4\beta^2\right)\right] \tag{1.30}$$

Finding the global minimum for this energy surface with respect to the collective quadrupole coordinates (β,γ) corresponds to fixing an upper bound for the binding energy of the associated Hamiltonian. Once the global minimum is found, we not only obtain an estimate for the binding energy, but we can also associate a *shape* to the Hamiltonian. Indeed, the solution[5] (β_0,γ_0) of the variational procedure can be related to the collective quadrupole parameters, describing an ellipsoid in the intrinsic framework of the geometrical model. The coherent state formalism sets up a bridge between the IBM and geometrical models (see chapter 2 and 3 for an introduction on geometrical models).

The coherent-state formalism does not only provide a convenient tool to study ground-state properties (such as e.g. binding energies and separation energies) of a given Hamiltonian in particular. We can also study the structural changes in the solutions of the Hamiltonian when the parameters of the model are varied, which brings us into the domain of *quantum phase transitions* [Iac87] The study of a quantum phase transition is the study of a system which is composed from two sub-Hamiltonians $\hat{H}_1$ and $\hat{H}_2$ that are incompatible with one another in the sense that they correspond to different physics cases within the same Hilbert space

$$\hat{H} = \xi\hat{H}_1 + (1-\xi)\hat{H}_2 \tag{1.31}$$

The IBM is tailor made for such systems as we have three classes of Hamiltonians that correspond to different physical situations i.e. the three limits of the model, $U(5)$, $O(6)$ and $SU(3)$. In principle, one needs to diagonalize the Hamiltonian (1.31) as the parameter ξ varies from one limit to the other. However, the coherent-state formalism helps to shed light on the problem. Since the energy surface is a function of a number of variables and control parameters, catastrophe theory [Gil81] can be used to study the qualitative changes of the expression (1.30) as the parameters are varied. It has been found [Lóp95] that the ground-state properties of the IBM Hamiltonian (1.31) are subject to considerable changes

[5] or class of solutions, as is e.g. the case in $O(5)$ symmetric IBM Hamiltonians.

around the critical point ξ_c So, the next question is of course to what extent these changes persist in the original IBM Hamiltonian around the critical point. This resulted in a number of studies (e.g. [Cej03, Gar05, Hei06]) concentrating on the transitions from one limit to another.

Not only the IBM is suitable to study quantum phase transitions; many more models can be used to explore this phenomenon. However, there exists a particularly convenient model for the study of quantum *shape* phase transitions: the geometrical or Bohr-Mottelson collective model [Boh53], which will be discussed in detail in chapter 2. Considering two different collective potentials $V_1(\beta, \gamma)$ and $V_2(\beta, \gamma)$, characterising different underlying physics, we can construct a Hamiltonian in the spirit of the quantum phase transitions (1.31). In particular, a transition from a spherical to a γ-independent β-deformed system can be simulated by means of the potentials

$$V_1(\beta, \gamma) = \tfrac{1}{2}\beta^2, \tag{1.32}$$

$$V_2(\beta, \gamma) = \tfrac{1}{4}(1 - \beta^2)^2. \tag{1.33}$$

Thus, the composite Hamiltonian (1.31) can be written as

$$\hat{H} = \hat{T} + V_\xi(\beta) \tag{1.34}$$

$$= \hat{T} + \tfrac{1}{2}\xi\beta^2 + \tfrac{1}{4}(1 - \xi)(1 - \beta^2)^2. \tag{1.35}$$

The total potential is plotted in figure (1.4) for different values of ξ. Qualitatively, the potential can be divided in two different classes, depending on ξ. For $\xi \geqslant 1/2$, the potential has a spherical minimum , while for $\xi < 1/2$, a deformed minimum results and starts to grow. This means that the value $\xi = 1/2$ draws the border between the two classes. Catastrophe theory teaches us that the criticality conditions of the potential are fulfilled at $\xi = \frac{1}{2}$, corresponding to a β^4 potential. Now it would be very interesting to know the solutions of the Hamiltonian in the immediate neighbourhood of the critical point in an analytic way. Then it can serve as a benchmark for the study of the structural changes around the critical point. Unfortunately, the β^4 potential is not analytically solvable [Gar05], although an approximation exists [Iac00].

The characterising property of a critical potential is the flat behaviour of the potential around the origin, as can be seen in figure (1.4). An analytically solvable potential with a similar behaviour at the origin, is the infinite square-well poten-

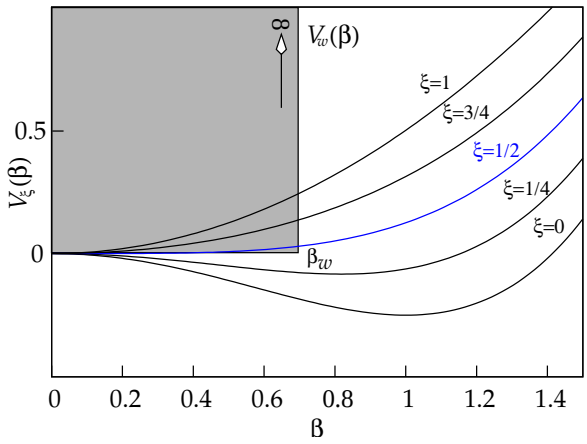

Figure 1.4: The potential of the Hamiltonian (1.35) for different values of ξ (shifted to $V(\beta = 0) = 0$). The infinite well potential $V_w(\beta)$ is also depicted to show that the infinite well is able to mimic the flat behaviour of the β^4 critical potential around $\beta = 0$.

tial (see figure (1.4))

$$V_w(\beta) = \begin{cases} 0 & \beta < \beta_w, \\ \infty & \beta \geqslant \beta_w. \end{cases} \tag{1.36}$$

As a consequence, $V_w(\beta)$ can serve as a substitute for the critical point potential, going from a spherical- towards a deformed system [Iac00]. The eigenfunctions of $V_w(\beta)$ are the Bessel functions, constrained in such a way that the zeros of the functions coincide with the wall of the potential (β_w). At the same time, this boundary condition provides the quantization of the spectrum. A remarkable feature of the eigenvalues of $V_w(\beta)$ is that, although the eigenvalues are directly related to the positioning of the wall, the scaled relative spectrum is *independent* from β_w. This suggests, together with the Bessel solutions, that the structure of the Hamiltonian is mainly determined by the flat behaviour of the potential, something which is necessary to be a good candidate for the description of critical point potentials. As a result, $V_w(\beta)$ was baptised as the $E(5)$ solution for critical points, since the Bessel functions provide a representation for plane waves in the 5D Euclidean space.

Much attention has been paid to $E(5)$ within this introductory chapter, since it was the germ for many other studies on quantum shape phase transitions. On

the one hand, a number of theoretical projects have been put on track, finding a firm basis in either analytic or algebraic models and techniques. On the other hand, it also stimulated a number of experimental groups to explore the nuclear chart in search for unambiguous fingerprints of shape phase transitions. Giving a complete overview of all present state-of-the-art achievements, is a tremendous if not overwhelming task. For this purpose, the reader is kindly referred to a recent overview [Cas07] on the growing field of quantum shape phase transitions.

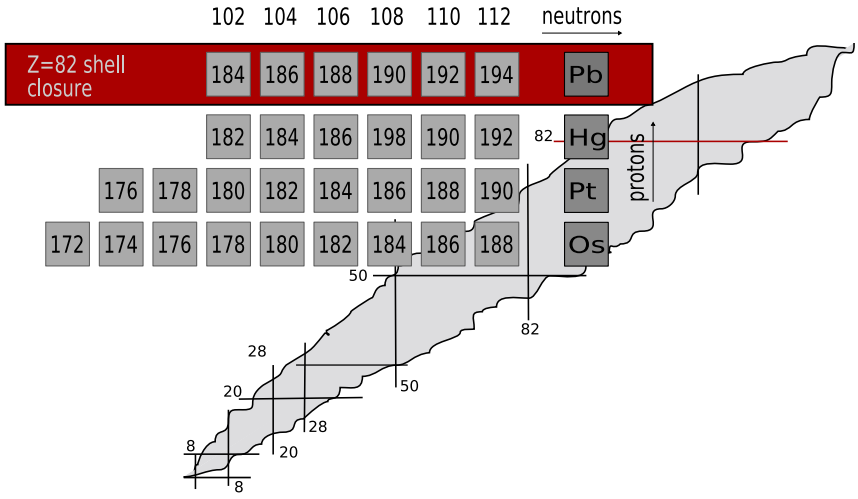

Figure 1.5: The nuclear chart around the $Z = 82$ shell closure. Only the even-even nuclei are depicted.

The work described here is also inspired by the field of shape phase transitions. Around the $Z = 82$ closed shell region (see figure 1.5), a number of structural changes occur in the low-energy structure of atomic nuclei, as has been pointed out by experiments and theoretical models. In the Os isotopes e.g. one can find indications for triaxial deformations, whereas the Pt isotopes are more considered to be β-deformed γ-independent rotors. Moreover, in the Pb isotopes, three different shape configurations coexist within a small excitation energy range. From a theoretical point of view, the interpretation mainly comes from a large variety of models, starting from potential energy surfaces over mean-field descriptions to truncated shell-model calculations (IBM). Therefore, we intend to deliver a complementary and consistent description within the geometrical model, in which the concept of shapes is naturally incorporated.

The following chapters are devoted to solving the Bohr Hamiltonian (2.13). In chapter 2, analytic and algebraic techniques are presented and used to solve for schematic types of Hamiltonians. In chapter 3, we discuss a pure algebraic technique in the spirit of Cartan-Weyl, in order to solve general types of collective Hamiltonians.

Where there is matter, there is geometry.
Johannes Kepler

2

GEOMETRICAL MODEL: ANALYTIC AND ALGEBRAIC APPROACHES

ABSTRACT

A broad introduction to the geometric Bohr-Mottelson is presented with the emphasise on analytically solvable potentials. It is shown, by means of the time-honoured harmonic oscillator potential, how special-function theory and algebraic techniques can be exploited to solve the differential eigenvalue equations in the intrinsic framework. These ideas are applied to the case of triaxiality. Two schematic types of triaxial deformed potentials are introduced. A first one describing soft triaxial rotors with general triaxiality, while the second has a fixed triaxiality yet respecting the periodic symmetry of the collective model. Both potentials are solved (approximately) and confronted with experimental data.

Section 2.1 The Geometrical Model

2.1.1 The shape of the nucleus

The Geometrical Model is a macroscopic model in the sense that it looks to the *geometry* of the surface and its excitation modes, provoked by the collective behaviour of the underlying nucleons. Due to the strong attractive nucleon-nucleon interaction, this surface will roughly be spherical. However, deviations from this highly symmetric shape are possible. An appropriate way to incorporate such deviations from a spherical shape, is to carry out a multipole expansion of the

radial dependence $R(\theta, \phi)$ as [Eis87, Boh98]

$$R(\theta, \phi) = R_0[1 + \sum_\lambda \alpha^\lambda \cdot Y_\lambda(\theta, \phi)], \tag{2.1}$$

with $Y_{\lambda\mu}(\theta, \phi)$ the spherical harmonics. It is significant to start from this multipole expansion since every term has a physical meaning. The $\lambda = 0$ term is a volume term, associated with *monopole* excitations[1]. For small deviations ($\alpha_\mu^\lambda \ll 1$), the $\lambda = 1$ *dipole* term is merely a translation of the centre of mass, and is therefore neglected. This leaves the $\lambda = 2$ *quadrupole* term as the first important deformation mode of the atomic nucleus at low excitation energy. We can truncate equation (2.1) to[2]

$$R(\theta, \phi) = R_0[1 + \alpha \cdot Y_2(\theta, \phi)]. \tag{2.2}$$

This equation describes an ellipsoid in the laboratory frame. To move over to the intrinsic frame (where the ellipsoids main axis' are chosen as a reference frame), we need to carry out a 3D rotation over the Euler angles (θ_i). Now, the ellipsoids surface is described by the intrinsic variables a_μ, which are connected to the laboratory variables α_ν by means of the rotation

$$a_\mu = \sum_\nu D^2_{\nu\mu}(\theta_i)\alpha_\nu \tag{2.3}$$

with $D^2_{\nu\mu}(\theta_i)$ the Wigner-D functions [Ros57]. Since the variables a_μ are chosen such as to describe the ellipsoid in the intrinsic frame, we have

$$a_2 = a_{-2}, \quad a_1 = a_{-1} = 0, \tag{2.4}$$

which leaves 2 independent variables (a_0, a_2) to describe the ellipsoid. It is convenient to rewrite them as

$$\begin{aligned} a_0 &= \beta \cos\gamma \\ a_2 &= \tfrac{1}{\sqrt{2}}\beta \sin\gamma \end{aligned} \tag{2.5}$$

with β the 5D radial variable and γ a polar coordinate. For general values of the intrinsic variables (β, γ), we obtain a general ellipsoid with 3 different lengths of the main axis'. Nevertheless, the rotational symmetry of the ellipsoid can (partially) be restored for some specific values

[1] As no volume conservation is apparent from equation (2.1), the monopole variable can be constrained with this purpose.

[2] From this point onwards, the quadrupole variables α_μ^2 will be abbreviated to α_μ.

1. Independent from γ, if $\beta = 0$ the ellipsoid reduces to a sphere. This is depicted in figure 2.1 (a).

2. For $\beta > 0$ and $\gamma = (2n+1)\frac{\pi}{3}$, two of the three main axis have equal length. Since the 3$^{\text{rd}}$ axis has a shorter length than the other 2, we obtain an *oblate* shape (see figure 2.1 (b))

3. Another case for which the $O(2)$ symmetry is restored around one of the main axis is the case for which $\beta > 0$ and $\gamma = 2n\frac{\pi}{3}$. Here, one of the axis' is relatively longer than the other two so we obtain a *prolate* shape (see figure 2.1 (c)).

4. Figure 2.1 (d) shows the special case for which $\gamma = (n + \frac{1}{2})\frac{\pi}{3}$. This corresponds to an ellipsoid where the ratios of the axis lengths differ maximally from 1, which will be denoted as the case of *maximal triaxiality*. Although this object is not symmetric in the geometrical sense, one can exploit the symmetry in the moments of inertia to describe the rotational dynamics of this type of ellipsoid (see section 2.4)

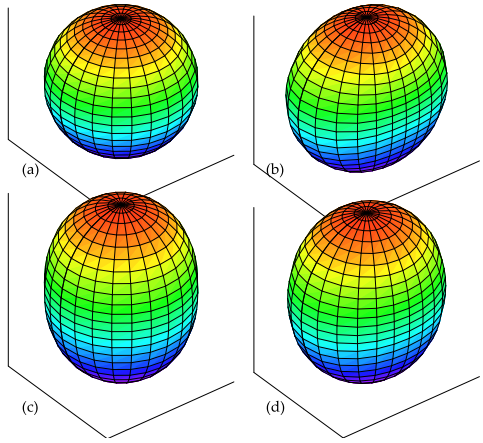

Figure 2.1: The different shapes for the ellipsoid, depending on the intrinsic variables (β, γ). A spherical (a), oblate (b), prolate (c) shape are depicted. Figure (d) shows an ellipsoid for which the triaxiality is maximal.

2.1.2 Inserting the dynamics

Until now, we have considered the atomic nucleus as a static object. Because of the Heisenberg principle, the surface will undergo excitations from the energetically favourable configuration, the so called vibrations and rotations. In a classical picture, the surface oscillations can be obtained from the Lagrangian

$$\mathcal{L} = T(\dot{\alpha}) - V(\alpha) \tag{2.6}$$

$$= \tfrac{B_2}{2}\dot{\alpha}\cdot\dot{\alpha} - V(\alpha), \tag{2.7}$$

with B_2 the mass parameter, associated with the surface stiffness. Going over to a classical Hamilton description, we introduce the canonic conjugate momenta π_μ so that the Hamiltonian can be written as

$$H = \tfrac{1}{2B_2}\pi\cdot\pi + V(\alpha). \tag{2.8}$$

As the nucleus is a quantum mechanical system, we need to quantise the surface oscillations. To do so, we replace the classical conjugate momenta by its quantum mechanical counterpart, in such a way that the following basic commutation rules are fulfilled

$$[\hat{\pi}_\mu, \hat{\alpha}_\nu] = -i\hbar\delta_{\mu\nu}, \qquad (\forall\mu,\nu). \tag{2.9}$$

A standard realisation of this relation is

$$\hat{\alpha}_\nu \to \alpha_\nu, \qquad \hat{\pi}_\mu \to -i\hbar\frac{\partial}{\partial\alpha_\mu}. \tag{2.10}$$

As a result, the classical Hamiltonian transforms into its quantum mechanical analogon.

$$\hat{H} = \tfrac{1}{2B_2}\hat{\pi}\cdot\hat{\pi} + V(\alpha). \tag{2.11}$$

Although the kinetic energy term in equation (2.11) has a simple form, it is far from clear at first sight what kind of physics it contains. In order to obtain a better comprehension, it is convenient to move over to the intrinsic frame of the ellipsoid. Starting from the standard realisation of the variables and conjugate momenta (2.10), Aage Bohr used the prescriptions from curved-coordinates vector analysis [Pod28] to derive the kinetic energy term in the intrinsic variables [Boh52]

$$\hat{T}_B = -\frac{\hbar^2}{2B_2}\left[\frac{1}{\beta^4}\frac{\partial}{\partial\beta}\beta^4\frac{\partial}{\partial\beta} + \frac{1}{\beta^2\sin 3\gamma}\frac{\partial}{\partial\gamma}\sin 3\gamma\frac{\partial}{\partial\gamma}\right] + \frac{\hbar^2}{8B_2}\sum_{i=1,2,3}\frac{\hat{L}_i'^2}{\beta^2\sin^2(\gamma-\frac{2\pi i}{3})}. \tag{2.12}$$

If we rewrite the potential energy $V(\alpha)$ in terms of the intrinsic variables and add it to the kinetic energy (2.12), we obtain the *Bohr Hamiltonian*

$$\hat{H}_B = \hat{T}_B + V(\beta, \gamma) \tag{2.13}$$

In (2.12), we notice that $\hat{T}_B$ is built up from 3 different terms.

1. A first term $\hat{T}_\beta$, accounting for the kinetic energy of the β-excitations.

$$\hat{T}_\beta = -\frac{\hbar^2}{2B_2}\frac{1}{\beta^4}\frac{\partial}{\partial\beta}\beta^4\frac{\partial}{\partial\beta}, \tag{2.14}$$

2. the second term $\hat{T}_\gamma$ describes the kinetic energy, associated with the γ-excitations

$$\hat{T}_\gamma = -\frac{\hbar^2}{2B_2}\frac{1}{\beta^2\sin 3\gamma}\frac{\partial}{\partial\gamma}\sin 3\gamma\frac{\partial}{\partial\gamma}, \tag{2.15}$$

3. The third term $\hat{T}_{\text{rot}}$ is referred to as the rotational term since it has the structure of a rotational Hamiltonian

$$\hat{T}_{\text{rot}} = \frac{\hbar^2}{8B_2}\sum_{i=1,2,3}\frac{\hat{L}_i'^2}{\beta^2\sin^2(\gamma - \frac{2\pi i}{3})}, \tag{2.16}$$

   with $\hat{L}_i'$ the component of the angular momentum around the intrinsic i-axis and the functions $\beta^2\sin^2(\gamma - \frac{2\pi i}{3}) \equiv \mathcal{J}_i$ denote the moments of inertia with respect to the i-axis. These are called *soft* moments of inertia, since they are different from those derived from a rigid rotor system (see section 2.3.1)

Although the 3 different terms describe different aspects of the collective excitations, they are still coupled. The coupling to the β excitations is rather loose and can be dealt with in some specific cases, depending on the potential in the Hamiltonian [Wil56]. Much stronger is the coupling of the γ-excitations to the rotational degrees of freedom by means of the γ-dependent moments of inertia $\mathcal{J}_i$, appearing in $\hat{T}_{\text{rot}}$. As a consequence, the γ-rotational motion can only be decoupled in some very specific situations in which an approximate treatment of the Hamiltonian is justified. However, since $\hat{T}_\gamma$ and $\hat{T}_{\text{rot}}$ are tightly connected in an algebraic way, the decoupling is not always necessary (see chapter 3.2).

Besides the kinetic energy in the Bohr Hamiltonian (2.13), the potential energy term also plays a role and accounts generally for the major part of the physics in

the Hamiltonian. This potential can either be constructed from a microscopic theory [Kum74] or through phenomenological considerations. If the latter strategy is followed, one can choose an analytically solvable potential that contains the basic physics, or resort to a more general expression in terms of the collective variables. Since the collective variables α_μ describe small amplitude deviations (2.2), most potentials can be written as an angular momentum scalar Taylor expansion in α. Unfortunately, the Taylor expansion of a potential is not analytically solvable, so one needs to construct a suitable basis to construct a matrix representation of the Hamiltonian to diagonalise, a topic which will be discussed in detail in chapter 3. The advantage of analytically solvable potentials is the clear parameter dependency of the solutions. These parameters are of utmost importance in fixing the potential and as such, a transparent one-to-one correspondence can be achieved of the solutions of the Hamiltonian with the physics described by the parameters. Therefore, it is of interest to construct analytically solvable potentials, and to confront them with experimental data. In the following section, a brief overview of solvable potentials is presented. Much attention will be given to the Davidson potential because of its "potential" use in the description of triaxial modes of motion (see next section 2.3.2).

Section 2.2 How to solve the Bohr Hamiltonian?

2.2.1 Decoupling the Hamiltonian

The question whether a potential can be analytically solvable is closely connected with the question if the potential enables a decoupling of the Hamiltonian. The Bohr Hamiltonian lives in a 5D Hilbert space, which means that it is represented by a second-order differential equation with 5 variables. If it would be possible to decouple this 5D equation into 5 different 1D equations, one would be able to solve these 5 equations separately, depending on the solvability of the decoupled potentials. As already mentioned, it is impossible to separate the γ- from the rotational degrees of freedom in an exact way, so the best one can get is the case where the β degree of freedom is decoupled from the others. This can be accomplished using a potential of the Wilets & Jean type [Wil56]

$$V(\beta,\gamma) = V_1(\beta) + \frac{V_2(\gamma)}{\beta^2}. \tag{2.17}$$

In the case of this potential, the Bohr Hamiltonian separates in two differential equations

$$\Big\{ -\frac{1}{\beta^4}\frac{\partial}{\partial\beta}\beta^4\frac{\partial}{\partial\beta} + u_1(\beta) - \varepsilon + \frac{\omega}{\beta^2}\Big\}\xi(\beta) = 0, \tag{2.18}$$

$$\Big\{ -\frac{1}{\sin 3\gamma}\frac{\partial}{\partial\gamma}\sin 3\gamma\frac{\partial}{\partial\gamma} + \sum_{i=1,2,3}\frac{\hat{L}_i'^2}{4\sin^2(\gamma - 2\pi i/3)} + u_2(\gamma) - \omega\Big\}\psi(\gamma,\theta_\iota) = 0, \tag{2.19}$$

where ω is the separation constant, $\varepsilon = (2B_2/\hbar^2)E$ and $u_k = (2B_2/\hbar^2)V_k$ (k=1,2). It is clear from these equations that we can only solve the Bohr Hamiltonian exactly whenever ω is determined exactly. At present, only one class of potentials $V_2(\gamma)$ is known for which equation (2.19) can be solved analytically, i.e. $V_2(\gamma) = 0$, which is denoted as the class of γ-*independent* potentials [Wil56]. In this particular case, equation (2.19) reduces to

$$\Big\{ -\frac{1}{\sin 3\gamma}\frac{\partial}{\partial\gamma}\sin 3\gamma\frac{\partial}{\partial\gamma} + \sum_{i=1,2,3}\frac{\hat{L}_i'^2}{4\sin^2(\gamma - 2\pi i/3)} - \omega\Big\}\psi(\gamma,\theta_\iota) = 0. \tag{2.20}$$

It is of particular importance to know the solutions (ω and $\psi(\gamma,\theta_i)$) of this differential equation. Not only because the coupling constant ω is needed as input in equation (2.18) in the case of γ-independent potentials, but the complete set of eigenfunctions $\psi(\gamma,\theta_i)$ can serve as a suitable basis for the matrix representation of a more general type of potentials.
Many techniques have been proposed in the literature to solve equation (2.20), relying either on algebraic or analytic methods. Shortly after the development of the Bohr Hamiltonian, it was realised that, making use of elementary group theory [Rak57], the coupling constant ω takes the values

$$\omega = v(v+3), \qquad (v \in \mathbb{N}), \tag{2.21}$$

where v is called the *seniority*. However, finding the associated eigenfunctions with ω was a less elementary task. The major complication in solving equation (2.20) is that the solutions $\psi(\gamma,\theta_i)$ must exhibit a good angular momentum quantum number L (and subsequently M), as the Bohr Hamiltonian is rotationally invariant. Therefore, one needs to seek for solutions of the form[3] [Eis87]

$$\psi^L_M(\gamma,\theta_i) = \sum_K g^K(\gamma)[D^{L*}_{MK}(\theta_i) + (-)^L D^{L*}_{M-K}] \tag{2.22}$$

[3]Note that the symmetrisation of the wavefunction according to the choice of the intrinsic frame is already implemented.

since the complex conjugate Wigner-D functions form good angular momentum tensors [Ros57]. The summation over the magnetic quantum number K along the intrinsic z' axis goes according the following rule

$$K = \begin{cases} K = 0, 2, \ldots L, & L = \text{even} \\ K = 2, 4, \ldots L-1, & L = \text{odd} \end{cases} \tag{2.23}$$

As a consequence, we need to find the functions $g^K(\gamma)$ of (2.22). Pioneering work has been carried out by Bès [Bès59], who determined the explicit γ-soft wavefunctions through a coupled differential-equation method. Unfortunately, this technique becomes tremendously complicated for spin states, higher than $L = 6$. Therefore, other techniques have been developed, based on the 5D harmonic oscillator potential and its underlying $SU(1,1) \times O(5)$ group structure. Here, the angular momentum invariance causes complications in the sense that the 3D orthogonal group is not naturally contained in the reduction of $SU(1,1) \times O(5)$. As a consequence one is forced to construct explicit wavefunctions, starting either from basic building blocks [Cor76, Cha76, Cha77] or from a projective coherent state formalism [Ghe78], constituting an orthonormal basis [Spi80, Góź80] with good angular momentum L. Even within the last decennium, some new techniques have been introduced. First, the vector coherent state formalism [Row94a, Row94b, Row95, Tur06] and much more recently an algebraic tractable model [Row04, Row05b, Tur05] were developed, enabling the construction of quadrupole harmonic oscillator representations with good angular momentum L. Without elaborating on the different techniques and the subtleties involved, we summarise here the reduction rules for L within a seniority v [Cha76, Fra94]

$$v = 3\nu_\Delta + \mu, \qquad (\nu_\Delta, \mu) \in \mathbb{N} \times \mathbb{N}, \tag{2.24}$$

$$L = \mu, \mu+1, \ldots, 2\mu-2, 2\mu. \tag{2.25}$$

This reduction scheme is illustrated in table 2.1 up to seniority $v = 6$. From this table, it can be seen that a degeneracy occurs in the $L = 6$ states for the seniority $v = 6$. For higher seniorities, this degeneracy persists, and is also present for other spin states. As a consequence, one of the two quantum numbers (ν_Δ, μ) is needed to distinguish between the different L states. Preference goes to ν_Δ. Although it is impossible to obtain ν_Δ from the eigenvalues of any operator, it has a physical meaning since it can be associated with the maximal number of triplets coupled to angular momentum $L = 0$. We call ν_Δ the *additional-* or *missing* quantum number, needed to unambiguously label the basis states.

Once ω is determined (2.21), it is used as input in equation (2.18). We obtain

v	(ν_Δ, μ)	L
0	(0,0)	0
1	(0,1)	2
2	(0,2)	2,4
3	(0,3)	3,4,6
	(1,0)	0
4	(0,4)	4,5,6,8
	(1,1)	2
5	(0,5)	5,6,7,8,10
	(1,2)	2,4
6	(0,6)	6,7,8,9,10,12
	(1,3)	3,4,6
	(2,0)	0

Table 2.1: Reduction rule for the possible L states within a seniority v. States upto $v = 6$ are presented to show that degeneracies in the L states are plausible (here: $L = 6$).

$$\Big\{ -\frac{1}{\beta^4}\frac{\partial}{\partial\beta}\beta^4\frac{\partial}{\partial\beta} + u_1(\beta) - \varepsilon + \frac{v(v+3)}{\beta^2} \Big\}\xi(\beta) = 0. \tag{2.26}$$

A vast number of γ-independent solvable potentials has been introduced in the literature, so instead of presenting a gallery of potentials we refer the reader to a recent overview on the use of solvable potentials in the Bohr-Mottelson model [For05a]. In the next subsection, we limit ourselves to a discussion of the 5D harmonic oscillator potential and its Davidson extension.

2.2.2 The 5D harmonic oscillator

The harmonic oscillator was historically the first collective potential ever introduced and solved [Boh52]. The physical legimitation for the use of such a schematic potential comes from classical arguments: if we consider the atomic nucleus as a macroscopic charged liquid drop, we need to supply energy to deform it from the spherical shape, due to the surface stiffness and the change in Coulomb energy. These energy contributions are of the order β^2, so we can write

$$V(\beta) = \tfrac{1}{2}C\beta^2. \tag{2.27}$$

Since the harmonic oscillator is a γ-independent potential, it can be catalogued as a trivial Wilets & Jean type of potential, and can be decoupled (see (2.18))

$$\Big\{ -\frac{1}{\beta^4}\frac{\partial}{\partial\beta}\beta^4\frac{\partial}{\partial\beta} + \frac{v(v+3)}{\beta^2} + k^2\beta^2 \Big\}\xi(\beta) = \varepsilon\xi(\beta), \tag{2.28}$$

with $k^2 = B_2C/\hbar^2$. If we rewrite $\xi(\beta) = \beta^v e^{-\frac{k\beta^2}{2}} f(\beta)$, we obtain

$$\frac{\partial^2 f(\beta)}{\partial\beta^2} + \left[\frac{2v+4}{\beta} - 2k\beta\right]\frac{\partial f(\beta)}{\partial\beta} + [\varepsilon - k(2v+5)]f(\beta) = 0, \tag{2.29}$$

which is equivalent to

$$xF''(x) + [v + \tfrac{5}{2} - x]F'(x) + \tfrac{1}{4}[\tfrac{\varepsilon}{k} - (2v+5)]F(x) = 0, \tag{2.30}$$

if $x = k\beta^2$. Equation (2.30) is the differential equation for the associated Laguerre polynomials [Arf01] of order $v + \frac{3}{2}$, so the total solution reads

$$\xi_n^v(\beta) = N\beta^v L_n^{v+\frac{3}{2}}(k\beta^2)e^{-\frac{k\beta^2}{2}}. \tag{2.31}$$

This solution is normalised if $n = \frac{1}{4}[\frac{\varepsilon}{k} - (2v+5)]$ is an integer, which leads towards the discrete eigenvalues of the total Hamiltonian

$$E = \hbar\Omega(2n + v + \tfrac{5}{2}), \tag{2.32}$$

with $\Omega = \sqrt{C/B_2}$ and the normalisation constant N is then given by

$$N = \sqrt{\frac{2k^{v+\frac{5}{2}}n!}{\Gamma(n+v+\frac{5}{2})}}. \tag{2.33}$$

Figure 2.2 organises the spectrum (equation (2.32)) according the quantum numbers. A remarkable fact about the harmonic oscillator potential is the large degeneracy in the spectrum, due to the linear dependence on the quantum numbers. These properties serve as major indications to investigate whether an atomic nucleus has a vibrational-like structure. Although it is very unlikely to encounter or discover a pure vibrational nucleus in experimental data, it still is a good benchmark for collective nuclear structure physics, partly because it has a simple and elegant structure that is not too far removed from real experimental data and partly because it can be fully solved and understood.

To solve for the harmonic oscillator, we made use of a class of special functions,

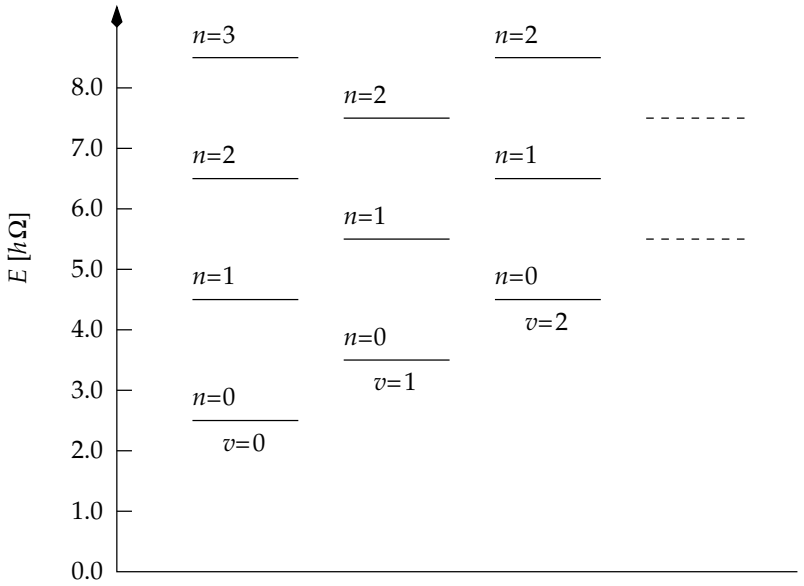

Figure 2.2: The spectrum of a 5D harmonic oscillator potential (2.32), organised according to the seniority v. The degeneracy in L for a given v state is not given in the figure.

i.e. the associated Laguerre polynomials. However, there exist other techniques to solve the eigenvalue differential equations. One among them makes use of symmetries or Lie algebras. The following treatment strongly resembles the discussion of pairing in section 1.2.2, although in the present case, the generators are expressed using differential operators instead of the second quantisation representations. We start by defining the following three operators

$$\begin{aligned}
\hat{B}_1 =& \frac{1}{4}\left[\frac{1}{k}\left(-\frac{1}{\beta^4}\frac{\partial}{\partial\beta}\beta^4\frac{\partial}{\partial\beta}+\frac{v(v+3)}{\beta^2}\right)-k\beta^2\right], \\
\hat{B}_2 =& -\frac{i}{2}\left[\frac{5}{2}+\beta\frac{\partial}{\partial\beta}\right], \\
\hat{B}_3 =& \frac{1}{4}\left[\frac{1}{k}\left(-\frac{1}{\beta^4}\frac{\partial}{\partial\beta}\beta^4\frac{\partial}{\partial\beta}+\frac{v(v+3)}{\beta^2}\right)+k\beta^2\right].
\end{aligned} \tag{2.34}$$

By calculating the commutation relations, we notice that they close according the non-compact Lie algebra of $SU(1,1)$, which is the non-compact isomorphic twin

of $SU(2)$ [Wyb74, Iac06]

$$[\hat{B}_1, \hat{B}_2] = -i\hat{B}_3, \quad [\hat{B}_2, \hat{B}_3] = i\hat{B}_1, \quad [\hat{B}_3, \hat{B}_1] = i\hat{B}_2. \tag{2.35}$$

Since $SU(1,1)$ is a rank 1 algebra, two quantum numbers are required to unambiguously label the irreducible representations. So we need two non-identical commuting operators to associate a quantum number to. The first one can be chosen from (2.34) (we choose $\hat{B}_3$) and the second one is the quadratic Casimir operator, given by

$$\hat{\mathcal{C}}_{SU(1,1)} = \hat{B}_3^2 - \hat{B}_2^2 - \hat{B}_1^2. \tag{2.36}$$

The irreducible representations (irreps) $|\lambda n\rangle$are defined by means of [Row96]

$$\hat{\mathcal{C}}_{SU(1,1)}|\lambda n\rangle = \tfrac{1}{4}\lambda(\lambda-2)|\lambda n\rangle, \qquad (\lambda \in \mathbb{R}^+), \tag{2.37}$$

$$\hat{B}_3|\lambda n\rangle = \tfrac{1}{2}(\lambda+2n)|\lambda n\rangle, \qquad (n \in \mathbb{N}). \tag{2.38}$$

To know the action of the other generators on this basis, it is convenient to introduce the raising and lowering operators, defined by

$$\hat{B}_\pm = \hat{B}_1 \pm i\hat{B}_2, \qquad \hat{B}_0 = \hat{B}_3. \tag{2.39}$$

These operators close according to the following commutation relations

$$[\hat{B}_0, \hat{B}_\pm] = \pm\hat{B}_\pm, \qquad [\hat{B}_-, \hat{B}_+] = 2\hat{B}_0, \tag{2.40}$$

and their action on the irreps is [Row96]

$$\hat{B}_+|\lambda n\rangle = \sqrt{(\lambda+n)(n+1)}|\lambda, n+1\rangle, \tag{2.41}$$

$$\hat{B}_-|\lambda n\rangle = \sqrt{(\lambda+n-1)n}|\lambda, n-1\rangle, \tag{2.42}$$

$$\hat{B}_0|\lambda n\rangle = \tfrac{1}{2}(\lambda+2n)|\lambda n\rangle, \tag{2.43}$$

hence, their name.
Although λ is defined from a group-theoretical point of view, it has a clear-cut connection with the physics of γ-independent potentials. Rewriting the Casimir operator (2.36) making use of the explicit β-realisation (2.34) of the $SU(1,1)$ algebra, we obtain

$$\hat{\mathcal{C}}_{SU(1,1)}) = \tfrac{1}{4}(v+\tfrac{5}{2})(v+\tfrac{1}{2}). \tag{2.44}$$

As a consequence, we can associate the Casimir quantum number λ with the seniority quantum number v

$$\lambda(\lambda-2) = (v+\tfrac{5}{2})(v+\tfrac{1}{2}), \tag{2.45}$$

which has $\lambda = v + \frac{5}{2}$, as an only solution since only positive values of λ are allowed. Moreover, the quantum number n can also be connected to a physical quantity. In the case of a harmonic oscillator potential, we recognise the decoupled differential equation (2.28) as the generator $\hat{B}_0$ of the $SU(1,1)$ algebra, up to a factor

$$4k\hat{B}_0|\xi\rangle = \varepsilon|\xi\rangle. \tag{2.46}$$

Because $|\xi\rangle$ is an eigenstate of $\hat{B}_0$, it must be an irreps (2.38), so we obtain the eigenvalue ε in a straightforward way as

$$\varepsilon = 2k(2n + \lambda). \tag{2.47}$$

Taking the various definitions of ε, k, Ω and λ into account, we regain the energy expression for the harmonic oscillator (2.32)

$$E_{nv} = \hbar\Omega(2n + v + \tfrac{5}{2}), \tag{2.48}$$

which means that the $SU(1,1)$ quantum number n can be associated to the β-phonons of the 5D harmonic oscillator.

As a conclusion, in the present subsection we have shown that different paths can lead towards the same solution of a problem. One can e.g. transform the involved differential equations until a "well-known" form appears. Unfortunately, this a method that might turn out to be rather technically involved. Another method makes use of symmetries. This method has a major advantage over the former that it is less technical in the calculations although the connection with the physics might not be immediately clear. However, even for more complicated problems than the harmonic oscillator potential, symmetries might shed light on the physics in a given problem and the solutions, as will be shown for the Davidson potential.

2.2.3 The Davidson potential as an extension of the harmonic oscillator

Davidson introduced the potential, bearing his name, to study the rotation-vibrational coupling of diatomic molecules [Dav32] in 3D. However, this potential can also be used in the collective Bohr-Mottelsen model as a γ-independent potential with a deformed minimum at $\beta_0 > 0$ as proposed by [Ell86]. The potential has the form

$$V(\beta) = \frac{C}{2}\left(\beta^2 + \frac{\beta_0^4}{\beta^2}\right), \tag{2.49}$$

and is depicted in figure 2.3 for different values of β_0. It can be seen as an extension of the harmonic oscillator potential, since it adds a centrifugal term to the β^2 potential. This centrifugal term is parametrised in such a way that the potential has a minimum at β_0.

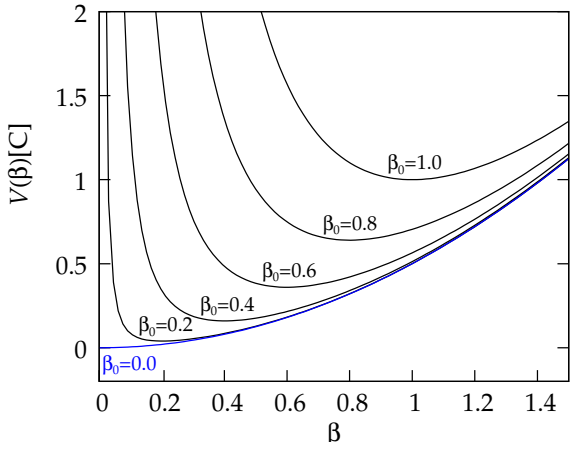

Figure 2.3: The Davidson potential for different values of β_0

The Bohr Hamiltonian can be solved in a similar way as for the harmonic oscillator. If we replace the seniority v in the expressions of the $SU(1,1)$ generators (2.34) by the parameter $\tilde{v}$, defined by

$$\tilde{v}(\tilde{v}+3) = v(v+3) + k^2\beta_0^4 \tag{2.50}$$

(with $k^2 = B_2C/\hbar^2$), the Hamiltonian can once again be associated with the generator $\hat{B}_0$. So the energy spectrum of the Davidson potential becomes

$$E^D_{n\tilde{v}} = \hbar\Omega(2n + \tilde{v} + \tfrac{5}{2}). \tag{2.51}$$

This potential can be used to study the transition from a spherical into a β-deformed system, as all observables can be calculated analytically along the transition path [Bon04]. In figure 2.4, the excitation energy is plotted as a function of the deformation parameter β_0. On the left side, we start from a vibrational spectrum, and move towards the situation in which all $n = 0$ states are lowered in the energy spectrum to form a ground band.

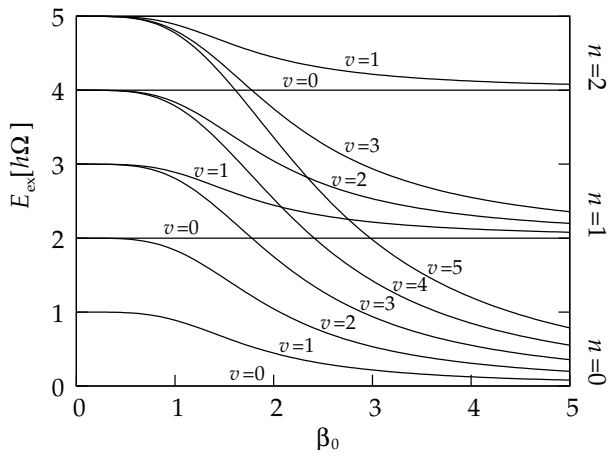

Figure 2.4: The excitation energy spectrum of the Davidson potential as a function of the deformation parameter β_0.

To summarise, it is shown by means of an example that symmetries or special-function theory can come in very handy when solving γ-independent potentials in the Bohr Hamiltonian. Moreover, the only known analytically solvable potentials are γ-independent [For05a]. This is due to the fact that, for n-dimensional systems with $n \geqslant 2$, the only two completely exactly solvable systems are the Davidson and Kratzer problems which can be regarded respectively as extensions of the harmonic oscillator and Coulomb potentials in n dimensions [Iac06] (see [For03] for a discussion within the framework of the collective model). From a nuclear physicists point of view, this is not a satisfactory situation since it is very unlikely to find fingerprints for pure γ-independent structures in experimental data (as e.g. the degeneracy in the seniority quantum number v). Therefore, we also require solvable potentials for γ-*dependent* potentials, in order to describe prolate, oblate, triaxial or even more complicated structures in the collective model.

To cope with prolate (or oblate) structures, the rotation-vibration (RV) model was developed in which the rotations of an axial deformed object are coupled to the vibrations of the surface [Fae62, Eis87]. This model is an approximative model, since it is only valid in the vicinity of ($\beta_0 > 0, \gamma = 0$) and corrections are to be treated in a perturbative way. Nevertheless, the RV model still serves as a good benchmark for axial soft rotational nuclei. In the next section, a similar strategy is followed as the RV model to solve for triaxial modes of motion, though a poten-

tial is chosen in the spirit of Wilets & Jean to decouple the β- from the γ-rotational degrees of freedom in an exact way.

Section 2.3 Triaxiality in the Bohr Hamiltonian

2.3.1 From rigid...

Historically, non-axial or triaxial nuclei were first addressed by means of a *rigid* model, which came as a limiting case of the Bohr-Mottelson model [Dav58, Dav59]. Within the language of the BM model, an atomic nucleus is considered rigid if it takes an infinite amount of energy to deform the nucleus from its equilibrium shape. The potential $V(\beta, \gamma)$ in the Bohr Hamiltonian must then be of the following form

$$V(\beta, \gamma) = \delta(\beta - \beta_0)\delta(\gamma - \gamma_0). \tag{2.52}$$

As a consequence, the kinetic excitations disappear in the Bohr Hamiltonian (2.13), and we are left with (2.16)

$$\hat{H}_{\text{rot}} = \frac{\hbar^2}{8B_2} \sum_{i=1,2,3} \frac{\hat{L}_i'^2}{\beta_0^2 \sin^2(\gamma_0 - \frac{2\pi i}{3})}, \tag{2.53}$$

where the (β, γ) variables have been frozen to the rigid values (β_0, γ_0). The form of $\hat{H}_{\text{rot}}$ suggests that the dynamics is restricted to rotations of a rigid body, with the moments of inertia given by

$$\mathcal{J}_i = 4B_2\beta_0^2 \sin^2(\gamma_0 - \tfrac{2\pi i}{3}). \tag{2.54}$$

These are called the *soft* moments of inertia, since they result from the BM model, which considers the atomic nucleus to be soft as a starting point. Therefore, the triaxial rigid Davydov Hamiltonian (2.53) can be interpreted as a rotational Hamiltonian originating from the rigid limit of the Bohr Hamiltonian.
However, this is not the only path leading towards a rotational Hamiltonian. If we consider the atomic nucleus to be a rigid body as a starting point, we can also deduce a quantum mechanical rotational Hamiltonian starting from a semi-classical point of view [Cas31]

$$\hat{H}_{\text{rigid}} = \sum_{i=1,2,3} \frac{(\hbar\hat{L}_i')^2}{2\mathcal{J}_i}. \tag{2.55}$$

Alternatively to the collective model, the moments of inertia are now derived from classical mechanics [Hey99]

$$\mathcal{J}_i = \tfrac{2}{5} m A R_0^2 \left[1 - \sqrt{\tfrac{5}{4\pi}} \beta_0 \cos(\gamma_0 - \tfrac{2\pi i}{3}) \right], \tag{2.56}$$

with m the nucleon mass. These moments of inertia are clearly different from the

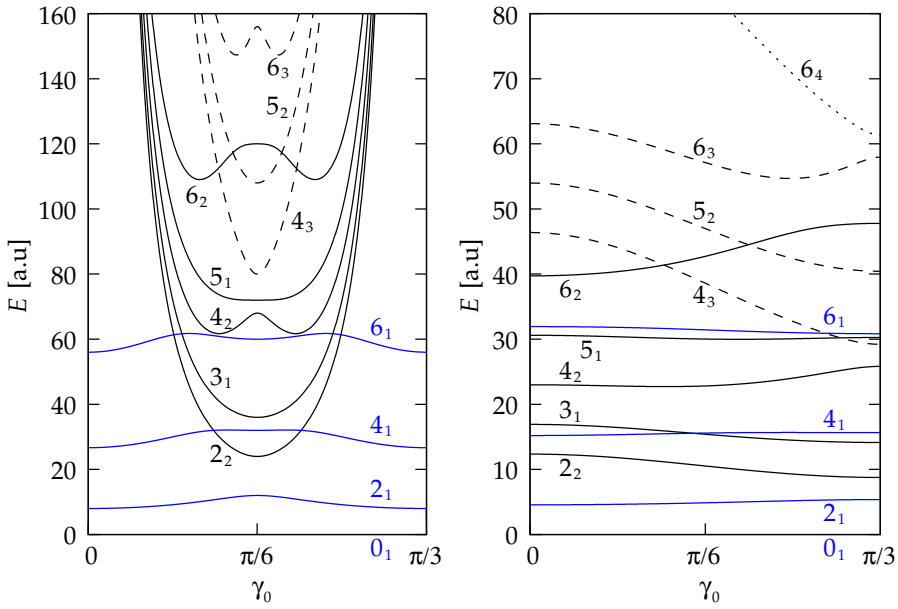

Figure 2.5: The spectrum of the rigid rotor, using the different expressions for the moments of inertia $\mathcal{J}_i$. On the left-hand side, the frozen soft moments of inertia from the Bohr Hamiltonian are used (2.54), while on the right-hand side the classical moments of inertia (2.56) are chosen. The energy is measured relative to $\hbar^2/(8B_2)$ on the left-hand side and to $5\hbar^2/(4mAR_0^2)$ on the right-hand side where $\beta_0 = 1$ is chosen to enhance the visualisation of the effects.

soft ones, derived in the framework of the collective model, which will have a serious effect on the energy spectrum. In figure 2.5, both the spectrum[4] for the Davydov Hamiltonian (left-hand side), as for the semi-classical rotational Hamiltonian (right-hand side) is shown, as a function of the triaxiality γ_0. Significant similarities and differences can be observed. The overall trend of the ground band

[4]Details of the calculation are given in appendix A.1

(in blue) is very much the same in both situations, though for the other bands, large discrepancies arise, especially in the limits of axial symmetry ($\gamma_0 = 0, \pi/3$). Since one of the soft moments of inertia (2.54) identically vanishes for axial symmetry, we obtain divergencies in the spectrum of the Davydov model (figure 2.5, left-hand side). From a classical point of view, it is incomprehensible how a moment of inertia could vanish, as it would take a zero amount of energy to accelerate the rotation of this axial rigid body around the corresponding main axis. This anomaly is an artefact, stemming from the forced decoupling of the rotations from the γ-softness of the ellipsoid. Moreover, the rotation-vibration model proves that the coupling of the γ-degree of freedom to the rotations along the axial symmetry axis eliminates the divergencies, so the $K \neq 0$ bands are substantially lowered in the spectrum. For triaxial modes, this coupling is less significant, and since the moments of inertia have a finite value, the $K \neq 0$ are observed in the spectrum. From figure 2.5 (right-hand side), we can see that the semi-classical model does not suffer from these divergencies (as long as β_0 stays sufficiently small).

It is clear from this discussion that the only unknown parameters in the rigid triaxial rotor model are the moments of inertia $\mathcal{J}_i$. To determine these parameters, we can compare them with the moments of inertia, as extracted from experimental data [Boh98, Hey99]. As a result, we find that the experimental moments of inertia lie in between the classical rigid moments of inertia and the ones obtained from the Davydov model[5]. In this respect, a recent study [Woo04] relaxed the functional dependence of the moments of inertia, treating them as free parameters in a fit to experimental data. This led to an improvement of the description of nuclear observables, suggesting that the semi-classical or irrotational Davydov interpretation of (triaxial) rotations might have to be abandoned. However, it is not clear to what extent the softness could compensate for the corrections, obtained by the free parameter fit. Eventually, the softness needs to be taken into account, as any rigid model cannot explain the occurrence of multiple $L = 0$ collective states in the low-energy structure of atomic nuclei, something which is observed frequently in experimental data, as e.g. in the Os isotopes.

2.3.2 ... to soft

From the former discussion, it becomes clear that the rigid triaxial model served well as a first attempt, though the softness needs to be incorporated if a complete description of the low-energy structure is desired. This means that the Bohr

[5] with the assumption of an irrotational mass parameter B_2. (see equation 2.65).

Hamiltonian is to be solved -something which is a nontrivial task- for potentials with a γ dependence. Making use of schematic harmonic oscillator potentials in β and γ, the Bohr Hamiltonian can be solved *approximately* [Dav60, Dav61], or one can also resort to more general expressions of the potentials which need to be diagonalised in a basis, obtained from e.g. the γ-independent solutions (see section 2.2). However, the transparency provided by analytic solutions is lost with the latter strategy. For this purpose, we studied a schematic potential of the form [For06]

$$V(\beta,\gamma) = \frac{\hbar^2}{2B_2}\left[A_D\beta^2 + \frac{C(\gamma-\gamma_0)^2 + B_D}{\beta^2}\right], \tag{2.57}$$

which exhibits a minimum at ($\beta = \sqrt[4]{B_D/A_D}, \gamma = \gamma_0$). This is a potential of the Wilets & Jean type, thus the γ-degrees of freedom can be decoupled exactly from the β degree of freedom. Concerning the β-excitations, we obtain a Davidson type of potential (eq. (2.49)), which has been elaborately discussed in section 2.2.3. For the decoupled γ excitations, we now obtain (2.19)

$$\Big\{-\frac{1}{\sin 3\gamma}\frac{\partial}{\partial\gamma}\sin 3\gamma\frac{\partial}{\partial\gamma} + \sum_{i=1,2,3}\frac{\hat{L}_i'^2}{4\sin^2(\gamma-2\pi i/3)} + C(\gamma-\gamma_0)^2 - \omega\Big\}\psi(\gamma,\theta_t) = 0. \tag{2.58}$$

Since we are mainly interested in triaxial modes, we can assume that γ_0 is significantly different from 0 or $\pi/3$ ($\gamma_0 \sim [\pi/12, \pi/4]$), which justifies the following approximations

- Because the rigid triaxial Davydov model is not divergent in the triaxial region, we can again freeze out the γ dependence in the moments of inertia

$$A_i = \frac{1}{4\sin^2(\gamma-\frac{2\pi i}{3})} \rightarrow \frac{1}{4\sin^2(\gamma_0-\frac{2\pi i}{3})}. \tag{2.59}$$

- The excitations are localised around the triaxial minimum γ_0, so we can approximate the kinetic energy term to (with $x \equiv \gamma - \gamma_0$)

$$-\frac{1}{\sin 3\gamma}\frac{\partial}{\partial\gamma}\sin 3\gamma\frac{\partial}{\partial\gamma} \sim -\frac{1}{\sin 3\gamma_0}\frac{\partial}{\partial x}\sin 3\gamma_0\frac{\partial}{\partial x} = -\frac{\partial^2}{\partial x^2}. \tag{2.60}$$

As a consequence, we obtain a 1D harmonic oscillator Hamiltonian around a triaxial minimum γ_0, to which the rigid Davydov rotor is added with the corre-

sponding triaxiality parameter

$$\Big\{ -\frac{\partial^2}{\partial x^2} + \sum_{i=1,2,3} A_i \hat{L}_i'^2 + Cx^2 - \omega \Big\} \psi(x, \theta_i) = 0. \tag{2.61}$$

This equation can be decoupled into a γ-vibrational and a rotational part which is reflected in the solution of the decoupling coefficient ω

$$\omega = \sqrt{C}(2n_\gamma + 1) + \omega_{\text{rot}}. \tag{2.62}$$

The vibrational term $\sqrt{C}(2n_\gamma + 1)$ comes from the harmonic oscillator term and ω_{rot} is the solution of the rotational part. In some particular cases, ω_{rot} can be determined analytically, as long as the Hilbert space stays reasonably small. E.g. for the $L = 2$ states e.g., we obtain the result (see appendix A.1)

$$\omega_{\text{rot}}(L = 2) = 2 \sum_i A_i \pm 2 \sqrt{\sum_i A_i^2 - \sum_{i<j} A_i A_j}, \tag{2.63}$$

identically to the Davydov triaxial rotor. Combining the results from the three decoupled equations (Davidson, 1D Harmonic oscillator and Davydov rotor), we obtain the total approximative solution of the Davidson deformed triaxial rotor

$$E^{L_i}_{n_\beta n_\gamma} = \frac{\hbar^2}{B_2} \sqrt{A_D} \left[2n_\beta + 1 + \sqrt{\tfrac{9}{4} + \sqrt{C}(2n_\gamma + 1) + \omega^{L_i}_{\text{rot}} + B_D} \right]. \tag{2.64}$$

Now that we have an analytic solution, it is interesting to confront them with experimental data in regions of the nuclear chart where evidence for triaxial modes has been observed, such as in the chain of Os isotopes.

2.3.3 Applications in the Os-isotopes

The Os isotopes have been the subject of many studies concerning the collectivity and geometry around the $Z = 82$ shell closure (see figure 1.5). Starting from a microscopic effective nucleon-nucleon interaction, self-consistent Hartree-Fock-Bogoliubov (HFB) calculations have been carried out, constructing ground state energy surfaces as a function of the deformation variables β and γ [Kum68, Ans86, Ans88]. The main result from these calculations was that the Os isotopes experience a transition from a prolate to an oblate structure for increasing mass number A, exhibiting soft triaxial minima in the energy surface along the transition line, depending on the interaction. More recently, the Davydov model (section 2.3.1) has been revisited to extract the rigid deformation parameters of the Os

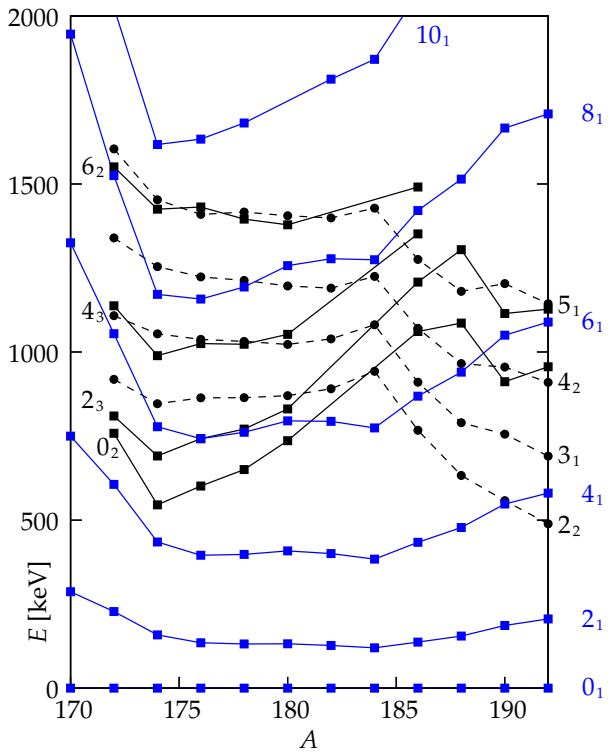

Figure 2.6: Experimental spectra of Os isotopes. Data is taken from the Nuclear Data Sheets [Fir89, Bro94, Sin95b, Sin95a, Bag98, Bro99, Sin02, Sin03, Bag03, Wu03, Bas06]

isotopes and neighbouring isotopic chains [Ess97]. The transition was found to be much smoother than the HFB predictions. This might be due to the softness of the calculated energy surfaces, as it is argued in [Ess97] that the evaluated rigid values correspond to the root mean square values of soft β and γ solutions, which will evolve more smoothly along the transition path than the values minimising the energy surface. Another study worth mentioning makes use of K-shape invariants to extract the β and γ values of a given nucleus [Wer05]. Although this technique starts from the Davydov model, it relies heavily on experimental data in order to extract the K-shape invariants and subsequently the deformation variables β and γ. A recent IBM study [McC05] also covered the Os isotopes, making use of the consistent-Q Hamiltonian (see section 1.2.3). It should be noted that the geometrical interpretation of the IBM1 consistent-Q formalism does not

allow triaxial minima in the energy surface (1.30), as the Hamiltonian is truncated up to 2-boson interactions. To enable a triaxial geometry in the IBM, we either incorporate higher-order interactions, or consider the proton-neutron IBM (IBM2) [Cap04, Cap05]. A numerical study of the Os isotopes in the framework of IBM2 has been carried out [Bij80], although no geometrical interpretation has been given in the mentioned work.

A study of the triaxial deformed Davidson potential (2.57) can give a valuable contribution to the discussion, since the parameters in the model (B_2,A_D,B_D,C and γ_0) all have a direct physical meaning. The β deformation and softness is governed by the mass parameter B_2 and the Davidson parameters A_D and B_D, while the γ softness is controlled by C and the triaxiality by γ_0. Fitting these parameters to the experimental data will result in a good or a bad description. If the present approach is successful, we can associate physical significance to the parameters. If it fails,the assumption of the Os isotopes as triaxial soft rotors is wrong, which means that we need to resort to other models for a better understanding of the Os isotopes. However at any time, it is good to keep in mind the schematic nature of the potential.

The experimental energy spectra of the Os isotopes are plotted in figure 2.6. We use these spectra to fit the parameters. From the theoretical energy formula (2.64), we learn that the excitation energy is independent from the ratio $\sqrt{A_D}/B_2$. Moreover, the relative spectrum (normalised to the first $L = 2^+$ state) is not affected by the ratio $\sqrt{A_D}/B_2$, which leaves us 3 independent parameters (B_D, C and γ_0) to fit the data. The chosen states, considered in our theoretical fit, are the 2_1^+ and 4_1^+ from the ground band, and the band heads of the supposed $(n_\beta = 0, n_\gamma = 0, K^* = 2)$ and $(n_\beta = 0, n_\gamma = 1, K^* = 0)$ bands. The K^* quantum number is used as a label to distinguish between different L_i-states in the determination of ω_{rot}. We use the notation K^* so as to make the connection with the K quantum number of the axial rigid rotor clear(see figure 2.5). A typical theoretical normalised energy spectrum (for ^{188}Os) is given in figure 2.7, where the comparison is made with experiment

Calculations have been carried out for the whole chain of Os isotopes with $A = 172 - 192$, except for ^{182}Os, where no information was available on the supposed $n_\gamma = 1$ band. Extensive comparison of the theoretical calculations and the experimental energy spectra has been given in figure 2.8. It can be seen from figure 2.8 (a) that the groundband is well described by the theory. This is not very surprising since the $L = 4_1$ and $L = 6_1$ excitation energy have been chosen as

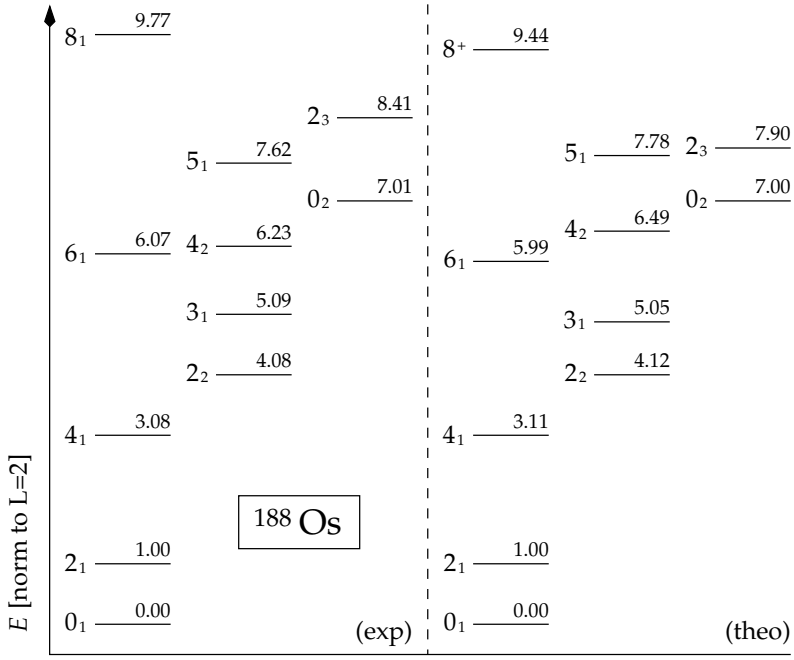

Figure 2.7: Normalised excitation spectrum for ^{188}Os, experimentally (exp) and theoretically (theo) (figure adopted from [For06])

experimental input in the fit. Moreover, the ratio $\sqrt{A_D}/B_2$ has been chosen to reproduce the excitation energy of the $L = 2_1$ ground band member. Nevertheless, the $L = 8_1$ and $L = 10_1$ are still well described by the model (the deviations are around or below 100 keV for each A), which proves that the ground band indeed is a collective rotational band, as was tacitly assumed.

The other bands are more interesting with respect to the model description. There is much data available for the $K^* = 2$ band, which is presented in figure 2.8 (b). The $L = 2_2^+$ is very well described (in magnitude and in trend), which does not come as a surprise neither as it is contained in the fitting procedure. From this figure 2.8 (b), we clearly see that the spectrum can be divided in two parts with $A = 184$ as the breaking point. For heavier masses ($A > 184$), we notice the band rapidly dropping in excitation energy, suggesting that the collectivity rises from this point. This is also the region where the band is best described by the model. However, it should be noted that the staggering effect is more washed out in the

experimental spectrum as compared with the calculated structure, which can be seen from the behaviour of the 4_2^+ state. This might be a side-effect of the harsh decoupling of the γ vibrations from the triaxial vibrations in the model, since the $K = 2$ band is rather sensitive to this coupling. The $K^* = 2$ band of the isotopes with the lower masses ($A < 184$) is less well reproduced quantitatively, although the general constant slope is also observed in the calculations. Since the model we are working with is a pure phenomenological model, we cannot provide a fundamental reason for the structural changes at $A = 184$ within this framework.

The next band to be discussed is the $n_\gamma = 1$ band, depicted in figure 2.8 (c). This band is suggested to be based on γ-vibrations of the nucleus around the equilibrium γ_0. The $L = 0_2^+$ bandhead is, as expected, well described since it is contained in the fit. The other states follow a similar trend as the $K^* = 2$ band with respect to the $A = 184$ break point. However, one cannot make conclusive statements from the data because for the masses ($A > 184$), few data is known from the Nuclear Data Sheets. Relying on the data for ^{186}Os, it seems that the γ band is quenched beyond $A = 184$. This is something which is not reproduced by the model. On the other side, the constant slope for the lower masses is well predicted, although the scaling is, just like for the $K^* = 2$ band, underestimated.

It is interesting to study the variation of the parameters along the series of isotopes. In figure 2.9, the fitted parameters (B_D, C and γ_0) are given. We can again roughly divide the results into two regions. For masses below $A = 184$, the parameters C and B_D are relatively small, which means that the potential (2.57) is rather soft. Nevertheless, there is an upward slope with increasing mass. This is reflected in the excitation energy of the $n_\gamma = 1$ band head 0_2^+, which follows a similar slope as the parameter C (see figure 2.8 (c)). The triaxiality γ_0 stays more or less constant $\gamma_0 \sim 14^\circ$ in this region, which is also observed in the evolution of the $K^* = 2$ band (see figure 2.8 (b)). For masses larger than 184, the situation becomes more rigid and the triaxiality increases. As a consequence, the situation evolves towards a triaxial rigid rotor, something which can be seen in the experimental spectrum, where the $K^* = 2$ band drops below the $n_\gamma = 1$ band. This is also indicated by the comparison of γ_0 with other methods in figure 2.9 (c). From this figure it is clearly seen that the comparison is best with the method of [Ess97] (black circles), which is related to the rigid triaxial Davydov model.

The parameters (B_D, C and γ_0) are obtained from the fitting procedure. Therefore, we are left with two free parameters (B_2 and A_D) to describe experimental observables. As can be seen from the energy formula (2.64), the ratio $\sqrt{A_D}/B_2$

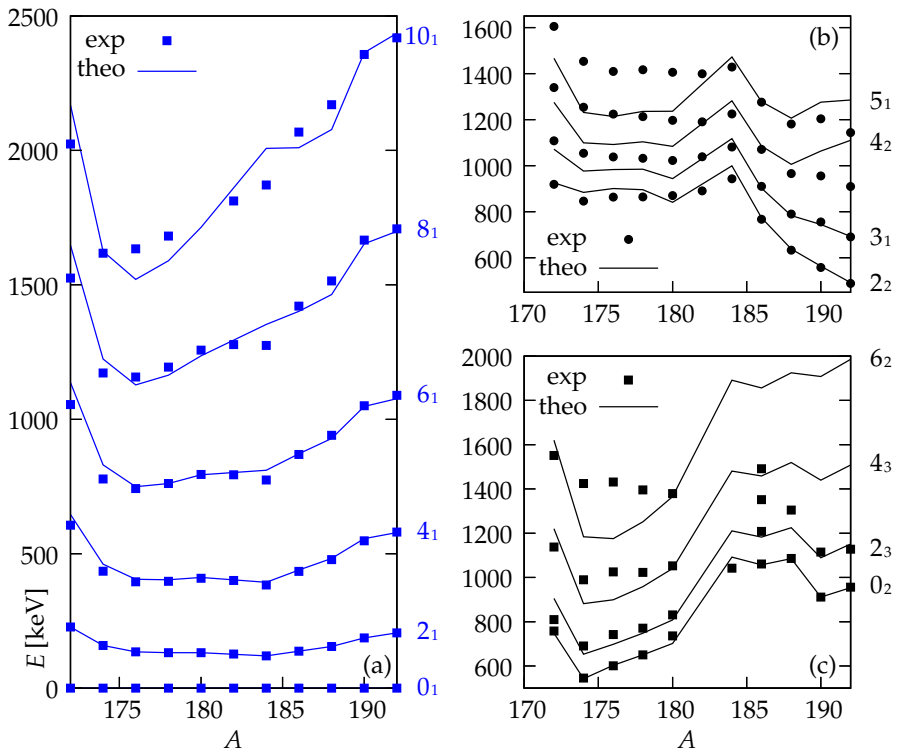

Figure 2.8: Comparison of experimental data with the calculated values. On the left-hand side (a), the groundband results are given, while un the upper right side, the results for the $(n_\beta = 0, n_\gamma = 0, K^* = 2)$ are presented. In the lower right-hand side (c), the $(n_\beta = 0, n_\gamma = 1, K^* = 0)$ γ-band is given. The labelling of the spins refers to figure 2.6.

can be adjusted to match the scale of the theoretical calculation versus the experimental spectrum. In the present calculation, it is used to match the excitation energy of the 2_1^+ state. As a consequence, we only need one extra condition to complete the determination of the set of parameters.
One strategy to do so is to assume that the mass parameter B_2 can be obtained using *irrotational* collective motion [Flü41, Eis87]. In this case, the mass parameter is given by

$$B_2 = \tfrac{1}{2}\rho R_0^5, \tag{2.65}$$

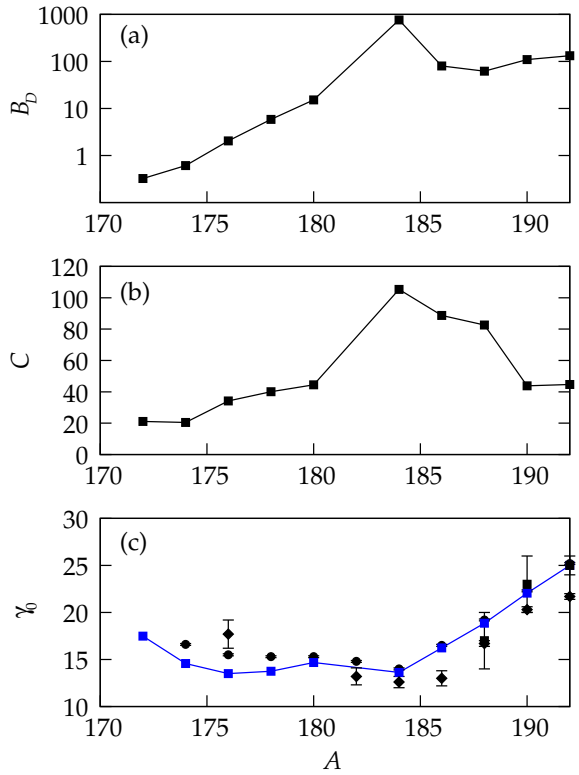

Figure 2.9: Plot of the fitted parameters B_D (a), C (b) and γ_0 (c). In the lowest panel (c), the calculated values of γ_0 are given in blue and compared to those obtained with other methods as described in the text (circles (γ_e) and diamonds (γ_b) refer to [Ess97], whereas squares are taken from [Wer05])

with ρ the mass density of the nucleus and R_0 defined by means of equation (2.2). We are able to verify this expression using the known quadrupole moments of the nucleus. The quadrupole moment is defined by

$$Q = \sqrt{\frac{16\pi}{5}} \frac{3ZR_0^2}{4\pi} \begin{pmatrix} 2 & 2 & 2 \\ -2 & 0 & 2 \end{pmatrix} \langle 2_1^+ || \alpha^* || 2_1^+ \rangle, \tag{2.66}$$

and can be calculated for the triaxial Davidson potential. The result is given by (the derivation is presented in detail in appendix A.2)

$$Q = \sqrt{\frac{1}{5\pi}}\frac{6}{7}ZR_0^2\frac{\Gamma(\tilde{v}+1/2)}{A_D^{1/4}\Gamma(\tilde{v})}(1-\frac{1}{4\sqrt{C}})[\cos\gamma_0(a_2^2-a_0^2)+2a_2a_0\sin\gamma_0]. \qquad (2.67)$$

This expression contains A_D as the only free parameter. If we assume irrotational flow for the mass parameter and fix A_D to fit the scale of the spectrum, A_D is no longer a free parameter for the quadrupole moment (2.67). The results of the irrotational flow assumption in calculating the quadrupole moments are given in figure 2.10. From the figure it is clearly seen that the sign and slope of the quadrupole moments are well reproduced, although the absolute value is overestimated by a factor of 2.5 in average. This shows that the assumption of irrotational flow is not validated and we better leave the mass parameter as a free parameter. However, it should be stressed that the Davidson potential does not allow an unambiguous fit from the energy spectrum alone. Therefore, we need to resort to the quadrupole moments in order to obtain a reasonable estimate of the mass parameter B_2. This will be the philosophy when dealing with more general types of potentials to describe nuclear observables such as energy spectra, quadrupole moments and electromagnetic transitions that require a more detailed and refined determination of the eigenstates, as will be discussed in the following chapters.

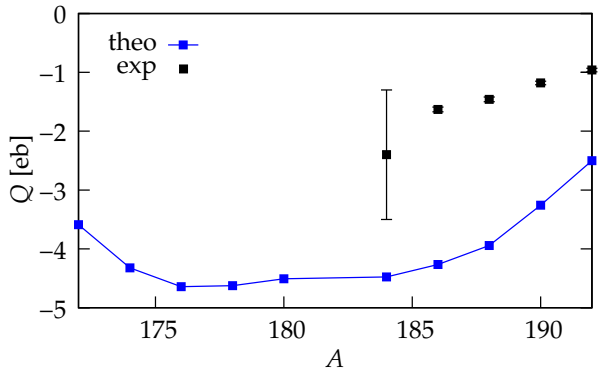

Figure 2.10: Plot of the quadrupole moments of the first excited 2_1^+ state of the Os isotopes. The experimental data is taken from [Rag89].

To conclude, it is possible to give a description of triaxial modes of motion using a very schematic potential of the Davidson type (2.57) that can be confronted

with experimental data to a reasonable extent. Energy spectra are rather well described and can be interpreted according to the parameters in the fitting procedure. However, it should be stressed that the proposed potential is very schematic. Since the potential in γ is a harmonic oscillator potential, the symmetry of choice of the intrinsic framework is violated. To restore this symmetry, we need to work with potentials that are periodic in γ with periodicity $\pi/3$. Typical terms respecting this symmetry are of the form $\cos 3\gamma$, and can be handled within the general collective model of the Frankfurt group [Gne71, Eis87], the recently proposed algebraic tractable model by the Toronto group [Row04, Row05b, Tur05] or the Cartan framework, discussed in the next chapter. The drawback of the latter models is that the analytical solvability is completely lost, and therefore, it would be informative to have a benchmarking periodic potential at hand that can be solved in an (approximative) analytical way. Such a potential can be found in the form of a Pöschl-Teller Potential of the second kind, and will be discussed in the next section.

Section 2.4 A solvable periodic potential

2.4.1 Spectrum of the Pöschl-Teller potential of the second kind

We can start from a potential of the Wilets & Jean type to decouple the β-degree of freedom so we can focus on the study of a periodic potential in γ. The decoupled γ-rotational differential equation is (2.19)

$$\Big\{ -\frac{1}{\sin 3\gamma}\frac{\partial}{\partial\gamma}\sin 3\gamma\frac{\partial}{\partial\gamma} + \sum_{i=1,2,3}\frac{\hat{L}_i'^2}{4\sin^2(\gamma-2\pi i/3)} + u_2(\gamma) - \omega\Big\}\psi(\gamma,\theta_\iota) = 0. \tag{2.68}$$

It is worth mentioning that in the specific case of $L^\pi = 0^+$ states, the rotational energy trivially vanishes, which leaves the γ-variable completely decoupled. If we choose the potential in γ to be completely soft ($u_2(\gamma) = 0$), the differential equation (2.68) reduces to the Legendre differential equation with $x = \cos(3\gamma)$, as already pointed out in [Boh52, Bès59]

$$\left\{9\frac{\partial}{\partial x}\left((1-x^2)\frac{\partial}{\partial x}\right) + \omega\right\}\psi(\gamma,\theta_\iota)_{L=0} = 0. \tag{2.69}$$

The normalised eigenfunctions of these equations are the Legendre polynomials if $\omega = 9\lambda(\lambda+1)$. Rewriting this as $\omega = 3\lambda(3\lambda+3)$, the correspondence to the

coupling constant $\omega = v(v+3)$ for γ-independent potentials is clear with $v = 3\lambda$ (see section 2.2.1).
Now we abandon the path of γ-independency and introduce the following potential [DB06]

$$u_2(\gamma) = \frac{\mu}{\sin^2 3\gamma}. \tag{2.70}$$

which is a Pöschl-Teller potential of the second kind [Iac06]. This potential, depicted in figure 2.11 (a), has some interesting characteristics. The behaviour is rather flat at the minimum, but diverges very quickly towards $\gamma = 0$ and $\gamma = \pi/3$. This will push the wavefunction away from the boundaries, imposing a localisation around $\gamma = \pi/6$. This effect is not as drastic as expected at first sight, because the components of the soft moments of inertia (2.54) exhibit a similar behaviour at the boundaries as can be seen in figure 2.11 (b). Moreover, in the specific case of $L = 3$, the rotational part reduces to an expression, proportional to $1/\sin^2 3\gamma$. Sandwiching the rotational part with the $L = 3$ state gives (using equations (A.16) in appendix A.1)

$$\langle 3M, K=2| \sum_i \frac{\hat{L}_i'^2}{4\sin^2(\gamma - \frac{2i\pi}{3})} |3M, K=2\rangle = \sum_i \frac{1}{\sin^2(\gamma - \frac{2i\pi}{3})} = \frac{9}{\sin^2 3\gamma}. \tag{2.71}$$

This particular result has been used to identify the associated Legendre functions $P^1_\lambda(\cos 3\gamma)$ [Arf01] with the $L = 3$ γ-independent wavefunctions [Bès59]. For other spin states, the situation is a little more complicated because of the occurrence of multiple K-states, though (2.71) suggests that the Pöschl-Teller potential can be considered as an average field covering for the rotational part of the Bohr Hamiltonian, which makes the potential physically liable.
Another interesting property of the potential is that the minimum is exactly located at $\gamma = \pi/6$. As already mentioned, the rotational Hamiltonian has an unexpected symmetry at maximal triaxiality. This symmetry is not of a geometrical nature, but comes from the moments of inertia. At $\gamma = \pi/6$, two of the three moments of inertia are equal, leading to a diagonal rotational Hamiltonian if the intrinsic projection axis of the angular momentum is chosen along the $1'$ axis. This was first observed by Meyer-Ter-Vehn [Mey75], and later exploited to find approximative solutions for potentials with a minimum at $\gamma = \pi/6$ [Bon05, For04, For05b]. Also in the present case, it will facilitate an approximative solution of the Hamiltonian.

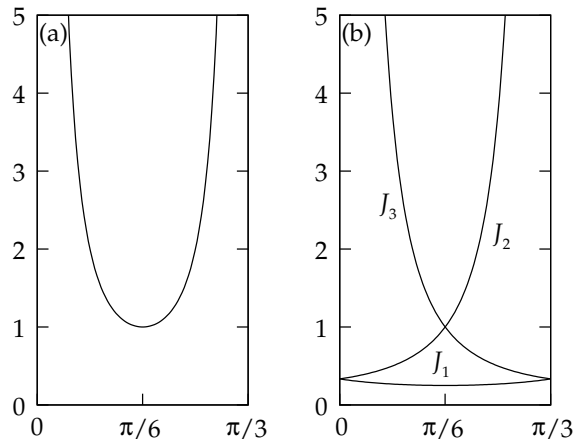

Figure 2.11: The potential (2.70) is depicted at the left side (a) and the inverse soft moments of inertia (2.54) $\mathcal{J}_i$ on the right side (b).

Inserting the potential (2.70) in (2.68) leads to

$$\Big\{ -\frac{1}{\sin 3\gamma}\frac{\partial}{\partial\gamma}\sin 3\gamma\frac{\partial}{\partial\gamma} + \sum_{i=1,2,3}\frac{\hat{L}_i'^2}{4\sin^2(\gamma - 2\pi i/3)} + \frac{\mu}{\sin^2 3\gamma} - \omega\Big\}\psi(\gamma,\theta_\iota) = 0. \tag{2.72}$$

Here the approximation comes into play. As the potential is minimal at $\gamma = \pi/6$, we can apply the freeze-out approximation (see section 2.3.2) and substitute the expectation value of $\gamma = \gamma_0 = \pi/6$ in the expressions of the moments of inertia. The rotational Hamiltonian then reads

$$\hat{H}_{rot} = \sum_{i=1,2,3}\frac{\hat{L}_i'^2}{4\sin^2(\gamma_0 - 2\pi i/3)} = \hat{L}'^2 - \frac{3}{4}\hat{L}_1'^2. \tag{2.73}$$

Therefore, we can further separate the differential equation(2.72) by imposing $\psi(\gamma,\theta_\iota) = \phi(\gamma)\mathcal{D}(\theta_\iota)$, obtaining the following set of differential equations

$$\left\{\frac{1}{\sin 3\gamma}\frac{\partial}{\partial\gamma}\sin 3\gamma\frac{\partial}{\partial\gamma} - \frac{\mu}{\sin^2 3\gamma} + \omega\right\}\phi(\gamma) = \eta\phi(\gamma), \tag{2.74}$$

$$\left\{\hat{L}'^2 - \frac{3}{4}\hat{L}_1'^2\right\}\mathcal{D}(\theta_\iota) = \eta\mathcal{D}(\theta_\iota). \tag{2.75}$$

The eigenvalues of equation (2.75) are easily found since $\hat{L}'^2$ is the quadratic Casimir operator of $O(3)$ and $\hat{L}'_1$ is the projection of the angular momentum on the $1'$-axis, which means that a diagonal representation can be found for both. These are the symmetrised Wigner $\mathcal{D}$-functions, quantised around the $1'$-axis, and are given by[6]

$$\mathcal{D}^L_{MR}(\theta_i) = \sqrt{\frac{2L+1}{16\pi^2(1+\delta_{R0})}}(D^{L*}_{MR} + (-1)^L D^{L*}_{M-R}). \tag{2.76}$$

We call R the eigenvalue of $\hat{L}'_1$ to distinguish it from the band quantum number K, associated with $\hat{L}'_3$, the projection on the $3'$-axis. Thus one obtains

$$\eta = L(L+1) - \frac{3}{4}R^2. \tag{2.77}$$

Equation (2.74) can now be written as (with $x = \cos(3\gamma)$)

$$\left\{\frac{\partial}{\partial x}\left((1-x^2)\frac{\partial}{\partial x}\right) - \frac{\mu'^2}{1-x^2}\right\}\phi(x) = (\eta' - \omega')\phi(x), \tag{2.78}$$

with $\mu' = \sqrt{\mu/9}$, $\eta' = \eta/9$ and $\omega' = \omega/9$. The eigensolutions are obtained in terms of the hypergeometric functions [Arf01]

$$\phi^{\lambda}_{\mu'}(x) \sim (1-x^2)^{\mu'/2}{}_2F_1\left(\mu' - \lambda, \mu' + \lambda + 1; \mu' + 1; \frac{1-x}{2}\right). \tag{2.79}$$

The hypergeometric functions are normalised when $\lambda = \mu' + i$ ($i \in \mathbb{N}$). A discrete eigenspectrum results for

$$\omega = 9\lambda(\lambda+1) + \eta, \tag{2.80}$$

or

$$\omega = 9\lambda(\lambda+1) + L(L+1) - \frac{3}{4}R^2. \tag{2.81}$$

Note that in case $\mu' \in \mathbb{N}$, the hypergeometric functions become the well known Legendre functions.
The main difference between the resulting spectrum (2.81) and a harmonic oscillator treatment [For04] is the specific form of the γ-excitation. Instead of a linear

[6] Note that the Euler angles define a rotation to the intrinsic frame so that the $1'$ axis is the projection axis.

spectrum, we obtain a quadratic spectrum in the quantum number λ. This is due to the typical behaviour of the chosen potential which causes a stronger confinement in comparison to the harmonic well. However, it should be stressed that, although the spectrum of the decoupling constant ω is quadratic, this does not imply that the total spectrum of the Bohr Hamiltonian needs to be quadratic in the quantum numbers, as it depends on the specific form of $u_1(\beta)$ in the Wilets & Jean potential. If we consider a potential of the Davidson type, we notice that ω (and therefore the γ-excitation) varies as a square-root, (2.64) so the total spectrum will rather be linear than quadratic in the quantum number λ [DB06].

Another point of interest is the classification of the lowest even L^+ state (see figure 2.12). Although we can construct a rotational $R = 0$ band on top of the $(L = 0, R = 0)$ state, the members of this band are not the lowest to be found in the spectrum for a fixed spin. Moreover, from eq. (2.81), it is easily seen that $L = R$ holds for the lowest state (which means that the system favours the spin maximally aligned with the 1′-axis). Nevertheless it is not preferable to organise these states as members of the groundband. Constructing the other states into bands results in staggering effects that totally wash out the rotational structure. Moreover, the E2-transitions between two states with equal R are enhanced above transitions between two states that differ in R (see next section). Therefore, a classification into bands according the quantum number R seems preferable.

2.4.2 Electromagnetic transitions

Electromagnetic transitions are an important observable of a model as they are very sensitive to the specific structure of the wavefunctions. The collective geometrical model is in lowest order approximation mainly based on quadrupole deformation. Therefore, the E2 transitions are the most meaningful fingerprints to investigate the wavefunctions. The operator for electric E2 transitions upto lowest order reads [Eis87]

$$\hat{T}(E2)_\mu = \frac{3ZR_0^2}{4\pi}\alpha^*_{2\mu}, \tag{2.82}$$

where

$$\alpha^*_{2\mu} = \beta\left[D^2_{\mu 0}\cos\gamma + \tfrac{1}{\sqrt{2}}\left(D^2_{\mu -2} + D^2_{\mu 2}\right)\sin\gamma\right]. \tag{2.83}$$

The reduced transition probability $B(E2; L_i \to L_f)$ is given by

$$B(E2; L_i \to L_f) = e^2 \sum_{\mu, M_f} |\langle L_f M_f|\hat{T}(E2)_\mu|L_i M_i\rangle|^2. \tag{2.84}$$

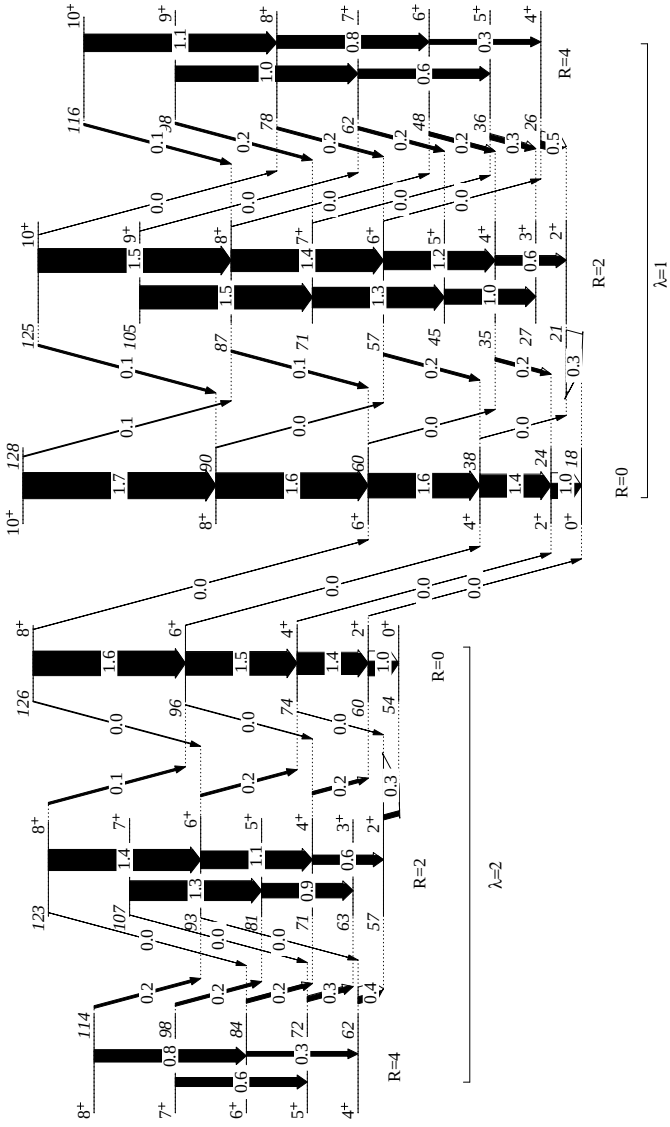

Figure 2.12: Spectrum corresponding to equation (2.81). Only the $R = 0, 2, 4$ band are given for the $\lambda = \lambda_{min} = 1$ (right-handside) and $\lambda = 2$ (left-handside) excitations. The $B(E2)_{rel}$ are given within the arrows and ω is depicted at the levels. All numbers are dimensionless.

Here we need the specific wavefunctions, corresponding to the eigenstates

$$\Psi_{n\lambda\mu' LMR}(\beta,\gamma,\theta_\iota) = \xi_n(\beta)\phi^\lambda_{\mu'}(\cos(3\gamma))\mathcal{D}^L_{MR}(\theta_\iota). \tag{2.85}$$

The function $\xi_n(\beta)$ corresponds with the nth solution of equation (2.18), $\phi^\lambda_{\mu'}(\cos(3\gamma))$ is given by (2.79) and $\mathcal{D}^L_{MR}(\theta_\iota)$, given by (2.76), is the symmetrised eigenfunction of the angular momentum. The $B(E2)$-values are then given by

$$\begin{aligned}
&B(E2; n_i\lambda_i L_i R_i \rightarrow n_f\lambda_f L_f R_f) \\
&\quad = e^2\left(\tfrac{3ZR_0^2}{4\pi}\right)^2 |\langle n_i|\beta|n_f\rangle|^2 \tfrac{2(2L_f+1)}{(16\pi^2)^2} \times |\langle L_f||D^{(2)}||L_i\rangle|^2 \\
&\quad \times \Bigg|\sqrt{2}\begin{pmatrix} L_f & 2 & L_i \\ -R_f & 0 & R_i\end{pmatrix}\langle\lambda_f|\cos\gamma|\lambda_i\rangle \\
&\quad + \sqrt{(1+\delta_{R_i0})(1+\delta_{R_f0})}\begin{pmatrix} L_{R_>} & 2 & L_{R_<} \\ -R_> & 2 & R_<\end{pmatrix}\langle\lambda_f|\sin\gamma|\lambda_i\rangle\Bigg|^2,
\end{aligned} \tag{2.86}$$

where $\xi_n(\beta) \equiv \langle\beta|n\rangle$, and $\phi^\lambda_{\mu'}(\cos(3\gamma)) \equiv \langle\gamma|\lambda\rangle$ (μ' has been omitted as it is equal for all basis states). An effective charge e is inserted and $\langle L_f||D^{(2)}||L_i\rangle$ is the reduced matrix element of the Wigner $D^{(2)}$-functions, with respect to both the projection on the intrinsic as well as the laboratory axis. This reduced matrix element can be deduced using well known formulas from angular momentum theory [Ros57]

$$\langle L_f||D^{(2)}||L_i\rangle = 8\pi^2. \tag{2.87}$$

As an example, the $B(E2)$-values within an $R = 0$ band are given by

$$\begin{aligned}
&B(E2; n\lambda L_i R_i = 0 \rightarrow n\lambda L_f R_f = 0) \\
&= e^2\left(\tfrac{3ZR_0^2}{4\pi}\right)^2 |\langle n|\beta|n\rangle|^2 (2L_f+1)\begin{pmatrix} L_f & 2 & L_i \\ 0 & 0 & 0\end{pmatrix}^2 |\langle\lambda|\cos\gamma|\lambda\rangle|^2.
\end{aligned} \tag{2.88}$$

If we restrict to transitions within bands with equal quantum number n of the β excitation, it is useful to express the $B(E2)$ values relative to

$$\begin{aligned}
&B(E2; n\lambda_{\min}2, 0 \rightarrow n\lambda_{\min}, 0, 0) \\
&= e^2\left(\tfrac{3ZR_0^2}{4\pi}\right)^2 |\langle n|\beta|n\rangle|^2 \tfrac{|\langle\lambda_{min}|\cos\gamma|\lambda_{min}\rangle|^2}{5},
\end{aligned} \tag{2.89}$$

which will be denoted as $B_{\mathrm{rel}}(E2)$. Thus, the relative transitions within one R band become (for the lowest λ excitation)

$$B_{rel}(E2; n\lambda_{min}L_iR \rightarrow n\lambda_{min}L_fR) = 5(2L_f+1)\begin{pmatrix} L_f & 2 & L_i \\ -R & 0 & R \end{pmatrix}^2. \tag{2.90}$$

We can compare these to the E2-transitions between states with different R quantum number (but equal $\lambda = \lambda_{min}$). Because of the symmetry of the $3j$ symbol (2.86), a selection rule prohibits transitions between two states unless $|\Delta R| = 2$. The relative $B(E2)_{rel}$ becomes

$$\begin{aligned} B_{\mathrm{rel}}(E2; n\lambda_{\mathrm{min}}L_iR_i \rightarrow n\lambda_{\mathrm{min}}L_fR_f) &= \frac{5(2L_f+1)}{2}\frac{|\langle\lambda_{\mathrm{min}}|\sin\gamma|\lambda_{\mathrm{min}}\rangle|^2}{|\langle\lambda_{\mathrm{min}}|\cos\gamma|\lambda_{\mathrm{min}}\rangle|^2} \\ &\times (1+\delta_{R_i0})(1+\delta_{R_f0})\begin{pmatrix} L_{R_>} & 2 & L_{R_<} \\ -R_> & 2 & R_< \end{pmatrix}^2. \end{aligned} \tag{2.91}$$

For the relative intraband transitions (2.90), only the rotational structure of the wavefunction is the decisive element, whereas for the relative interband transitions (2.91), the specific γ-dependence of the problem plays a significant role. Unfortunately, the γ-part cannot be manipulated by means of symmetry arguments, and it becomes inevitable to apply a numerical treatment in order to evaluate the matrix elements. Nevertheless, in the specific case of $\mu' \in \mathbb{N}$ (2.78), the solutions of the equations are the Associated Legendre Functions. Through the use of recursion relationships [Arf01] the matrix elements can easily be obtained numerically, as will be shown in the appendix A.3. For the sake of simplicity, we choose $\mu' = 1$ from now on. The matrix elements for $\lambda_{\mathrm{min}} = \mu' = 1$ become $\langle 1|\cos\gamma|1\rangle = 2187/2560$ and $\langle 1|\sin\gamma|1\rangle = 729\sqrt{3}/2560$ with the ratio $1/\sqrt{3}$. By substituting this ratio in equation (2.91), we can compare the relative interband transitions (2.91) with the intraband (2.90) transitions. These results are included in figure 2.12. We notice that the transitions within the $R = 0$ band are much stronger than those between the $L = R$ states. In order to obtain a good band classification, we rely on sequences of aligned E2-transitions, as would be the case from an experimental point of view. Classifying the $R = 0$ band as the groundband is thus justified (see figure 2.12) and other R-bands are constructed in a similar way.

Another point of interest are the relative transitions between different λ-excitation bands. Therefore, one needs the matrix elements $\langle\lambda|\cos\gamma|\lambda'\rangle$ and $\langle\lambda|\sin\gamma|\lambda'\rangle$. These can be calculated using the results derived in appendix A.3. The squared matrix elements $|\langle\lambda_{\mathrm{min}}|\cos\gamma|\lambda\rangle|^2$ relative to $|\langle\lambda_{\mathrm{min}}|\cos\gamma|\lambda_{\mathrm{min}}\rangle|^2$ are depicted in

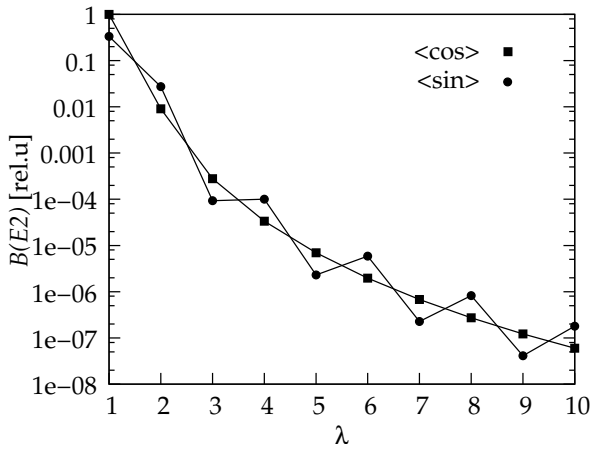

Figure 2.13: Relative squared matrix elements $|\langle 1|\cos\gamma|\lambda\rangle|^2/|\langle 1|\cos\gamma|1\rangle|^2$ (squares) and $|\langle 1|\sin\gamma|\lambda\rangle|^2/|\langle 1|\cos\gamma|1\rangle|^2$ (circles). It is clearly seen that the matrix elements diminish strongly for larger γ excitations. As a consequence, the transitions towards the lowest λ band originating from high λ are very small.

figure 2.13 and point out that the transitions within a fixed γ excitation band are much stronger than the bands which differ in λ quantum number (see also the results in table 2.2).

2.4.3 Justification of the approximation

The best way to justify the approximation is to solve the problem without it, which means: diagonalising the Hamiltonian. An adequate means to study the exact solutions of the problem is to choose an appropriate basis, calculate the matrix elements of the Hamiltonian in this basis, and perform a numerical diagonalisation. Since the decoupling of the β-part from the γ-rotational part is carried out in an exact way, we focus on the γ-rotational part only (2.72). It would have been interesting to make use of the basis of the algebraic tractable model as it is expressed in the language of the intrinsic variables (see section 2.2.1). Unfortunately, $1/\sin^2 3\gamma$ is not a proper seniority tensor. Even worse, it is an infinite sum of polynomials of good seniority tensor character $\cos 3\gamma$, leading to divergencies in the needed matrix elements. So we rather make use of the set of hypergeometric functions with fixed μ' as a basis for the γ-part, because these functions are

$\langle\lambda\vert\cos\gamma\vert\lambda'\rangle$	$\lambda'=1$	$\lambda'=2$	$\lambda'=3$	$\lambda'=4$	$\lambda'=5$
$\lambda=1$	0.854	0.081	-0.014	0.005	-0.002
$\lambda=2$	0.081	0.839	0.092	-0.018	0.007
$\lambda=3$	-0.014	0.092	0.834	0.097	-0.020
$\lambda=4$	0.005	-0.018	0.097	0.832	-0.099
$\lambda=5$	-0.002	0.007	-0.020	0.099	0.893

$\langle\lambda\vert\sin\gamma\vert\lambda'\rangle$	$\lambda'=1$	$\lambda'=2$	$\lambda'=3$	$\lambda'=4$	$\lambda'=5$
$\lambda=1$	0.493	-0.141	-0.008	-0.009	-0.001
$\lambda=2$	-0.141	0.484	-0.160	-0.010	-0.012
$\lambda=3$	-0.008	-0.160	0.481	-0.167	-0.011
$\lambda=4$	-0.009	-0.010	-0.167	0.480	-0.171
$\lambda=4$	-0.001	-0.012	-0.011	-0.171	0.479

Table 2.2: Matrix elements $\langle\lambda\vert\cos\gamma\vert\lambda'\rangle$ and $\langle\lambda\vert\sin\gamma\vert\lambda'\rangle$.

the eigensolutions of a differential equation

$$\Big\{-\frac{1}{\sin 3\gamma}\frac{\partial}{\partial\gamma}\sin 3\gamma\frac{\partial}{\partial\gamma}+\frac{(3\mu')^2}{\sin^2 3\gamma}-\omega\Big\}\phi^{\lambda}_{\mu'}(\cos(3\gamma))=0, \tag{2.92}$$

with $\omega = 9\lambda(\lambda+1)$. For the rotational part, the convenient basis consists of the symmetrised eigenfunctions of the angular momentum (2.76). So, a general solution of (2.72) can be written as

$$\psi_{L_iM}(\gamma,\theta_\iota)=\sum_{\lambda,R}{}^{L_i}c^R_\lambda\phi^{\lambda}_{\mu'}(\cos(3\gamma))\mathcal{D}^L_{MR}(\theta_\iota). \tag{2.93}$$

Calculating the matrix elements of the eigenvalue equation (2.72), one notices that one part of the eigenvalue equation is trivially diagonal (the part corresponding with the term between curly brackets in equation (2.92)), whereas the rotational part is not. Therefore, we still need to perform a numerical integration of the rotational part in the basis of the hypergeometrical functions

$$\begin{aligned}\langle\lambda LMR|\hat{H}_{\rm rot}|\lambda' LMR'\rangle = &\sum_{i=1,2,3}\langle LMR|\hat{L}_i'^2|LMR'\rangle\\ &\int_0^{\pi/3}\frac{\phi^{\lambda}_{\mu'}(\cos(3\gamma))\phi^{\lambda'}_{\mu'}(\cos(3\gamma))}{4\sin^2(\gamma-2\pi i/3)}\sin 3\gamma d\gamma.\end{aligned} \tag{2.94}$$

In order to compare with the analytically obtained solution, we choose $\mu'=1\in\mathbb{N}$. As a consequence, the hypergeometric functions can be recognised as Asso-

ciated Legendre Functions, for which the matrix elements can be derived using appropriate recursion relations (see appendix A.3). Thus, we are in the position to diagonalise the matrix. As a drawback of the model, the Hilbert space of the hypergeometric functions is infinite dimensional. To deal with this problem, we start from a selected number of basis states, corresponding with the lowest quantum numbers, and construct a truncated matrix to diagonalise. Following a standard procedure, we subsequently incorporate an increasing number of basis states with higher quantum numbers until convergence is obtained for the lowest excited states. Here, we require, for a fixed L, convergence up to 10^{-6} for the eigenstates corresponding to the 2 lowest γ-excitations. Once the eigenstates have been determined, $B(E2)$-values can be calculated, relative to the $B(E2; 2^+ \rightarrow 0^+)$ of the ground band. The results of the spectrum and $B(E2)_{rel}$ values are depicted in figure 2.14

One notices an overall good agreement between the analytically obtained spectrum using the approximation discussed before (see figure 2.12) and the full diagonalisation of the problem (see figure 2.14). On the one hand, one clearly recognises the connection between the states depicted in figure 2.14 and the analytically obtained states considering the excitation ω and occurrence in the spectra. On the other hand, there is a strong agreement in the interband and intraband $B(E2)_{rel}$ values resulting from the two calculations, enabling us to classify the states into different bands. This agreement can be understood quite easily by inspecting the specific structure of the wavefunctions (See coefficients in table 2.3), from which we notice that the low-lying states are all dominated by one specific state with quantum numbers (λ, R). Note, however, that we no longer label the bands with quantum numbers.

However, a closer inspection of figure 2.12 and figure 2.14 reveals some differences, e.g. the staggering effect within a band (figure 2.14), associated with the triaxiality of the system, melts away in the approximative solution because the γ-softness of the moments of inertia is not treated exactly. Also, a lowering of the excitation energies can be observed. Applying the approximation, we replace the specific γ-dependent moments of inertia by their expectation value at $\gamma_0 = \pi/6$. As a consequence, they do not longer act as a strongly localising potential at $\gamma_0 = \pi/6$. This delocalises the wavefunctions somewhat and consequently lowers the corresponding excitation energies.

Nonetheless, there still is a good overall good agreement between the analytical solution with approximation and the full diagonalisation of the problem, indicat-

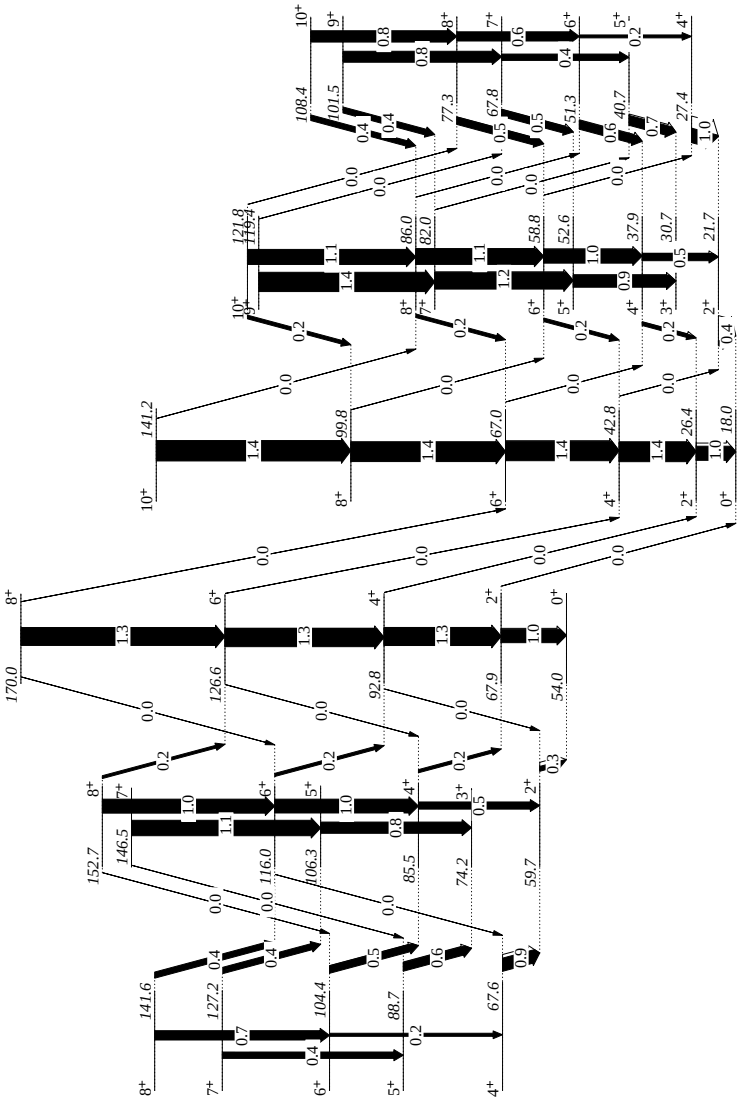

Figure 2.14: Spectrum obtained after diagonalisation. Only those states corresponding to the states given in figure 2.12 are given. The $B(E2)_{rel}$ are denoted by means of the arrows (numbers and relative thickness) and ω is given at each level. All numbers are dimensionless.

L^+	ω	$\lambda=1$			$\lambda=2$		
		$R=0$	$R=2$	$R=4$	$R=0$	$R=2$	$R=4$
0^+	18.0	1.000	.	.	0.000	.	.
	54.0	0.000	.	.	1.000	.	.
2^+	21.7	0.000	0.996	.	0.084	0.000	.
	26.4	-0.992	0.000	.	0.000	-0.112	.
	59.7	0.106	0.000	.	0.000	-0.988	.
	67.9	0.000	0.081	.	-0.984	0.000	.
3^+	30.7	.	0.997	.	.	0.000	.
	74.2	.	0.000	.	.	-0.994	.
4^+	27.4	0.076	0.000	0.991	0.000	0.109	0.000
	37.9	0.000	0.960	0.000	0.209	0.000	0.181
	42.8	-0.961	0.000	0.098	0.000	-0.244	0.000
	67.6	0.000	0.180	0.000	-0.026	0.000	-0.971
	85.5	0.221	0.000	0.079	0.000	-0.896	0.000
	92.8	0.000	-0.165	0.000	0.916	0.000	-0.101

Table 2.3: Coefficients ${}^{L_i}c_\lambda^R$ of the wavefunctions (eq. 2.93) of the low-lying states. Only states up to $L^\pi = 4^+$ depicted in figure 2.14 are given. (higher-spin states can be found in [DB06]

ing that the approximation may be considered as a meaningful choice.

2.4.4 A tentative example

The major drawback of the Pöschl-Teller potential (2.70) is its restriction to structure appearing near $\gamma = \pi/6$. As a consequence, this potential is not applicable to systems with more general triaxiality, as is the case for the triaxial deformed Davidson potential, unless the triaxiality is maximal. However, it appears that such cases do exist. According to the work by Esser [Ess97], a number of the Pt-isotopes can be interpreted as triaxial rigid rotors in the vicinity of maximal triaxiality. The most remarkable isotope is ^{196}Pt, in which the value of γ_b is identically 30°. So it would be interesting to see whether the Pöschl-Teller potential can be applied to this situation. In addition to the Pöschl-Teller potential in γ ($u_2(\gamma)$), a harmonic oscillator $u_1(\beta) = A_D\beta^2$ is chosen in the Wilets & Jean potential. This leads to the energy expression

$$E^{L_i}_{n_\beta \lambda R} = \frac{\hbar^2}{B_2}\sqrt{A_D}(2n_\beta + 1 + \sqrt{\tfrac{9}{4} + \omega^{L_i}}), \tag{2.95}$$

with ω^{L_i} given by equation (2.81). Similar to the discussion in the previous section 2.3.3, the spectrum scales with the ratio $\sqrt{A_D}/B_2$, so we fix this parameter to fit the 2_1^+ state exactly. This leaves only one parameter μ to fit the energy spectrum. One may notice that the parameter B_D of the Davidson potential is not included in the fit. This is due to the particular shape of the Pöschl-Teller potential $u_2(\gamma)$. Contrary to the harmonic oscillator potential in γ, the parameter μ in $u_2(\gamma)$ does not only control the γ softness of the potential, but also the β deformation since it takes over the role of B_D at the minimum ($u_2(\gamma) = \mu$ holds for $\gamma = \pi/6$). The result of the fit is given in figure 2.15

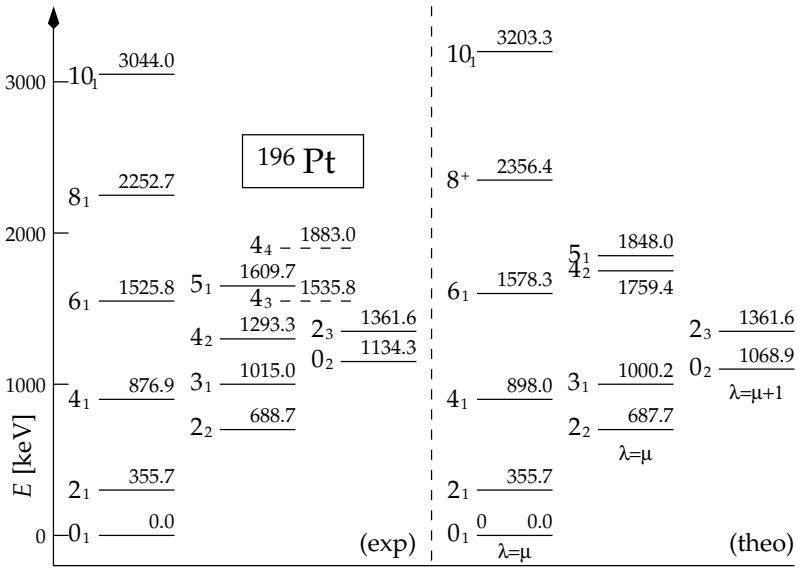

Figure 2.15: Experimental (exp) and theoretical (theo) spectrum of ^{196}Pt. The theoretical calculations are obtained with a Pöschl-Teller type of potential (2.70) with $\mu = 8.07285$. Bands are organised according to the occurrence of the spin in the spectrum. ($L = R$ for the ground band and $\lambda = \mu + 1$ band. The middle band has $R = 4$ for $L = 5$, $R = 2$ for $L = 3, 4$ and $R = 0$ for $L = 2$.

All states are quite well reproduced within 200 keV, with the exception of the $L = 4$ state in the second band. This might be due to the peculiar band structure as already discussed in section 2.4.1. There it was discussed that odd staggering modes arise when constructing the bands according to the occurency of the spins in the spectrum, as is done to meet the experimental level scheme. This is

a theoretical effect, and should not affect the description of the experimentally observed bands. Otherwise, the aberrant behaviour of the $L = 4$ state might be related to excitations outside of the collective quadrupole models space. Indeed, apart from $E2$ quadrupole transitions observed by via Coulomb excitation, considerable B(E4) strengths have been observed, pointing towards an admixture of quadrupole and hexadecupole degrees of freedom [Set91, Chu98], something which was studied in an extensive *sd*-*g* IBM-1 calculation[7] in [Set91]. Moreover, multiple 4^+ states have been found in a small energy region (close to 1500 keV) with considerable admixture of quadrupole and hexadecupole modes (dashed lines in figure 2.15), so it is difficult to single out one of them and associate that state with the $(R = 2)$ 4^+ state of the Pöschl-Teller potential.
Nevertheless, from the general resemblance of the energy spectrum between experiment and theory, we can conclude that the Pöschl-Teller potential stood the test. As a remark, the potential has been fitted to other Pt-isotopes that were found to lie in the vicinity of maximal triaxiality. Although the errors obtained by the different fits change little, it should be noted that ^{196}Pt rendered the best fit. This is not surprising, since it was already considered to be a case of maximal triaxiality [Ess97]. Therefore, only the results of this isotope are presented here.

In conclusion, solvable schematic potentials provide a powerful tool in the global understanding of collective modes of motion. We start from a typical physics case we are aiming to understand. Then we can construct a phenomenological potential, keeping the parametrisation as transparent as possible, keeping in mind that the potential needs to be solvable (up to physically justified approximations). Once the potential is solved, the solutions can be confronted to experimental data in order to grasp the influence of the parameters on the description of the data. In the present chapter, these ideas have been applied to the case of triaxiality. Two different potentials in the spirit of Wilets & Jean have been constructed, solved and compared to the bulk of experimental data. The general conclusion is that, despite the schematic nature of the potential, a good overall agreement of the models with the data is obtained, with physically meaningful parameters as a result. However, if we intend to extend our understanding of triaxial nuclei (e.g. fine tuning the quadrupole matrix elements in Q and B(E2) values), we have to reach beyond schematic models. These observables are very sensitive to the exact structure of the wave functions, so we need to solve more general types of potentials in a non-approximative framework. How to do so will be discussed in the following chapter.

[7] The g-boson is a hexadecupole boson with basis angular momentum $L = 4$ [Cas93].

Algebra is generous: she often gives more than is asked for.

Jean d'Alembert

3

GEOMETRICAL MODEL: A CARTAN'S PERSPECTIVE

ABSTRACT

General potentials are discussed. Starting from a semi-classical argument, a general form of potential is deduced. It is shown how the resulting Hamiltonian can be treated in an $SU(1,1) \times O(5)$ Cartan-Weyl basis. Matrix elements of the collective variables, as well as the canonic conjugate momenta and boson creation- and annihilation operators are obtained, making use of an intermediate state method in the natural basis. Applications in the spirit of shape phase transitions are presented.

Section 3.1 A general potential

3.1.1 A classical point of view

In the previous chapter, solvable schematic potentials have been used to study triaxiality in the chain of Os (and Pt) isotopes within the framework of the collective geometrical model. The parametrisation of these potentials is very transparent, which makes them ideal tools to examine the physics one is interested in. However, there is no underlying (microscopic) reason to justify the choice of the particular *form* of the potential so its validation is always a posteriori. Therefore, if we go beyond type-case studies (such as e.g. triaxiality) by trying to study collectivity in all its facets, we need a *general* type of potential, supported by physics arguments.

The form of this general type of potential can be deduced from a semi-classical argument. Starting from the nucleon wavefunctions, giving rise to a finite density $\rho(\vec{r})$, one can make the interaction between the particles also density dependent. As a result, the interaction density between two infinitesimal pieces of nuclear matter can be written as (see figure 3.1)

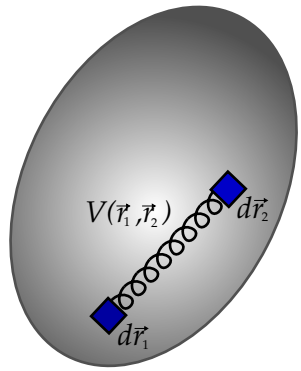

Figure 3.1: Classical construction of the collective potential $V(\alpha)$

$$\rho(\vec{r}_1)V_{\text{int}}(\vec{r}_1,\vec{r}_2)\rho(\vec{r}_2)d\vec{r}_1 d\vec{r}_2. \tag{3.1}$$

As a consequence, the total interaction energy of the atomic nucleus is given by

$$V_{\text{tot}} = \int d\vec{r}_1 \int d\vec{r}_2 \rho(\vec{r}_1)V_{\text{int}}(\vec{r}_1,\vec{r}_2)\rho(\vec{r}_2). \tag{3.2}$$

At this point, we can make use of the geometry of the problem. The collective model assumes that the atomic nucleus exhibits a homogeneous density with a sharp surface, described by the formula (2.2). The total interaction then becomes (in spherical coordinates)

$$V(\alpha) = \rho^2 \int_{r_1=0}^{R(\theta_1,\phi_1)} r_1^2 dr_1 d\Omega_1 \int_{r_2=0}^{R(\theta_2,\phi_2)} r_2^2 dr_2 d\Omega_2 V_{\text{int}}(\vec{r}_1,\vec{r}_2), \tag{3.3}$$

It is noteworthy that V_{tot} has become a function of the collective variables α. Thus, the cumulative interaction energy of the atomic nucleus not only depends on the microscopic interaction V_{int}, but also on the specific shape of the nucleus $R(\theta,\phi)$, which means that we can label $V_{\text{tot}}(\alpha)$ as a collective potential energy. The main ingredient in (3.3) is the interaction $V_{\text{int}}(\vec{r}_1,\vec{r}_2)$, which has typically a short-ranged

attractive nature, such as e.g. the Yukawa potential. Unfortunately, extracting an (analytic) expression for the collective potential $V(\alpha)$ from the Yukawa potential is extremely involved and goes beyond the scope of this introduction [Kra79, Jön96]. For this purpose we revert to a harmonic oscillator potential which is also an attractive interaction, although in a much more schematic way

$$V_{\text{int}}(\vec{r}_1, \vec{r}_2) = k|\vec{r}_1 - \vec{r}_2|^2 = k(r_1^2 + r_2^2 - 2r_1 r_2 \cos\theta_{12}), \tag{3.4}$$

with $\cos\theta_{12}$ the angle between the vectors $\vec{r}_1$ and $\vec{r}_2$. Substituting this interaction in equation (3.3) gives

$$\begin{aligned} V(\alpha) =& k\rho^2 \left[\int d\Omega_1 \int_0^{R_1} dr_1 r_1^4\right] \left[\int d\Omega_2 \int_0^{R_2} dr_2 r_2^2\right] \\ &+ k\rho^2 \left[\int d\Omega_1 \int_0^{R_1} dr_1 r_1^2\right] \left[\int d\Omega_2 \int_0^{R_2} dr_2 r_2^4\right] \\ &- k\rho^2 \int d\Omega_1 \int d\Omega_2 P_1(\cos\theta_{12}) \int_0^{R_1} dr_1 r_1^3 \int_0^{R_2} dr_2 r_2^3, \end{aligned} \tag{3.5}$$

with R_i the shorthand notation for $R(\theta_i, \phi_i)$ and $P_1(\cos\theta_{12})$ the rank 1 Legendre polynomial. Calculating the radial integrals, substituting the expression for the radius $R(\theta, \phi)$ and making use of the addition theorem and angular momentum theory [Ros57] in order to evaluate the integrals of polynomials of the spherical harmonics, we obtain the following expression for $V(\alpha)$ upto 4^{th} order in α

$$\begin{aligned} V(\alpha) = V_0[&(4\pi)^2 + 52\pi(\alpha\cdot\alpha) - 26\sqrt{\tfrac{10\pi}{7}}(\alpha\cdot[\alpha\alpha]^{(2)}) \\ &+ \tfrac{285}{7}(\alpha\cdot\alpha)^2 + \mathcal{O}(\alpha^5)], \end{aligned} \tag{3.6}$$

with $V_0 = 2kR_0^8/15$. This potential is a multipole decomposition where all terms are angular momentum scalars. In principle, this potential is a polynomial in α up to 8^{th} order, but since the deviations from the spherical shape (R_0) are small, we can neglect the higher-order terms. There are some more remarkable features. The potential (3.6) has a distinct spherical minimum, which is not surprising since we have started from an attractive interaction. Because of the presence of the $\alpha\cdot[\alpha\alpha]^{(2)}$, there is a small tendency towards oblate excitations. This is due to the attractive interaction, favouring a minimisation of the volume of the ellipsoid[1]. The only unphysical property of the harmonic oscillator, regarding the nucleon-nucleon interaction, is the range. Contrary to the Yukawa potential, the harmonic oscillator does not exhibit a short range interaction. However, it has been found

[1] Which is remarkable as more prolate than oblate nuclei are observed in experimental data.

that the typical range of the Yukawa potential (1.4fm) is still too large to successfully describe heavy-ion elastic scattering data within this framework, so one needed to modify the Yukawa potential for this purpose [Kra79, Jön96]. However, heavy-ion reactions require higher multipole order components of the surface than only the quadrupole deformations. For low-energy nuclear structure phenomena, we can limit the model to the quadrupole degrees of freedom α^2, which are small quantities by definition. As a consequence, every potential (3.3) can be written as a multipole expansion in the collective variables (e.g. expression (3.6)), with only the coefficients dependent of the interaction V_{int}. We obtain

$$\begin{aligned} V(\alpha) &= c_2(\alpha\cdot\alpha) + c_3(\alpha\cdot[\alpha\alpha]^{(2)}) + c_4(\alpha\cdot\alpha)^2 \\ &\quad + c_5(\alpha\cdot\alpha)(\alpha\cdot[\alpha\alpha]^{(2)}) + c_6(\alpha\cdot\alpha)^3 + d_6(\alpha\cdot[\alpha\alpha]^{(2)})^2 + \dots \end{aligned} \tag{3.7}$$

3.1.2 Dealing with the general potential

This potential (3.7) was the starting point for the General Collective Model (GCM) of the Frankfurt group [Gne71, Eis87]. Invoking higher-order terms, an extension of the standard Bohr kinetic energy term was proposed

$$\hat{T}_{GCM} = \tfrac{1}{2B_2}\hat{\pi}\cdot\hat{\pi} + B_3[\hat{\pi}\alpha]^{(2)}\cdot\hat{\pi} + \dots. \tag{3.8}$$

The physical motivation for this extension is that the higher-order multipoles in the kinetic energy can correct for the irrotational assumption on the nature of the mass parameter B_2 (see chapter 2.3.3 and [Flü41, Eis87]). The total GCM Hamiltonian contains a significant number of free parameters to fit to the experimental data. These parameters can be obtained from a microscopic theory [Kum74], though it is more pragmatic to directly fit them to the data. In this respect, Caprio [Cap03] introduced a more tractable version of the GCM, where only the standard Bohr kinetic energy term and potential energy terms up to order 4 are included. The Hamiltonian then reduces to

$$\hat{H} = \tfrac{1}{2B_2}\hat{\pi}\cdot\hat{\pi} + c_2(\alpha\cdot\alpha) + c_3(\alpha\cdot[\alpha\alpha]^{(2)}) + c_4(\alpha\cdot\alpha)^2. \tag{3.9}$$

Although this Hamiltonian is a simplified version with respect to the total GCM Hamiltonian, still it is able to account for most of the basic physics in the collective model, such as the harmonic oscillator, axial- and γ-soft rotational structures. This point can be clarified by transforming to the intrinsic representations of the collective model. The potential then becomes

$$V(\beta,\gamma) = c_2\beta^2 - \sqrt{\tfrac{2}{7}}c_3\beta^3\cos 3\gamma + c_4\beta^4. \tag{3.10}$$

This potential exhibits a spherical minimum whenever $(9c_3^2 - 112c_2c_4) \leq 0$ and a deformed minimum otherwise. In the latter case, an oblate minimum is found for $c_3 < 0$ and a prolate minimum for $c_3 > 0$. These two regions are clearly separated by $c_3 = 0$, corresponding to a γ-independent potential. In all cases, it is assumed that $c_4 > 0$ to ensure the localisation of the wavefunction. Thus, we learn that the potential (3.10) can reproduce the basis structures of the collective model, which is already sufficient for certain atomic nuclei such as e.g. ^{102}Pd [Cap03]. However, if we intend to include more complex structures such as triaxiality or shape coexistence, we definitely have to incorporate higher order terms (up to order 6).

Once the potential (3.7) is chosen, we need a powerful tool to solve the above Hamiltonian. One can start from a harmonic oscillator basis to construct the matrix representation of the Hamiltonian. As already discussed in chapter 2.2.2, the 5D harmonic oscillator is a γ-independent model and many techniques have been proposed in the literature to construct the γ-independent basis wavefunctions. Apart from those techniques, one particular method is worth mentioning as it starts from the Cartan-Weyl [Car94, Wyb74, Iac06] reduction scheme of the covering $SU(1,1) \times O(5)$ group. This strategy was followed by Hecht [Hec65] to construct fractional parentage coefficients for spin-2 phonons, that were subsequently used by the Frankfurt group in order to obtain the necessary matrix elements in the development of the GCM.

In the next section, the path of the natural Cartan-Weyl reduction is followed. It will be shown that the matrix elements of the quadrupole variable can be extracted within this basis, without making use of the explicit representations in terms of the collective variables [DB07]. In the end, it will turn out that the basic commutation relations of the collective variables suffice to fix the complete structure of the algebra, and furthermore the dynamics of the Hamiltonian.

Section 3.2 — Collective variables in the Cartan basis

3.2.1 The $SU(1,1) \times O(5)$ group structure

We start from the standard commutation relations[2]

$$[\pi_{\mu'}, \alpha_\mu] = -i\hbar\delta_{\mu\mu'}, \qquad [\pi_{\mu'}, \pi_\mu] = 0, \qquad [\alpha_{\mu'}, \alpha_\mu] = 0. \tag{3.11}$$

[2]Note that the variables have become operators, though we silently omit the operator symbol to avoid overload in the notation.

To establish the $SU(1,1) \times O(5)$ group structure, it is convenient to introduce the following recoupling formula

$$\begin{aligned}(\alpha \cdot \alpha)(\pi^* \cdot \pi^*) =& (\alpha \cdot \pi^*)(\alpha \cdot \pi^*) + 3i\hbar(\alpha \cdot \pi^*) \\ & - 2([\alpha\pi^*]^{(1)} \cdot [\alpha\pi^*]^{(1)} + [\alpha\pi^*]^{(3)} \cdot [\alpha\pi^*]^{(3)}),\end{aligned} \tag{3.12}$$

where the complex conjugate π^* is introduced to ensure for good angular momentum transformation properties. The 3 operators $(\alpha \cdot \alpha)$, $(\pi^* \cdot \pi^*)$ and $(\alpha \cdot \pi^*)$ generate the algebra of an $SU(1,1)$ group, which forms a direct product together with the $O(5)$ group, built from the 10 operators $[\alpha\pi^*]^{(1)}_M$ and $[\alpha\pi^*]^{(3)}_M$.
Both groups have a distinct physical interpretation in the intrinsic frame; $SU(1,1)$ is strongly linked with the excitations in the radial variable β, whereas $O(5)$ encompasses the γ-rotational excitations. Expressing the $SU(1,1)$ generators in terms of the intrinsic variables, we obtain the realisation[3] (2.34), with the only difference that the quadratic Casimir of $O(5)$ has been replaced by its eigenvalue $v(v+3)$. Comparison of the generator B_0, the recoupling formula (3.12) and equations (2.18 & 2.19) shows that the γ-rotational coupling coefficient $\omega = v(v+3)$ can be associated with the Casimir operator of $O(5)$. Therefore, we can associate $O(5)$ to the group encompassing the γ vibrations coupled to the rotational structure.

In a first part, we concentrate on the application of the Cartan-Weyl scheme on the $O(5)$ group, leaving a freedom of choice for a suitable $SU(1,1)$ basis, since there is an ambiguity involved whether the intrinsic or lab-frame realisation of the collective variables is used.

3.2.2 The Cartan-Weyl reduction of $O(5)$

The commutation relations of the operators L_M and O_M, defined by

$$[\alpha\pi^*]^{(1)}_M = \tfrac{i\hbar}{\sqrt{10}} L_M, \qquad [\alpha\pi^*]^{(3)}_M = \tfrac{i\hbar}{\sqrt{10}} O_M, \tag{3.13}$$

span the algebra of the $O(5)$ group

$$[L_m, L_{m'}] = -\sqrt{2}\langle 1m1m'|1m+m'\rangle L_{m+m'}, \tag{3.14}$$

$$[L_m, O_{m'}] = -2\sqrt{3}\langle 1m3m'|3m+m'\rangle O_{m+m'}, \tag{3.15}$$

$$\begin{aligned}[O_m, O_{m'}] = & -2\sqrt{7}\langle 3m3m'|1m+m'\rangle L_{m+m'} \\ & + \sqrt{6}\langle 3m3m'|3m+m'\rangle O_{m+m'}.\end{aligned} \tag{3.16}$$

[3] (up to a rotation)

The $M = 0$ projections $\{L_0, O_0\}$ form an intuitive choice of the Cartan subalgebra within the set $\{L_m, O_{m'}\}$. This set has the advantage of incorporating the angular momentum projection operator L_0 in the physical group reduction chain $O(5) \supset O(3) \supset O(2)$. Nevertheless, it is not explicitly contained in the natural Cartan-Weyl reduction chain $O(5) \supset O(4) \cong SU(2) \times SU(2)$ which can be realised through the following rotation [Cor76, Row94b]:

$$\begin{array}{ll} X_+ = -\frac{1}{5}(\sqrt{2}L_{+1} + \sqrt{3}O_{+1}), & Y_+ = -\frac{1}{\sqrt{5}}O_{+3}, \\ X_- = \frac{1}{5}(\sqrt{2}L_{-1} + \sqrt{3}O_{-1}), & Y_- = \frac{1}{\sqrt{5}}O_{-3}, \\ X_0 = \frac{1}{10}(L_0 + 3O_0), & Y_0 = \frac{1}{10}(3L_0 - O_0), \\ T_{-\frac{1}{2}\frac{1}{2}} = -\frac{1}{\sqrt{50}}(\sqrt{3}L_{+1} - \sqrt{2}O_{+1}), & T_{\frac{1}{2}\frac{1}{2}} = \frac{1}{\sqrt{10}}O_{+2}, \\ T_{\frac{1}{2}-\frac{1}{2}} = \frac{1}{\sqrt{50}}(\sqrt{3}L_{-1} - \sqrt{2}O_{-1}), & T_{-\frac{1}{2}-\frac{1}{2}} = -\frac{1}{\sqrt{10}}O_{-2}. \end{array} \tag{3.17}$$

The group reduction is immediately clear, as the sets $\{X_0, X_\pm\}$ and $\{Y_0, Y_\pm\}$ both span standard $SU(2)$ algebras. Furthermore all generators of the one $SU(2)$ algebra commute with all generators of the other. The commutation relations are given by

$$\begin{array}{ll} [X_0, X_\pm] = \pm X_\pm, & [X_+, X_-] = 2X_0, \\ [Y_0, Y_\pm] = \pm Y_\pm, & [Y_+, Y_-] = 2Y_0, \\ [X_0, Y_0] = 0, & [X_\pm, Y_\pm] = [X_\pm, Y_\mp] = 0. \end{array} \tag{3.18}$$

So the reduction is $O(5) \supset O(4) \cong SU(2)_X \times SU(2)_Y$. The non-$O(4)$ operators $T_{\mu\nu}$ can be identified as the 4 components of a bitensor of character $\{\frac{1}{2}, \frac{1}{2}\}$ within the $SU(2) \times SU(2)$ scheme, according to Racah's definition [Rac42]. The index μ denotes the bitensor component relative to the $SU(2)_X$ group, while ν is the component with respect to $SU(2)_Y$

$$[X_0, T_{\mu\nu}] = \mu T_{\mu\nu}, \tag{3.19}$$

$$[X_\pm, T_{\mu\nu}] = \sqrt{(\tfrac{1}{2} \mp \mu)(\tfrac{1}{2} \pm \mu + 1)}\, T_{\mu\pm1\nu}, \tag{3.20}$$

$$[Y_0, T_{\mu\nu}] = \nu T_{\mu\nu}, \tag{3.21}$$

$$[Y_\pm, T_{\mu\nu}] = \sqrt{(\tfrac{1}{2} \mp \nu)(\tfrac{1}{2} \pm \nu + 1)}\, T_{\mu\nu\pm1}. \tag{3.22}$$

The internal commutation relations of the T bitensor completes the Cartan-Weyl structure, which can be found in table (3.1).

Once the commutation relations have been determined within the Cartan-Weyl basis, it is instructive to construct the root diagram. Figure 3.2 shows 2 different realisations of the same root diagram, depending on the choice of the Cartan

$*$	$T_{-\frac{1}{2}-\frac{1}{2}}$	$T_{\frac{1}{2}-\frac{1}{2}}$	$T_{-\frac{1}{2}\frac{1}{2}}$	$T_{\frac{1}{2}\frac{1}{2}}$
$T_{-\frac{1}{2}-\frac{1}{2}}$	0	$\frac{1}{2}Y_-$	$\frac{1}{2}X_-$	$\frac{1}{2}(X_0+Y_0)$
$T_{\frac{1}{2}-\frac{1}{2}}$	$-\frac{1}{2}Y_-$	0	$\frac{1}{2}(X_0-Y_0)$	$-\frac{1}{2}X_+$
$T_{-\frac{1}{2}\frac{1}{2}}$	$-\frac{1}{2}X_-$	$-\frac{1}{2}(X_0-Y_0)$	0	$-\frac{1}{2}Y_+$
$T_{\frac{1}{2}\frac{1}{2}}$	$-\frac{1}{2}(X_0+Y_0)$	$\frac{1}{2}X_+$	$\frac{1}{2}Y_+$	0

Table 3.1: Multiplication table for the internal commutation relations of the T bitensor. The multiplication $*$ symbolises the standard commutation.

subalgebra. On the left side (Fig. 3.2(a)) a standard root diagram with respect to the $\{X_0, Y_0\}$ Cartan subalgebra is depicted, while on the right side (Fig. 3.2(b)), a more physical subalgebra $\{L_0, O_0\}$ is chosen as a reference frame. The latter framework has a visual advantage, since the projection of the generators on the L_0-axis is readily established. This enhances the insight in the problem of constructing wavefunctions with good angular momentum from the weight diagrams in the Cartan-Weyl basis (see section 3.3).

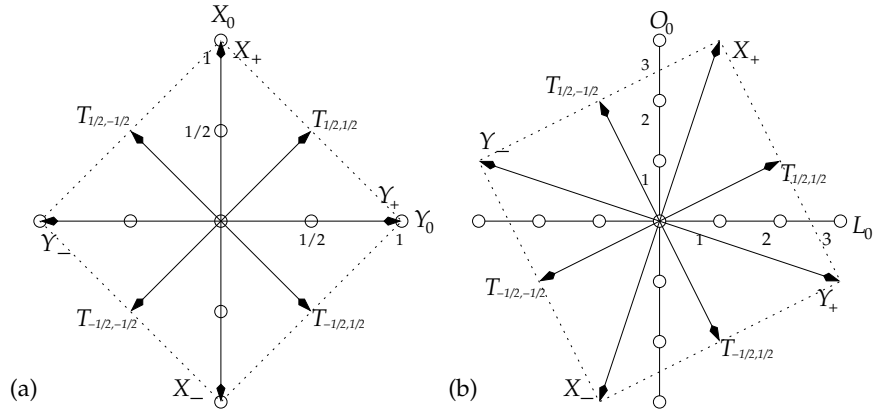

Figure 3.2: The root diagrams of the $O(5)$ algebra in the Cartan-Weyl basis for either the (a) natural $\{X_0, Y_0\}$ or (b) physical $\{L_0, O_0\}$ Cartan subalgebra.

3.2.3 Representations of $O(5)$

Every subgroup in the group reduction chain provides an associated Casimir operator. The quadratic Casimir operator of $O(5)$ can be constructed from the

Killing form [Wyb74]

$$\mathcal{C}_2[O(5)] = \tfrac{1}{5}(L \cdot L + O \cdot O), \tag{3.23}$$
$$= 2(X^2 + Y^2 - 2[TT]^{(00)}). \tag{3.24}$$

with $[TT]^{(00)}$ denoting the scalar Clebsch Gordan coupling with respect to both $SU(2)_X$ and $SU(2)_Y$, and X^2 and Y^2 the quadratic Casimir operator of the respective $SU(2)$ groups

$$X^2 = X_0^2 + \tfrac{1}{2}(X_+X_- + X_-X_+), \tag{3.25}$$
$$Y^2 = Y_0^2 + \tfrac{1}{2}(Y_+Y_- + Y_-Y_+). \tag{3.26}$$

Starting from the explicit expressions of the generators (see appendix B.1) in terms of the collective variables and the canonic conjugate momenta, the following operator identity can be proven

$$X^2 - Y^2 \equiv 0, \tag{3.27}$$

which is true in general for symmetric representations [Cor76]. The consequence of this identity is that we are left with 4 operators that commute among each others, i.e. the quadratic Casimir operator of $O(5)$, the quadratic Casimir operator of $SU(2)_X$ and $SU(2)_Y$ ($X^2 \equiv Y^2$) and the Cartan subalgebra $\{X_0, Y_0\}$ which are the respective linear Casimir operators of the $O(2)_X$ and $O(2)_Y$ subgroups. As a result, we obtain a representation which is determined by 4 independent quantum numbers

$$|vXM_XM_Y\rangle, \tag{3.28}$$

with

$$\mathcal{C}_2[O(5)]|vXM_XM_Y\rangle = v(v+3)|vXM_XM_Y\rangle, \tag{3.29}$$
$$X^2|vXM_XM_Y\rangle = Y^2|vXM_XM_Y\rangle = X(X+1)|vXM_XM_Y\rangle, \tag{3.30}$$
$$X_0|vXM_XM_Y\rangle = M_X|vXM_XM_Y\rangle, \tag{3.31}$$
$$Y_0|vXM_XM_Y\rangle = M_Y|vXM_XM_Y\rangle. \tag{3.32}$$

Now that the basis to work in is fixed, we can study the action of the generators as they hop through the representations with fixed quantum number v. Acting with the $O(4) \cong SU(2)_X \times SU(2)_Y$ generators on $|vXM_XM_Y\rangle$ is trivial because

of the well-known angular momentum theory

$$X_{\pm}|vXM_XM_Y\rangle = \sqrt{(X \mp M_X)(X \pm M_X + 1)}|vXM_X \pm 1, M_Y\rangle, \tag{3.33}$$

$$X_0|vXM_XM_Y\rangle = M_X|vXM_XM_Y\rangle, \tag{3.34}$$

$$Y_{\pm}|vXM_XM_Y\rangle = \sqrt{(X \mp M_Y)(X \pm M_Y + 1)}|vXM_X, M_Y \pm 1\rangle, \tag{3.35}$$

$$Y_0|vXM_XM_Y\rangle = M_Y|vXM_XM_Y\rangle. \tag{3.36}$$

The action of $T_{\mu\nu}$ on $|vXM_XM_Y\rangle$ is less trivial, though the bitensorial character of T can be well exploited. Since T is a $\{\frac{1}{2}\,\frac{1}{2}\}$ bitensor, it can only connect representations that differ $\frac{1}{2}$ in quantum number X

$$\begin{aligned} T_{\mu\nu}|vXM_XM_Y\rangle = a|v, X + \tfrac{1}{2}, M_X + \mu, M_Y + \nu\rangle \\ + b|v, X - \tfrac{1}{2}, M_X + \mu, M_Y + \nu\rangle. \end{aligned} \tag{3.37}$$

The coefficients a and b are not only dependent on v and X, but also on the projection quantum numbers μ, ν, M_X and M_Y. However, these projections can be filtered out by means of the Wigner-Eckart theorem. As the $SU(2)_X$ forms a direct product with $SU(2)_Y$, we can apply the theorem for both groups, independently from each other. As a result, the dependency on the projection quantum numbers is completely factored out in the Wigner-3j symbols. This leaves a double reduced matrix element [4] to be calculated:

$$\begin{aligned} a &= \langle v, X + \tfrac{1}{2}, M_X + \mu, M_Y + \nu|T_{\mu\nu}|vXM_XM_Y\rangle \\ &= (-)^k \begin{pmatrix} X + \frac{1}{2} & \frac{1}{2} & X \\ -M_X - \mu & \mu & M_X \end{pmatrix} \begin{pmatrix} X + \frac{1}{2} & \frac{1}{2} & X \\ -M_Y - \nu & \nu & M_Y \end{pmatrix} \\ &\quad \times \langle vX + \tfrac{1}{2}||T||vX\rangle, \end{aligned} \tag{3.38}$$

$$\begin{aligned} b &= \langle v, X - \tfrac{1}{2}, M_X + \mu, M_Y + \nu|T_{\mu\nu}|vXM_XM_Y\rangle \\ &= (-)^k \begin{pmatrix} X - \frac{1}{2} & \frac{1}{2} & X \\ -M_X - \mu & \mu & M_X \end{pmatrix} \begin{pmatrix} X - \frac{1}{2} & \frac{1}{2} & X \\ -M_Y - \nu & \nu & M_Y \end{pmatrix} \\ &\quad \times \langle vX - \tfrac{1}{2}||T||vX\rangle, \end{aligned} \tag{3.39}$$

with $k = 2X + 1 - M_X - M_Y - \mu - \nu$.
In order to calculate the double reduced matrix element, we have 2 types of expressions at hand. On the one hand the internal commutation relations of the

[4] In this section, we formally use the single reduced matrix notation in order to express the double reduced matrix, as any confusion between normal and double reduced matrix element is excluded within this section.

T bitensor (see table 3.1) and on the other hand the Casimir operator of $O(5)$ (3.24). First we consider the internal commutation relations, in which case it is instructive to proceed by means of an example although the obtained result is generally valid. Take e.g. the commutation relation $[T_{-\frac{1}{2}-\frac{1}{2}}, T_{\frac{1}{2}\frac{1}{2}}] = \frac{1}{2}(X_0 + Y_0)$, and sandwich it with the state $|vXM_XM_Y\rangle$

$$\begin{aligned}\langle vXM_XM_Y|T_{-\frac{1}{2}-\frac{1}{2}}T_{\frac{1}{2}\frac{1}{2}}|vXM_XM_Y\rangle - \langle vXM_XM_Y|T_{\frac{1}{2}\frac{1}{2}}T_{-\frac{1}{2}-\frac{1}{2}}|vXM_XM_Y\rangle \\ = \tfrac{1}{2}(M_X + M_Y).\end{aligned} \tag{3.40}$$

At this point, we can insert a complete set of intermediate states $|v'X'M'_XM'_Y\rangle$ between the two generators.

$$\begin{aligned}&\sum_{v'X'M'_XM'_Y} \langle vXM_XM_Y|T_{-\frac{1}{2}-\frac{1}{2}}|v'X'M'_XM'_Y\rangle\langle v'X'M'_XM'_Y|T_{\frac{1}{2}\frac{1}{2}}|vXM_XM_Y\rangle \\ &- \sum_{v'X'M'_XM'_Y} \langle vXM_XM_Y|T_{\frac{1}{2}\frac{1}{2}}|v'X'M'_XM'_Y\rangle\langle v'X'M'_XM'_Y|T_{-\frac{1}{2}-\frac{1}{2}}|vXM_XM_Y\rangle \\ &= \tfrac{1}{2}(M_X + M_Y).\end{aligned} \tag{3.41}$$

Due to symmetry considerations, a large amount of the matrix elements in the summation are identically zero. First of all the $SU(2)_X \times SU(2)_Y$ bitensor character of T dictates strict selection rules with respect to X, M_X and M_Y. As a result the summation over X', M'_X and M'_X is restricted to specific values which are completely governed by the Wigner-3j symbol in (3.38,3.39). Secondly, the components $T_{\mu\nu}$ of T are $O(5)$ generators, which cannot alter the seniority quantum number v. So, the summation over v' is reduced to one seniority $v' = v$.
Once the restriction in the summation is carried out, it is convenient to apply the Wigner-Eckart theorem (3.38,3.39) and after some tedious algebra we obtain a relationship for the double reduced matrix elements

$$\begin{aligned}&\frac{\langle vX||T||vX+\frac{1}{2}\rangle\langle vX+\frac{1}{2}||T||vX\rangle}{2X+2} - \frac{\langle vX||T||vX-\frac{1}{2}\rangle\langle vX-\frac{1}{2}||T||vX\rangle}{2X} \\ &= \frac{(2X+1)^2}{2}.\end{aligned} \tag{3.42}$$

The same procedure can be followed for the quadratic Casimir of $O(5)$. Sandwiching equation (3.24) with $|vXM_XM_Y\rangle$ yields

$$\begin{aligned}\langle vXM_XM_Y|(T_{-\frac{1}{2}\frac{1}{2}}T_{\frac{1}{2}-\frac{1}{2}} + T_{\frac{1}{2}-\frac{1}{2}}T_{-\frac{1}{2}\frac{1}{2}} - T_{-\frac{1}{2}-\frac{1}{2}}T_{\frac{1}{2}\frac{1}{2}} - T_{\frac{1}{2}\frac{1}{2}}T_{-\frac{1}{2}-\frac{1}{2}})|vXM_XM_Y\rangle \\ = v(v+3) - 4X(X+1).\end{aligned} \tag{3.43}$$

By inserting again a complete set, applying the Wigner-Eckart theorem and making use of the previously derived relation (3.42), we obtain the result

$$\begin{aligned} &-4\langle vX||T||vX+\tfrac{1}{2}\rangle\langle vX+\tfrac{1}{2}||T||vX\rangle \\ &\quad = (v-2X)(v+2X+3)(2X+1)(2X+2). \end{aligned} \tag{3.44}$$

This can slightly be rewritten, if one takes the Hermitian conjugate of the T bitensor into consideration.

$$T^{\dagger}_{\mu\nu} = (-1)^{\mu+\nu} T_{-\mu-\nu}. \tag{3.45}$$

It can be proven that this leads towards the following expression for the double reduced matrix elements

$$\langle v, X||T||v, X+\tfrac{1}{2}\rangle^{*} = -\langle v, X+\tfrac{1}{2}||T||v, X\rangle. \tag{3.46}$$

As a result, we can write

$$|\langle vX||T||vX+\tfrac{1}{2}\rangle|^2 = \tfrac{1}{4}(v-2X)(v+2X+3)(2X+1)(2X+2), \tag{3.47}$$

$$|\langle vX||T||vX-\tfrac{1}{2}\rangle|^2 = \tfrac{1}{4}(v-2X+1)(v+2X+2)(2X)(2X+1). \tag{3.48}$$

So the double reduced matrix elements are determined up to a phase. Here we fix the relative sign of $\langle vX||T||vX+\frac{1}{2}\rangle$ and $\langle vX||T||vX-\frac{1}{2}\rangle$ to be opposite, as it is the only way to obtain eigenstates with real angular momentum L in the physical basis (see section (3.3)).

Once that the double reduced matrix elements are determined, they can be plugged into equations (3.38,3.39), yielding the action of the bitensor T components.

$$\begin{aligned} &T_{\frac{1}{2}\frac{1}{2}}|vXM_XM_Y\rangle \\ &\quad = \frac{\sqrt{(X+M_X+1)(X+M_Y+1)(v-2X)(v+2X+3)}}{2\sqrt{(2X+1)(2X+2)}}|vX+\tfrac{1}{2}, M_X+\tfrac{1}{2}, M_Y+\tfrac{1}{2}\rangle \\ &\quad - \frac{\sqrt{(X-M_X)(X-M_Y)(v-2X+1)(v+2X+2)}}{2\sqrt{(2X)(2X+1)}}|vX-\tfrac{1}{2}, M_X+\tfrac{1}{2}, M_Y+\tfrac{1}{2}\rangle, \end{aligned} \tag{3.49}$$

$$\begin{aligned} &T_{\frac{1}{2}-\frac{1}{2}}|vXM_XM_Y\rangle \\ &\quad = \frac{\sqrt{(X+M_X+1)(X-M_Y+1)(v-2X)(v+2X+3)}}{2\sqrt{(2X+1)(2X+2)}}|vX+\tfrac{1}{2}, M_X+\tfrac{1}{2}, M_Y-\tfrac{1}{2}\rangle \\ &\quad + \frac{\sqrt{(X-M_X)(X+M_Y)(v-2X+1)(v+2X+2)}}{2\sqrt{(2X)(2X+1)}}|vX-\tfrac{1}{2}, M_X+\tfrac{1}{2}, M_Y-\tfrac{1}{2}\rangle, \end{aligned} \tag{3.50}$$

$$
\begin{aligned}
&T_{-\frac{1}{2}\frac{1}{2}}|vXM_XM_Y\rangle \\
&\quad= \frac{\sqrt{(X-M_X+1)(X+M_Y+1)(v-2X)(v+2X+3)}}{2\sqrt{(2X+1)(2X+2)}}|vX+\tfrac{1}{2},M_X-\tfrac{1}{2},M_Y+\tfrac{1}{2}\rangle \\
&\quad+ \frac{\sqrt{(X+M_X)(X-M_Y)(v-2X+1)(v+2X+2)}}{2\sqrt{(2X)(2X+1)}}|vX-\tfrac{1}{2},M_X-\tfrac{1}{2},M_Y+\tfrac{1}{2}\rangle, \qquad (3.51)
\end{aligned}
$$

$$
\begin{aligned}
&T_{-\frac{1}{2}-\frac{1}{2}}|vXM_XM_Y\rangle \\
&\quad= \frac{\sqrt{(X-M_X+1)(X-M_Y+1)(v-2X)(v+2X+3)}}{2\sqrt{(2X+1)(2X+2)}}|vX+\tfrac{1}{2},M_X-\tfrac{1}{2},M_Y-\tfrac{1}{2}\rangle \\
&\quad- \frac{\sqrt{(X+M_X)(X+M_Y)(v-2X+1)(v+2X+2)}}{2\sqrt{(2X)(2X+1)}}|vX-\tfrac{1}{2},M_X-\tfrac{1}{2},M_Y-\tfrac{1}{2}\rangle. \qquad (3.52)
\end{aligned}
$$

From these expressions it is clearly seen that no representations can be constructed with $X > \frac{v}{2}$, as the representations must have a positive definite norm. Combining these results with the standard quantum reduction rules for the $SU(2)$ group, we can label all basis states of a representation with fixed v as follows

$$X = 0 \ldots v/2, \quad M_X = -X \ldots X, \quad M_Y = -X \ldots X. \qquad (3.53)$$

Figure (3.3) gives a visual interpretation of the reduction rules for the representation $v = 2$.

3.2.4 Matrix elements of the collective coordinates

The Hamiltonian describing a system undergoing quadrupole collective excitations contains a potential $V(\alpha)$, written in terms of the collective variables α_μ. Even orders of α_μ are only dependent on β and can easily be handled by means of the $SU(1,1)$ generators. Odd powers of α_μ are a little more cumbersome, as they introduce also a γ dependency. Indeed, it turns out that

$$[\alpha\alpha]^{(2)} \cdot \alpha = -\sqrt{\tfrac{2}{7}}\beta^3 \cos 3\gamma, \qquad (3.54)$$

can be considered as the building block of the γ part of the potential $V(\beta,\gamma)$ in the intrinsic frame. Therefore, matrix elements of α_μ within a suitable basis are needed for the construction of the matrix representation of the Hamiltonian. As the chosen framework in the present paper is the Cartan-Weyl natural basis, we proceed within this basis and show that all matrix elements can be calculated by means of an algebraic procedure, similar to the one proposed in the preceding section.

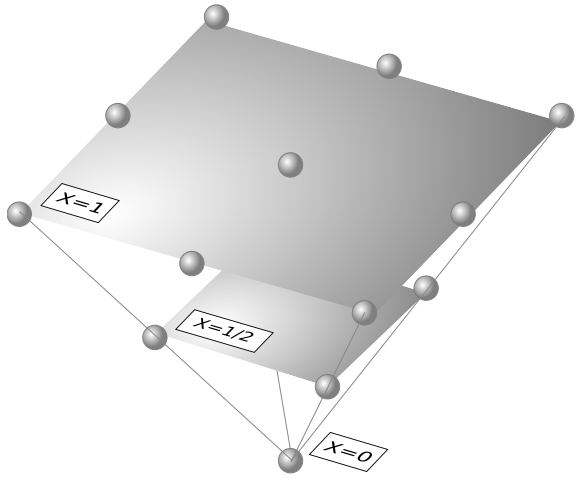

Figure 3.3: Visual interpretation of an $O(5)$ representation with $v = 2$. Every sphere denotes a single basis state. The representation is organised in planes with distinct X quantum number, which contain $(2X+1)^2$ (M_X, M_Y) projection states.

First, we need to establish the bitensor character of the collective variables α_μ with respect to $SU(2)_X \times SU(2)_Y$. Calculating the commutation relations of α_μ with the $SU(2)$ generators (which is done most conveniently using the explicit expressions given in appendix B.1), we can summarise them as

$$[X_0, \alpha^{\lambda\lambda}_{\mu\nu}] = \mu\alpha^{\lambda\lambda}_{\mu\nu}, \tag{3.55}$$

$$[X_\pm, \alpha^{\lambda\lambda}_{\mu\nu}] = \sqrt{(\lambda \mp \mu)(\lambda \pm \mu + 1)}\,\alpha^{\lambda\lambda}_{\mu\pm1\nu}, \tag{3.56}$$

$$[Y_0, \alpha^{\lambda\lambda}_{\mu\nu}] = \nu\alpha^{\lambda\lambda}_{\mu\nu}, \tag{3.57}$$

$$[Y_\pm, \alpha^{\lambda\lambda}_{\mu\nu}] = \sqrt{(\lambda \mp \nu)(\lambda \pm \nu + 1)}\,\alpha^{\lambda\lambda}_{\mu\nu\pm1}, \tag{3.58}$$

where the 5 collective variables have been relabelled as follows

$$\begin{aligned}&\left\{\alpha_2 = \alpha^{\frac12\frac12}_{\frac12\frac12}, \alpha_1 = \alpha^{\frac12\frac12}_{-\frac12\frac12}, \alpha_{-1} = \alpha^{\frac12\frac12}_{\frac12-\frac12}, \alpha_{-2} = \alpha^{\frac12\frac12}_{-\frac12-\frac12}\right\},\\ &\left\{\alpha_0 = \alpha^{00}_{00}\right\}.\end{aligned} \tag{3.59}$$

This clearly states that the 5 projections of α can be divided into the 4 components of a $\{\frac12\frac12\}$ bispinor and a single biscalar, according to Racah [Rac42]. We can again

define double reduced matrix elements

$$\begin{aligned}&\langle vXM_XM_Y|\alpha^{\lambda\lambda}_{\mu\nu}|v'X'M'_XM'_Y\rangle\\&\quad=(-)^k\begin{pmatrix}X&\lambda&X'\\-M_X&\mu&M'_X\end{pmatrix}\begin{pmatrix}X&\lambda&X'\\-M_Y&\nu&M'_Y\end{pmatrix}\langle vX||\alpha^{\lambda}||v'X'\rangle,\end{aligned}\tag{3.60}$$

with $k=2X-M_X-M_Y$. It is noteworthy that, contrary to the matrix elements of the generators $T_{\mu\nu}$, v' is not necessarily equal to v. To obtain explicit expressions for the double reduced matrix elements, we start from the commutation relations

$$[T_{\mu\nu},\alpha^{\frac12\frac12}_{\mu'\nu'}]=\frac{(-)^{(\mu+\nu)}}{\sqrt{2}}\delta_{-\mu\mu'}\delta_{-\nu\nu'}\alpha^{00}_{00},\tag{3.61}$$

$$[T_{\mu\nu},\alpha^{00}_{00}]=\frac{1}{\sqrt{2}}\alpha^{\frac12\frac12}_{\mu\nu},\tag{3.62}$$

$$[\alpha^{\lambda\lambda}_{\mu\nu},\alpha^{\lambda'\lambda'}_{\mu'\nu'}]=0.\tag{3.63}$$

First a relationship between $\langle vX||\alpha^0||v'X'\rangle$ and $\langle vX||\alpha^{\frac12}||v'X'\rangle$ needs to be established. This can be accomplished using the commutation relations (3.61). We consider the specific case $[T_{\frac12\frac12},\alpha^{\frac12\frac12}_{\frac12\frac12}]=0$ and construct the following matrix elements

$$\langle vX\pm\tfrac12,M_X+\tfrac12,M_Y+\tfrac12|[T_{\frac12\frac12},\alpha^{\frac12\frac12}_{\frac12\frac12}]|v'X\mp\tfrac12,M_X-\tfrac12,M_Y-\tfrac12\rangle,\tag{3.64}$$

$$\langle vXM_XM_Y|[T_{\frac12\frac12},\alpha^{\frac12\frac12}_{\frac12\frac12}]|v'XM_X-1,M_Y-1\rangle,\tag{3.65}$$

in terms of the double reduced matrix elements. This can be achieved by inserting a complete set of basis states between the generator $T_{\frac12\frac12}$ and the variable $\alpha^{\frac12\frac12}_{\frac12\frac12}$, then making use of the $T_{\mu\nu}$ matrix elements (3.49) obtained in the previous subsection and the Wigner-Eckart theorem (3.60). The outcome of these tedious although straightforward calculations are, respectively for (3.64) (with minus and positive sign) and (3.65)

$$\begin{aligned}&\langle vX-\tfrac12||\alpha^{\frac12}||v'X\rangle\frac{\sqrt{(v'-2X)(v'+2X+3)}}{\sqrt{2X}}\\&\quad-\langle vX||\alpha^{\frac12}||v'X+\tfrac12\rangle\frac{\sqrt{(v-2X+1)(v+2X+2)}}{\sqrt{2X+2}}=0,\end{aligned}\tag{3.66}$$

$$\langle vX+\tfrac{1}{2}||\alpha^{\frac{1}{2}}||v'X\rangle\frac{\sqrt{(v'-2X+1)(v'+2X+2)}}{\sqrt{2X+2}} - \langle vX||\alpha^{\frac{1}{2}}||v'X-\tfrac{1}{2}\rangle\frac{\sqrt{(v-2X)(v+2X+3)}}{\sqrt{2X}} = 0, \tag{3.67}$$

$$\frac{\langle vX+\frac{1}{2}||\alpha^{\frac{1}{2}}||v'X\rangle}{\sqrt{(v-2X)(v+2X+3)}}\left[\frac{(v'+1)(v'+2)}{2X}-\frac{(v+1)(v+2)}{2X+2}\right] + \frac{\langle vX||\alpha^{\frac{1}{2}}||v'X+\frac{1}{2}\rangle}{\sqrt{(v'-2X)(v'+2X+3)}}\left[\frac{(v+1)(v+2)}{2X}-\frac{(v'+1)(v'+2)}{2X+2}\right]=0. \tag{3.68}$$

The same procedure can be repeated for the commutation relation $[T_{\frac{1}{2}\frac{1}{2}},\alpha^{\frac{1}{2}\frac{1}{2}}_{-\frac{1}{2}\frac{1}{2}}]=0$. We obtain again (3.66) and (3.67), accompanied by the following expression

$$\begin{aligned}&\tfrac{\langle vX+\frac{1}{2}||\alpha^{\frac{1}{2}}||v'X\rangle}{\sqrt{(v-2X)(v+2X+3)}}\left[(v-2X)(v+2X+3)-(v'-2X+1)(v'+2X+2)\right]\\ &+\tfrac{\langle vX||\alpha^{\frac{1}{2}}||v'X+\frac{1}{2}\rangle}{\sqrt{(v'-2X)(v'+2X+3)}}\left[(v-2X+1)(v+2X+2)-(v'-2X)(v'+2X+3)\right]\\ &=0.\end{aligned} \tag{3.69}$$

Combining (3.68) with (3.69) gives a homogeneous set of two equations in two variables $\langle vX+\frac{1}{2}||\alpha^{\frac{1}{2}}||v'X\rangle$ and $\langle vX||\alpha^{\frac{1}{2}}||v'X+\frac{1}{2}\rangle$, rendering the trivial zero solution, unless the determinant of the associated matrix identically vanishes. This is only possible when $v'=v\pm1$, which proves the common knowledge that α forms an $O(5)$-tensor of rank 1.

Finally, we repeat the procedure for $[T_{\frac{1}{2}\frac{1}{2}},\alpha^{\frac{1}{2}\frac{1}{2}}_{-\frac{1}{2}-\frac{1}{2}}]=-\frac{1}{\sqrt{2}}\alpha^{00}_{00}$. Besides (3.66) and (3.67), we obtain the expression

$$\begin{aligned}&\tfrac{\langle vX+\frac{1}{2}||\alpha^{\frac{1}{2}}||v'X\rangle}{\sqrt{(v-2X)(v+2X+3)}}\Big[X(v'+1)(v'+2)\\ &\qquad-(X+1)(v+1)(v+2)+2(2X+1)^2\Big]\\ &+\tfrac{\langle vX||\alpha^{\frac{1}{2}}||v'X+\frac{1}{2}\rangle}{\sqrt{(v'-2X)(v'+2X+3)}}\Big[X(v+1)(v+2)\\ &\qquad-(X+1)(v'+1)(v'+2)+2(2X+1)^2\Big]\\ &=-2\sqrt{2}\sqrt{(2X+1)(2X+2)}\langle vX||\alpha^0||v'X\rangle.\end{aligned} \tag{3.70}$$

Solving the set of equations (3.69) and (3.70) (or equivalently (3.68) and (3.70)) results in expressions of all possible double reduced matrix elements of $\alpha^{\frac{1}{2}}$ as a function of the double reduced matrix elements of α^0.
From this point on, we will explicitly take into account that the α variable connects representations with $\Delta v = 1$, omitting all other matrix elements which are identically zero. For $v' = v + 1$ we obtain

$$\langle v, X + \tfrac{1}{2}||\alpha^{\frac{1}{2}}||v+1, X\rangle = -\tfrac{1}{\sqrt{2}}\sqrt{\tfrac{2X+2}{2X+1}}\sqrt{\tfrac{v-2X}{v+2X+3}}\langle vX||\alpha^0||v+1, X\rangle, \quad (3.71)$$

$$\langle v, X||\alpha^{\frac{1}{2}}||v+1, X+\tfrac{1}{2}\rangle = \tfrac{1}{\sqrt{2}}\sqrt{\tfrac{2X+2}{2X+1}}\sqrt{\tfrac{v+2X+4}{v-2X+1}}\langle vX||\alpha^0||v+1, X\rangle, \quad (3.72)$$

and for $v' = v - 1$

$$\langle v, X + \tfrac{1}{2}||\alpha^{\frac{1}{2}}||v-1, X\rangle = \tfrac{1}{\sqrt{2}}\sqrt{\tfrac{2X+2}{2X+1}}\sqrt{\tfrac{v+2X+3}{v-2X}}\langle vX||\alpha^0||v-1, X\rangle, \quad (3.73)$$

$$\langle v, X||\alpha^{\frac{1}{2}}||v-1, X+\tfrac{1}{2}\rangle = -\tfrac{1}{\sqrt{2}}\sqrt{\tfrac{2X+2}{2X+1}}\sqrt{\tfrac{v-2X-1}{v+2X+2}}\langle vX||\alpha^0||v-1, X\rangle. \quad (3.74)$$

So, we only have to determine the biscalar double reduced matrix elements. Although the commutation relations (3.63) seem trivial, they are convenient in the derivation of the $\{00\}$ double reduced matrix elements. If we consider only the non-trivial commutation relations for which $\lambda = \frac{1}{2}$ and $\lambda' = \frac{1}{2}$, and apply again the same procedure which has been used throughout the present paper, we obtain the following result:

$$\frac{\sum_{v'}\langle vX||\alpha^{\frac{1}{2}}||v'X+\frac{1}{2}\rangle\langle v'X+\frac{1}{2}||\alpha^{\frac{1}{2}}||vX\rangle}{2X+2} - \frac{\sum_{v'}\langle vX||\alpha^{\frac{1}{2}}||v'X-\frac{1}{2}\rangle\langle v'X-\frac{1}{2}||\alpha^{\frac{1}{2}}||vX\rangle}{2X} = 0. \quad (3.75)$$

Now, taking all derived expressions (3.66),(3.67) and (3.71) to (3.74) into account, we can rewrite the relation (3.75) as

$$\frac{(2v+5)}{(v-2X+1)(v+2X+3)}\langle vX||\alpha^0||v+1X\rangle\langle v+1X||\alpha^0||vX\rangle = \frac{(2v+1)}{(v+2X+2)(v-2X)}\langle vX||\alpha^0||v-1X\rangle\langle v-1X||\alpha^0||vX\rangle. \quad (3.76)$$

This relation differs from the previously derived expressions with respect to the quantum numbers. The expressions (3.66) to (3.74) relate matrix elements with different X connections, though the seniority connection (v to $v' = v \pm 1$) was fixed. Now, (3.76) relates matrix elements with different seniority connection,

leaving the X quantum number unaltered.
At last, in order to obtain explicit expressions, we return to the geometry of the problem. It has been mentioned earlier that the operator $\alpha \cdot \alpha$ commutes with all the generators of $O(5)$, making it an $O(5)$ scalar. Therefore, this operator can be treated as a constant with respect to the $O(5)$ scheme. We call this constant β^2, referring to the radial deformation parameter in (2.5). As a consequence, we can write

$$\langle vXM_XM_Y|\alpha \cdot \alpha|vXM_XM_Y\rangle = \beta^2. \tag{3.77}$$

The procedure used culminates into closed expressions of the matrix elements. By inserting a complete set of basis states between the variables of (3.77), we can rewrite this expression in terms of double reduced matrix elements:

$$\begin{aligned}\beta^2 = \frac{1}{(2X+1)^2}\sum_{v'}[&\langle vX||\alpha^0||v'X\rangle\langle v'X||\alpha^0||vX\rangle \\ &+ \langle vX||\alpha^{\frac{1}{2}}||v'X+\tfrac{1}{2}\rangle\langle v'X+\tfrac{1}{2}||\alpha^{\frac{1}{2}}||vX\rangle \\ &+ \langle vX||\alpha^{\frac{1}{2}}||v'X-\tfrac{1}{2}\rangle\langle v'X-\tfrac{1}{2}||\alpha^{\frac{1}{2}}||vX\rangle].\end{aligned} \tag{3.78}$$

All these different matrix elements can be reduced to a single one by means of the reduction rules (3.66) to (3.76). As a result, we obtain

$$\langle vX||\alpha^0||v+1X\rangle\langle v+1X||\alpha^0||vX\rangle = \tfrac{(v-2X+1)(v+2X+3)}{(2v+3)(2v+5)}(2X+1)^2\beta^2 \tag{3.79}$$

$$\langle vX||\alpha^0||v-1X\rangle\langle v-1X||\alpha^0||vX\rangle = \tfrac{(v-2X)(v+2X+2)}{(2v+1)(2v+3)}(2X+1)^2\beta^2. \tag{3.80}$$

Taking into account that $\alpha_0^\dagger = \alpha_0$, we can write

$$\langle vX||\alpha^0||v'X\rangle^* = \langle v'X||\alpha^0||vX\rangle, \tag{3.81}$$

and summarise

$$|\langle v,X||\alpha^0||v+1,X\rangle|^2 = \tfrac{(v-2X+1)(v+2X+3)}{(2v+3)(2v+5)}(2X+1)^2\beta^2, \tag{3.82}$$

$$|\langle v,X||\alpha^0||v-1,X\rangle|^2 = \tfrac{(v-2X)(v+2X+2)}{(2v+1)(2v+3)}(2X+1)^2\beta^2, \tag{3.83}$$

which is equivalent to

$$\langle v,X||\alpha^0||v+1,X\rangle = \sqrt{\tfrac{(v-2X+1)(v+2X+3)}{(2v+3)(2v+5)}}(2X+1)\beta, \tag{3.84}$$

$$\langle v,X||\alpha^0||v-1,X\rangle = \sqrt{\tfrac{(v-2X)(v+2X+2)}{(2v+1)(2v+3)}}(2X+1)\beta, \tag{3.85}$$

because α_0 is a hermitian operator.
Making use of the relations (3.71-3.74), we can construct all double reduced matrix elements of the α variable. Taking the appropriate Wigner-3j coefficients into account, the total matrix elements of the α variable can easily be derived. As an example we evaluate the matrix element

$$\begin{aligned}&\langle vXM_XM_Y|\alpha^{00}_{00}|v'XM_XM_Y\rangle \\ &\quad = (-)^k \begin{pmatrix} X & 0 & X \\ -M_X & 0 & M_X \end{pmatrix} \begin{pmatrix} X & 0 & X \\ -M_Y & 0 & M_Y \end{pmatrix} \langle vX||\alpha^0||v',X\rangle,\end{aligned} \tag{3.86}$$

with $k = 2X - M_X - M_Y$. This leads to the closed expression

$$\langle vXM_XM_Y|\alpha^{00}_{00}|v+1,XM_XM_Y\rangle = \beta\sqrt{\tfrac{(v-2X+1)(v+2X+3)}{(2v+3)(2v+5)}}, \tag{3.87}$$

$$\langle vXM_XM_Y|\alpha^{00}_{00}|v-1,XM_XM_Y\rangle = \beta\sqrt{\tfrac{(v-2X)(v+2X+2)}{(2v+1)(2v+3)}}. \tag{3.88}$$

There is a subtlety involved with equation (3.77). β^2 can either be regarded as the radial variable in the 5-dimensional Euclidean space, which is a constant by definition under rotations of the $O(5)$ orthogonal group, or it can be recognised as a generator of the aforementioned $SU(1,1)$ algebra. In the latter scheme, the $O(5)$ Hilbert space needs to be extended to incorporate this $SU(1,1)$ basis. Then, it is more convenient to move over to a boson creation and annihilation realisation

$$b^\dagger_\mu = \tfrac{1}{\sqrt{2}}(\sqrt{k}\alpha_\mu + \tfrac{i}{\sqrt{k\hbar}}\pi^*_\mu), \qquad \tilde{b}_\mu = \tfrac{1}{\sqrt{2}}(\sqrt{k}\alpha_\mu - \tfrac{i}{\sqrt{k\hbar}}\pi^*_\mu), \tag{3.89}$$

with $[b_\mu, b^\dagger_\nu] = \delta_{\mu\nu}$ and $\tilde{b}_\mu = (-1)^\mu b_{-\mu}$, as it gives immediately rise to the $SU(1,1)$ algebra spanned by

$$B_+ = \tfrac{1}{2}b^\dagger \cdot b^\dagger, \quad B_- = \tfrac{1}{2}\tilde{b}\cdot\tilde{b}, \quad B_0 = \tfrac{1}{4}(b^\dagger\cdot\tilde{b} + \tilde{b}\cdot b^\dagger), \tag{3.90}$$

which is closely connected to the $SU(1,1)$ algebra, defined with the intrinsic realisation (see equations (2.34) in section 2.2.2). The only difference between the $SU(1,1)$ algebra in the previous chapter and this $SU(1,1)$ is that the quadratic Casimir of $O(5)$, emerging from (3.90) has been replaced by its eigenvalue $v(v+3)$. This will be discussed in more detail in section 3.2.6.
A similar technique, as presented for the collective variables in the $O(5)$ basis, can be applied to obtain the matrix elements of the boson creation and annihilation operators (3.89) in the $SU(1,1)$ basis. However, as the boson operators are built from the collective variables ánd the canonic conjugate momenta, we also require the matrix elements of the canonical conjugate momenta in the $O(5)$ basis.

3.2.5 Matrix elements of the canonical conjugate momenta

The calculation of the matrix elements of π^*_μ is very parallel to the algorithm, discussed in the previous section. Indeed, it can be proven that the canonical conjugate momenta have the same transformation properties as the variables in the Cartan-Weyl basis. Relabelling the conjugate momenta as

$$\left\{\pi^*{}_2 = \pi^{*\,\frac{1}{2}\,\frac{1}{2}}_{\frac{1}{2}\,\frac{1}{2}}, \pi^*{}_1 = \pi^{*\,\frac{1}{2}\,\frac{1}{2}}_{-\frac{1}{2}\,\frac{1}{2}}, \pi^*{}_{-1} = \pi^{*\,\frac{1}{2}\,\frac{1}{2}}_{\frac{1}{2}\,-\frac{1}{2}}, \pi^*{}_{-2} = \pi^{*\,\frac{1}{2}\,\frac{1}{2}}_{-\frac{1}{2}\,-\frac{1}{2}}\right\},$$
$$\left\{\pi^*{}_0 = \pi^{*\,00}_{\;\;00}\right\}, \tag{3.91}$$

we can see that the five projections can also be divided in four components of a $\{\frac{1}{2}\frac{1}{2}\}$ bispinor and a $\{00\}$ biscalar, by means of the definition given by Racah [Rac42]

$$[X_0, \pi^{*\lambda\lambda}_{\mu\nu}] = \mu\pi^{*\lambda\lambda}_{\mu\nu}, \tag{3.92}$$
$$[X_\pm, \pi^{*\lambda\lambda}_{\mu\nu}] = \sqrt{(\lambda\mp\mu)(\lambda\pm\mu+1)}\,\pi^{*\lambda\lambda}_{\mu\pm1\nu}, \tag{3.93}$$
$$[Y_0, \pi^{*\lambda\lambda}_{\mu\nu}] = \nu\pi^{*\lambda\lambda}_{\mu\nu}, \tag{3.94}$$
$$[Y_\pm, \pi^{*\lambda\lambda}_{\mu\nu}] = \sqrt{(\lambda\mp\nu)(\lambda\pm\nu+1)}\,\pi^{*\lambda\lambda}_{\mu\nu\pm1}. \tag{3.95}$$

Moreover, the commutation relations with the non-$SU(2)$ generators $T_{\mu\nu}$ give the same results as equations (3.61) and (3.62)

$$[T_{\mu\nu}, \pi^{*\,\frac{1}{2}\,\frac{1}{2}}_{\mu'\nu'}] = \frac{(-)^{(\mu+\nu)}}{\sqrt{2}}\delta_{-\mu\mu'}\delta_{-\nu\nu'}\pi^{*\,00}_{\;\;00}, \tag{3.96}$$
$$[T_{\mu\nu}, \pi^{*\,00}_{\;\;00}] = \frac{1}{\sqrt{2}}\pi^{*\,\frac{1}{2}\,\frac{1}{2}}_{\mu\nu}. \tag{3.97}$$

As a consequence, we can copy the results from the previous section, as long as they are only relying on the bitensor and biscalar transformation properties in the Cartan-Weyl basis. We obtain for $v' = v+1$

$$\langle vX+\tfrac{1}{2}||\pi^{*\frac{1}{2}}||v+1X\rangle = -\tfrac{1}{\sqrt{2}}\sqrt{\tfrac{2X+2}{2X+1}}\sqrt{\tfrac{v-2X}{v+2X+3}}\langle vX||\pi^{*0}||v+1X\rangle, \tag{3.98}$$
$$\langle vX||\pi^{*\frac{1}{2}}||v+1, X+\tfrac{1}{2}\rangle = \tfrac{1}{\sqrt{2}}\sqrt{\tfrac{2X+2}{2X+1}}\sqrt{\tfrac{v+2X+4}{v-2X+1}}\langle vX||\pi^{*0}||v+1, X\rangle, \tag{3.99}$$

and for $v' = v-1$

$$\langle vX+\tfrac{1}{2}||\pi^{*\frac{1}{2}}||v-1, X\rangle = \tfrac{1}{\sqrt{2}}\sqrt{\tfrac{2X+2}{2X+1}}\sqrt{\tfrac{v+2X+3}{v-2X}}\langle vX||\pi^{*0}||v-1, X\rangle, \tag{3.100}$$
$$\langle vX||\pi^{*\frac{1}{2}}||v-1X+\tfrac{1}{2}\rangle = -\tfrac{1}{\sqrt{2}}\sqrt{\tfrac{2X+2}{2X+1}}\sqrt{\tfrac{v-2X-1}{v+2X+2}}\langle vX||\pi^{*0}||v-1X\rangle, \tag{3.101}$$

with $\langle vX||\pi^{*\lambda}||v'X'\rangle$ the double reduced matrix elements, defined by

$$\begin{aligned}&\langle vXM_XM_Y|\pi^{*\lambda\lambda}_{\mu\nu}|v'X'M'_XM'_Y\rangle\\&=(-)^k\begin{pmatrix}X&\lambda&X'\\-M_X&\mu&M'_X\end{pmatrix}\begin{pmatrix}X&\lambda&X'\\-M_Y&\nu&M'_Y\end{pmatrix}\langle vX||\pi^{*\lambda}||v'X'\rangle,\end{aligned}\tag{3.102}$$

($k=2X-M_X-M_Y$).
So now we are at the point of calculating the biscalar double reduced matrix element. Since the α double reduced matrix elements are known, it is convenient to start from the generator (see appendix B.1)

$$X_+=\tfrac{i}{\hbar}(\alpha_2\pi^*_{-1}-\alpha_{-1}\pi^*_2).\tag{3.103}$$

Sandwiching this generator and making use of the intermediate state method, together with reduction rules (3.98 to 3.101) gives

$$\begin{aligned}&\tfrac{2v+5}{(v-2X+1)(v+2X+3)}\langle vX||\alpha^0||v+1,X\rangle\langle v+1,X||\pi^{*0}||vX\rangle\\&-\tfrac{2v+1}{(v+2X+2)(v-2X)}\langle vX||\alpha^0||v-1,X\rangle\langle v-1,X||\pi^{*0}||vX\rangle\\&=-i\hbar(2X+1)^2.\end{aligned}\tag{3.104}$$

Now we can insert the geometry of the problem. If we take the $SU(1,1)$ generator $\alpha\cdot\pi^*$, it can be proven that the intrinsic realisation of this operator is

$$\alpha\cdot\pi^*=i\hbar\beta\frac{\partial}{\partial\beta}.\tag{3.105}$$

Once again, this operator can be considered as a constant in the $O(5)$ basis, since the $SU(1,1)$ generators commute with all generators of $O(5)$. Sandwiching this generator results in

$$\begin{aligned}&\tfrac{(v+3)(2v+5)}{(v+2X+3)(v-2X+1)}\langle vX||\alpha^0||v+1,X\rangle\langle v+1,X||\pi^{*0}||vX\rangle\\&+\tfrac{v(2v+1)}{(v+2X+2)(v-2X)}\langle vX||\alpha^0||v-1,X\rangle\langle v-1,X||\pi^{*0}||vX\rangle\\&=i\hbar(2X+1)^2\beta\frac{\partial}{\partial\beta}.\end{aligned}\tag{3.106}$$

Combining equation (3.104) with (3.106), and substituting the closed expressions for the double reduced α matrix elements, we obtain

$$\langle v+1,X||\pi^{*0}||vX\rangle=\sqrt{\tfrac{(v+2X+3)(v-2X+1)}{(2v+3)(2v+5)}}(2X+1)i\hbar\left[\frac{\partial}{\partial\beta}-\frac{v}{\beta}\right],\tag{3.107}$$

$$\langle v-1,X||\pi^{*0}||vX\rangle=\sqrt{\tfrac{(v+2X+2)(v-2X)}{(2v+1)(2v+3)}}(2X+1)i\hbar\left[\frac{\partial}{\partial\beta}+\frac{v+3}{\beta}\right],\tag{3.108}$$

or, inserting the Wigner-3j symbols

$$\langle v+1XM_XM_Y|\pi^{*0}|vXM_XM_Y\rangle = \sqrt{\tfrac{(v+2X+3)(v-2X+1)}{(2v+3)(2v+5)}}i\hbar\left[\frac{\partial}{\partial\beta}-\frac{v}{\beta}\right], \tag{3.109}$$

$$\langle v-1XM_XM_Y|\pi^{*0}|vXM_XM_Y\rangle = \sqrt{\tfrac{(v+2X+2)(v-2X)}{(2v+1)(2v+3)}}i\hbar\left[\frac{\partial}{\partial\beta}+\frac{v+3}{\beta}\right]. \tag{3.110}$$

These expressions in terms of the partial derivatives in β are remarkable though not surprising, as similar expressions have been found for the canonical conjugate momentum in the framework of the factorisation method [Inf51, Row05a][5]. Nevertheless, we can verify the validity of equation (3.109) and (3.110) twofold. The first verification checks the hermiticity of the matrix elements. We know that $\pi_0^\dagger = \pi_0$ so the hermitian conjugates of the matrix elements[6] read

$$\langle vXM_XM_Y|\pi_0^*|v'XM_XM_Y\rangle^\dagger = \langle v'XM_XM_Y|\pi_0^*|vXM_XM_Y\rangle. \tag{3.111}$$

We proceed with $v' = v-1$,

$$\begin{aligned}&\langle vXM_XM_Y|\pi_0^*|v-1XM_XM_Y\rangle^\dagger \\ &\quad= \sqrt{\tfrac{(v+2X+2)(v-2X)}{(2v+1)(2v+3)}}(-i\hbar)\left[\left(\frac{\partial}{\partial\beta}\right)^\dagger-\frac{v-1}{\beta}\right].\end{aligned} \tag{3.112}$$

It can be shown by means of equation (3.105) that

$$\left(\frac{\partial}{\partial\beta}\right)^\dagger = -\frac{4}{\beta}-\frac{\partial}{\partial\beta}, \tag{3.113}$$

which confirms the first check, when substituting in equation (3.112).
A second check involves the kinetic energy term $\pi^*\cdot\pi^*$. Rewriting equation (3.12), making use of the intrinsic variable β while recognising the quadratic Casimir of $O(5)$ (3.24), we obtain an alternative expression for the kinetic energy

$$\pi^*\cdot\pi^* = -\hbar^2\left(\frac{1}{\beta^4}\frac{\partial}{\partial\beta}\beta^4\frac{\partial}{\partial\beta}-\frac{\mathcal{C}_2[O(5)]}{\beta^2}\right). \tag{3.114}$$

[5] Differences with formulas (107,108) of [Row05a] are due to the inclusion of the volume element β^4 in the mentioned work.

[6] The $O(5)$ matrix elements are actually still operators in the $SU(1,1)$ space, hence the hermitian conjugate instead of complex conjugate.

The matrix element $\langle vXM_XM_Y|\pi^*\cdot\pi^*|vXM_XM_Y\rangle$ then becomes

$$\langle vXM_XM_Y|\pi^*\cdot\pi^*|vXM_XM_Y\rangle = -\hbar^2\left(\frac{1}{\beta^4}\frac{\partial}{\partial\beta}\beta^4\frac{\partial}{\partial\beta} - \frac{v(v+3)}{\beta^2}\right), \quad (3.115)$$

as only the quadratic Casimir affects the $O(5)$ basis state. To check the matrix elements of the conjugate momenta, we can apply the intermediate state method on the matrix element, combining it with the trivial commutation relation $[\pi^*_\mu, \pi^*_\nu] = 0$:

$$\begin{aligned}
&\langle vXM_XM_Y|\pi^*\cdot\pi^*|vXM_XM_Y\rangle \\
&\quad= \tfrac{1}{(2X+1)^2}\tfrac{(2v+3)(2v+5)}{(v+2X+3)(v-2X+1)}\langle vX||\pi^{*0}||v+1,X\rangle\langle v+1,X||\pi^{*0}||vX\rangle \\
&\quad= -\hbar^2\left(\frac{\partial}{\partial\beta}+\frac{v+4}{\beta}\right)\left(\frac{\partial}{\partial\beta}-\frac{v}{\beta}\right) \\
&\quad= -\hbar^2\left(\frac{1}{\beta^4}\frac{\partial}{\partial\beta}\beta^4\frac{\partial}{\partial\beta} - \frac{v(v+3)}{\beta^2}\right), \qquad (3.116)
\end{aligned}$$

which is exactly the expression of the kinetic energy operator in the Cartan-Weyl basis. More than just a test for the matrix elements of the conjugate momenta, these checks can also act as verifications for the matrix elements of the collective coordinates, as they where used during the calculation of the conjugate momenta matrix elements.

3.2.6 $SU(1,1)$ from the $U(5)$ boson realisation

Starting from the boson creation and annihilation operators (3.89), several algebras can be created. One among them is the $U(5)$ algebra, which is spanned by the following 25 generators [Iac87, Fra94]

$$\mathcal{G}_{LM} = [b^\dagger\tilde{b}]^L_M, \quad (3.117)$$

with $L = 0,\ldots,4$ and $M = -L,\ldots,L$. Filtering the odd L generators from the set of $U(5)$ generators, we obtain the 10 generators of $O(5)$, which comprises the 3 angular momentum generators of $O(3)$ ($L = 1$). It is noteworthy that this $O(5)$ algebra equals the one defined by L_M and O_M, defined in equation (3.13), up to a factor.
Another algebra is the one associated with $SU(1,1)$ [Ui68, Ari76, Ari79]. Indeed, reconsidering the operators (3.90)

$$B_+ = \tfrac{1}{2}b^\dagger\cdot b^\dagger, \quad B_- = \tfrac{1}{2}\tilde{b}\cdot\tilde{b}, \quad B_0 = \tfrac{1}{4}(b^\dagger\cdot\tilde{b}+\tilde{b}\cdot b^\dagger), \quad (3.118)$$

we notice that they close under the standard $SU(1,1)$ commutation relations

$$[B_0, B_\pm] = \pm B_\pm, \qquad [B_-, B_+] = 2B_0. \tag{3.119}$$

The action of these generators on a given representation $|\lambda n\rangle$ is [Row96]

$$B_+|\lambda n\rangle = \sqrt{(\lambda+n)(n+1)}|\lambda n+1\rangle, \tag{3.120}$$

$$B_-|\lambda n\rangle = \sqrt{(\lambda+n-1)n}|\lambda n-1\rangle, \tag{3.121}$$

$$B_0|\lambda n\rangle = \tfrac{1}{2}(\lambda+2n)|\lambda n\rangle, \tag{3.122}$$

$$\mathcal{C}_{SU(1,1)}|\lambda n\rangle = \tfrac{1}{4}\lambda(\lambda-2)|\lambda n\rangle, \tag{3.123}$$

where the quadratic Casimir operator is given by [Wyb74]

$$\mathcal{C}_{SU(1,1)} = B_0^2 - B_0 - B_+B_-. \tag{3.124}$$

This operator, expressed in terms of the (α,π^*) realisation, renders the following important identity

$$\mathcal{C}_{SU(1,1)} = \tfrac{1}{4}(\mathcal{C}_2[O(5)] + \tfrac{5}{4}). \tag{3.125}$$

As a consequence, the seniority v can be related to the Casimir quantum number λ of $SU(1,1)$:

$$\lambda(\lambda-2) = v(v+3) + \tfrac{5}{4} \rightarrow \lambda = v + \tfrac{5}{2}. \tag{3.126}$$

This relation points out that, although the mutual generators of $SU(1,1)$ and $O(5)$ commute, the two algebras are still connected by means of the quadratic Casimir quantum number, i.e. the seniority v. Consequently, we require both bases to calculate the matrix elements of the boson creation and annihilation operators. We start from the $SU(1,1)$ basis, defined by $|\lambda n\rangle$, and later incorporate the $O(5)$ Cartan-Weyl representations. First, we deduce selection rules for the matrix elements in the $SU(1,1)$ basis. For this purpose, we write down the commutation relations

$$\begin{array}{ll} [B_-, b_\mu^\dagger] = \tilde{b}_\mu, & [B_-, \tilde{b}_\mu] = 0, \\ [B_0, b_\mu^\dagger] = \frac{1}{2}b_\mu^\dagger, & [B_0, \tilde{b}_\mu] = -\frac{1}{2}\tilde{b}_\mu, \\ [B_+, b_\mu^\dagger] = 0, & [B_+, \tilde{b}_\mu] = -b_\mu^\dagger. \end{array} \tag{3.127}$$

Calculating the matrix elements of the commutation relations with B_0

$$\langle\lambda' n'|[B_0, b_\mu^\dagger]|\lambda n\rangle = \tfrac{1}{2}\langle\lambda' n'|b_\mu^\dagger|\lambda n\rangle, \tag{3.128}$$

$$\langle\lambda' n'|[B_0, \tilde{b}_\mu]|\lambda n\rangle = -\tfrac{1}{2}\langle\lambda' n'|\tilde{b}_\mu|\lambda n\rangle, \tag{3.129}$$

gives rise to the selection rules

$$\lambda' + 2n' - \lambda - 2n - 1 = 0 \qquad \text{for } \langle \lambda' n' | b^\dagger_\mu | \lambda n \rangle, \tag{3.130}$$
$$\lambda' + 2n' - \lambda - 2n + 1 = 0 \qquad \text{for } \langle \lambda' n' | \tilde{b}_\mu | \lambda n \rangle. \tag{3.131}$$

More selection rules can be obtained from the other commutation relations:

$$\langle \lambda' n' + 1 | [B_+, b^\dagger_\mu] | \lambda n - 1 \rangle = 0, \tag{3.132}$$
$$\langle \lambda' n' + 1 | [B_+, \tilde{b}_\mu] | \lambda n \rangle = -\langle \lambda' n' + 1 | b^\dagger_\mu | \lambda n \rangle, \tag{3.133}$$
$$\langle \lambda' n' | [B_-, b^\dagger_\mu] | \lambda n \rangle = \langle \lambda' n' | \tilde{b}_\mu | \lambda n \rangle, \tag{3.134}$$
$$\langle \lambda' n' | [B_-, \tilde{b}_\mu] | \lambda n + 1 \rangle = 0. \tag{3.135}$$

The above relations result in the following four equations

$$\sqrt{(\lambda' + n')(n' + 1)} \langle \lambda' n' | b^\dagger_\mu | \lambda n - 1 \rangle - \sqrt{(\lambda + n - 1) n} \langle \lambda' n' + 1 | b^\dagger_\mu | \lambda n \rangle = 0, \tag{3.136}$$
$$\sqrt{(\lambda' + n')(n' + 1)} \langle \lambda' n' | \tilde{b}_\mu | \lambda n \rangle - \sqrt{(\lambda + n)(n + 1)} \langle \lambda' n' + 1 | \tilde{b}_\mu | \lambda n + 1 \rangle = -\langle \lambda' n' + 1 | b^\dagger_\mu | \lambda n \rangle, \tag{3.137}$$
$$\sqrt{(\lambda' + n')(n' + 1)} \langle \lambda' n' + 1 | b^\dagger_\mu | \lambda n \rangle - \sqrt{(\lambda + n - 1) n} \langle \lambda' n' | b^\dagger_\mu | \lambda n - 1 \rangle = \langle \lambda' n' | \tilde{b}_\mu | \lambda n \rangle, \tag{3.138}$$
$$\sqrt{(\lambda' + n')(n' + 1)} \langle \lambda' n' + 1 | \tilde{b}_\mu | \lambda n + 1 \rangle - \sqrt{(\lambda + n)(n + 1)} \langle \lambda' n' | \tilde{b}_\mu | \lambda n \rangle = 0, \tag{3.139}$$

which is a homogeneous set of four equations in four variables (the matrix elements). This means that these matrix elements are identically zero unless the determinant of the matrix identically vanishes. Solving the determinant, realising that the four matrix elements are chosen such that the selection rule $\lambda' + 2n' - \lambda - 2n + 1 = 0$ holds (3.130 & 3.131) for all of them, we obtain the general selection rules

$$\{\lambda' = \lambda - 1, n' = n\}, \tag{3.140}$$
$$\{\lambda' = \lambda + 1, n' = n - 1\}. \tag{3.141}$$

Thus the non-vanishing matrix elements are

$$\begin{array}{ll} \langle \lambda + 1, n | b^\dagger_\mu | \lambda n \rangle, & \langle \lambda + 1, n - 1 | \tilde{b}_\mu | \lambda n \rangle, \\ \langle \lambda - 1, n + 1 | b^\dagger_\mu | \lambda n \rangle, & \langle \lambda - 1, n | \tilde{b}_\mu | \lambda n \rangle. \end{array} \tag{3.142}$$

Although we already knew that α_μ and π^*_μ are $v = 1$ $O(5)$ tensors, this was not explicitly taken into account in the calculation, but emerged naturally from the selection criteria. However, these selection rules also contain a physical interpretation. It is comprehended from the definition of the generator B_+ that n denotes the number of boson pairs coupled to angular momentum zero. Since B_0 counts the total number of bosons, λ can be associated to the number of pairs not coupled to zero, i.e. the seniority v. To conclude, the allowed solutions of the homogeneous set of equations are summarised. Some solutions relate the matrix elements with different pair number n

$$\sqrt{\lambda+n+1}\langle\lambda+1,n|b^\dagger_\mu|\lambda n\rangle = \sqrt{\lambda+n}\langle\lambda+1,n+1|b^\dagger_\mu|\lambda n+1\rangle, \tag{3.143}$$

$$\sqrt{n+1}\langle\lambda-1,n|b^\dagger_\mu|\lambda,n-1\rangle = \sqrt{n}\langle\lambda-1,n+1|b^\dagger_\mu|\lambda n\rangle, \tag{3.144}$$

and

$$\sqrt{n}\langle\lambda+1,n|\tilde{b}_\mu|\lambda n+1\rangle = \sqrt{n+1}\langle\lambda+1,n-1|\tilde{b}_\mu|\lambda n\rangle, \tag{3.145}$$

$$\sqrt{\lambda+n-1}\langle\lambda-1,n+1|\tilde{b}_\mu|\lambda,n+1\rangle = \sqrt{\lambda+n}\langle\lambda-1,n|\tilde{b}_\mu|\lambda n\rangle, \tag{3.146}$$

while other relate the matrix elements of creation and annihilation operators

$$\sqrt{n}\langle\lambda+1,n|b^\dagger_\mu|\lambda n\rangle = \sqrt{\lambda+n}\langle\lambda+1,n-1|\tilde{b}_\mu|\lambda n\rangle, \tag{3.147}$$

$$\sqrt{\lambda+n-1}\langle\lambda-1,n+1|b^\dagger_\mu|\lambda n\rangle = \sqrt{n+1}\langle\lambda-1,n|\tilde{b}_\mu|\lambda n\rangle. \tag{3.148}$$

From this point onwards, we proceed by including the $O(5)$ basis. As the creation and annihilation operator matrix elements can be related by means of equation (3.147) and (3.148), we only consider $b^\dagger$ ($\tilde{b}$ is analogous). Both the collective coordinates α_μ and canonical conjugate momenta π^*_μ can be divided in the four components of a bispinor and a single biscalar in the $SU(2)_X \times SU(2)_Y$ subgroup of the Cartan-Weyl reduction (see equation (3.59) and (3.91)). As the bosons creation operators are merely a sum of the two (see equation 3.89), the transformation properties are preserved. We can now relabel the operators

$$\left\{b^\dagger{}_2 = b^{\dagger\,\frac{1}{2}\frac{1}{2}}_{\frac{1}{2}\frac{1}{2}}, b^\dagger{}_1 = b^{\dagger\,\frac{1}{2}\frac{1}{2}}_{-\frac{1}{2}\frac{1}{2}}, b^\dagger{}_{-1} = b^{\dagger\,\frac{1}{2}\frac{1}{2}}_{\frac{1}{2}-\frac{1}{2}}, b^\dagger{}_{-2} = b^{\dagger\,\frac{1}{2}\frac{1}{2}}_{-\frac{1}{2}-\frac{1}{2}}\right\}, \tag{3.149}$$

$$\left\{b^\dagger{}_0 = b^{\dagger\,00}_{00}\right\}. \tag{3.150}$$

Applying the Wigner-Eckart theorem twice we can extract a double reduced matrix element. The only difference with the previously defined double matrix elements is the presence of the $SU(1,1)$ quantum number n and λ. However, as the

latter quantum number is in one-to-one correspondence with v ($\lambda = v + 5/2$), it will be omitted not to overload the notation. So we can write

$$\begin{aligned}&\langle nvXM_XM_Y|b^{\dagger\,\lambda\lambda}_{\mu\nu}|n'v'X'M'_XM'_Y\rangle \\ &= (-)^k \begin{pmatrix} X & \lambda & X' \\ -M_X & \mu & M'_X \end{pmatrix} \begin{pmatrix} X & \lambda & X' \\ -M_Y & \nu & M'_Y \end{pmatrix} \langle nvX||b^{\dagger\,\lambda}||n'v'X'\rangle,\end{aligned} \tag{3.151}$$

with $k = 2X - M_X - M_Y$. The commutation relations of $b^\dagger$ with the components of the T bispinor are also identical to (3.61-3.62) and (3.96-3.97)

$$[T_{\mu\nu}, b^{\dagger\,\frac{1}{2}\frac{1}{2}}_{\mu'\nu'}] = \frac{(-)^{(\mu+\nu)}}{\sqrt{2}}\delta_{-\mu\mu'}\delta_{-\nu\nu'}b^{\dagger\,00}_{00}, \tag{3.152}$$

$$[T_{\mu\nu}, b^{\dagger\,00}_{00}] = \frac{1}{\sqrt{2}}b^{\dagger\,\frac{1}{2}\frac{1}{2}}_{\mu\nu}. \tag{3.153}$$

As a result, we can write all $\{\frac{1}{2}\frac{1}{2}\}$ double reduced matrix elements as a function of $\{00\}$, similar to equations (3.71) to (3.74). Taking the $SU(1,1)$ selection rules for n and λ into account (3.140 & 3.141), we can incorporate them in the relations for the matrix elements. Thus we obtain for $v' = v + 1$:

$$\begin{aligned}&\langle nv, X + \tfrac{1}{2}||b^{\dagger\,\frac{1}{2}}||n-1, v+1, X\rangle \\ &\quad = -\tfrac{1}{\sqrt{2}}\sqrt{\tfrac{2X+2}{2X+1}}\sqrt{\tfrac{v-2X}{v+2X+3}}\langle vX||b^{\dagger\,0}||n-1, v+1, X\rangle,\end{aligned} \tag{3.154}$$

$$\begin{aligned}&\langle nv, X||b^{\dagger\,\frac{1}{2}}||n-1, v+1, X+\tfrac{1}{2}\rangle \\ &\quad = \tfrac{1}{\sqrt{2}}\sqrt{\tfrac{2X+2}{2X+1}}\sqrt{\tfrac{v+2X+4}{v-2X+1}}\langle vX||b^{\dagger\,0}||n-1, v+1, X\rangle,\end{aligned} \tag{3.155}$$

and for $v' = v - 1$:

$$\begin{aligned}&\langle nv, X + \tfrac{1}{2}||b^{\dagger\,\frac{1}{2}}||n, v-1, X\rangle \\ &\quad = \tfrac{1}{\sqrt{2}}\sqrt{\tfrac{2X+2}{2X+1}}\sqrt{\tfrac{v+2X+3}{v-2X}}\langle nvX||b^{\dagger\,0}||n, v-1, X\rangle,\end{aligned} \tag{3.156}$$

$$\begin{aligned}&\langle nv, X||b^{\dagger\,\frac{1}{2}}||n, v-1, X+\tfrac{1}{2}\rangle \\ &\quad = -\tfrac{1}{\sqrt{2}}\sqrt{\tfrac{2X+2}{2X+1}}\sqrt{\tfrac{v-2X-1}{v+2X+2}}\langle nvX||b^{\dagger\,0}||n, v-1, X\rangle.\end{aligned} \tag{3.157}$$

At the end, we only need to determine two double reduced $\{00\}$ matrix elements. For this purpose, we have two additional expressions at hand: the commutation relation $[\tilde{b}_0, b^\dagger_0] = 1$ and the $SU(1,1)$ generator $B_+ = \frac{1}{2}b^\dagger \cdot b^\dagger$. We construct the

following matrix elements

$$\langle nvXM_XM_Y|[\tilde{b}_0, b_0^\dagger]|nvXM_XM_Y\rangle = 1, \tag{3.158}$$

$$\langle n+1, vXM_XM_Y|b^\dagger \cdot b^\dagger|nvXM_XM_Y\rangle = 2\sqrt{(\lambda+n)(n+1)}. \tag{3.159}$$

Applying the intermediate state method, making use of the relations (3.143 to 3.148) and (3.154 to 3.157), we obtain the closed result

$$\begin{aligned}\langle n+1vX||b^{\dagger 0}||n, v+1, X\rangle\langle n, v+1, X||b^{\dagger 0}||nvX\rangle \\ = \tfrac{(v+2X+3)(v-2X+1)}{(2v+5)(2v+3)} 2(2X+1)^2\sqrt{(\lambda+n)(n+1)},\end{aligned} \tag{3.160}$$

$$\begin{aligned}\langle n+1vX||b^{\dagger 0}||n+1, v-1, X\rangle\langle n+1, v-1, X||b^{\dagger 0}||nvX\rangle \\ = \tfrac{(v+2X+2)(v-2X)}{(2v+1)(2v+3)} 2(2X+1)^2\sqrt{(\lambda+n)(n+1)}.\end{aligned} \tag{3.161}$$

Since $(b_0^\dagger)^\dagger = b_0 \equiv \tilde{b}_0$, we obtain the boson creation double reduced matrix elements

$$\langle n, v+1, X||b^{\dagger 0}||nvX\rangle = \sqrt{\tfrac{(v+2X+3)(v-2X+1)}{(2v+5)(2v+3)}}\sqrt{2}(2X+1)\sqrt{\lambda+n}, \tag{3.162}$$

$$\langle n+1, v-1, X||b^{\dagger 0}||nvX\rangle = \sqrt{\tfrac{(v+2X+2)(v-2X)}{(2v+1)(2v+3)}}\sqrt{2}(2X+1)\sqrt{n+1}, \tag{3.163}$$

and likewise for the boson annihilation double reduced matrix elements

$$\langle n-1, v+1, X||\tilde{b}^0||nvX\rangle = \sqrt{\tfrac{(v+2X+3)(v-2X+1)}{(2v+5)(2v+3)}}\sqrt{2}(2X+1)\sqrt{n}, \tag{3.164}$$

$$\langle n, v-1, X||\tilde{b}^0||nvX\rangle = \sqrt{\tfrac{(v+2X+2)(v-2X)}{(2v+1)(2v+3)}}\sqrt{2}(2X+1)\sqrt{\lambda+n-1}. \tag{3.165}$$

3.2.7 $SU(1,1)$ from the intrinsic realisation.

At the present point, we have all necessary ingredients to start the cooking. In principle, every term in the GCM Hamiltonian can be dealt with in the $SU(1,1) \times O(5)$ scheme, using the boson formalism of the previous chapter. Even powers of α and π^* are treated most easily in the $SU(1,1)$ basis, whereas the odd powers need to be addressed in the $O(5)$ basis. This can become quite involved, as every collective variable is expressed as the sum of a boson creation and annihilation operator. Since

$$[\alpha\alpha]^{(2)} \cdot \alpha = -\sqrt{\tfrac{2}{7}}\beta^3 \cos 3\gamma, \tag{3.166}$$

it is convenient to know the matrix elements of β in the $SU(1,1)$ basis. We can use the previously derived results for this purpose. The collective coordinate with angular momentum projection zero reads

$$\alpha_0 = \tfrac{1}{\sqrt{2k}}(b_0^\dagger + \tilde{b}_0). \tag{3.167}$$

Making use of the expressions (3.87) and (3.88) for the α_0 matrix element and (3.162) to (3.165) for the boson matrix elements, we can filter out the $O(5)$ dependency of the matrix elements. As a result, we are left with the β matrix elements

$$\begin{aligned} \langle \lambda+1, n|\beta|\lambda n\rangle &= \tfrac{1}{\sqrt{k}}\sqrt{\lambda+n}, & \langle \lambda+1, n-1|\beta|\lambda n\rangle &= \tfrac{1}{\sqrt{k}}\sqrt{n}, \\ \langle \lambda-1, n|\beta|\lambda n\rangle &= \tfrac{1}{\sqrt{k}}\sqrt{\lambda+n-1}, & \langle \lambda-1, n+1|\beta|\lambda n\rangle &= \tfrac{1}{\sqrt{k}}\sqrt{n+1}. \end{aligned} \tag{3.168}$$

It is noteworthy that the same matrix elements have been derived in the framework of the factorisation method [Row05a].

Section 3.3 Rotation to the physical basis

3.3.1 The rotation

The drawback of the Cartan-Weyl reduction is that its basis is not naturally compatible with the physical angular momentum quantum number L which emerges from experimental energy spectra. This comes from the fact that $L \cdot L$ does not commute with X^2, implying that a basis diagonalizing both operators is non-existent. Therefore, a rotation from the natural group chain $O(5) \supset O(4) \cong SU(2) \times SU(2)$ to the physical chain $O(5) \supset O(3) \supset O(2)$ is needed. Fortunately, the Casimir operator L_0 associated with the physical $O(2)$ group is diagonal in the Cartan-Weyl basis, leaving $L \cdot L$ the only operator to diagonalize.

$$L \cdot L = L_0^2 + \tfrac{1}{2}(L_+L_- + L_-L_+). \tag{3.169}$$

Rewriting the $O(3)$ generators in terms of the Cartan-Weyl generators gives

$$L_\pm = 2X_\pm + \sqrt{12}T_{\mp\frac{1}{2}\pm\frac{1}{2}}, \tag{3.170}$$

$$L_0 = X_0 + 3Y_0, \tag{3.171}$$

so that $L \cdot L$ can be written as

$$\begin{aligned} L \cdot L = {} & 4X^2 - 3[(X_0 - 3Y_0 + \tfrac{1}{2})(X_0 + Y_0 + \tfrac{1}{2}) - \tfrac{1}{4}] \\ & + 4\sqrt{3}[T_{-\frac{1}{2}\frac{1}{2}}X_- + T_{\frac{1}{2}-\frac{1}{2}}X_+] + 12T_{\frac{1}{2}-\frac{1}{2}}T_{-\frac{1}{2}\frac{1}{2}}. \end{aligned} \tag{3.172}$$

The action of all generators are known in the natural basis (see section 3.2.3), so the matrix elements of a matrix representation can easily be calculated. The dimension of the matrix is governed by the seniority quantum number since the generators involved in the expression $L \cdot L$ cannot alter the $O(5)$ quantum number, which means that there is an associated matrix with every v. This matrix is even further reducible if one takes the L_0 operator into account. Since L_0 can be written as $L_0 = X_0 + 3Y_0$, it is immediately diagonal in the Cartan-Weyl basis, making $M = M_X + 3M_Y$ a good quantum number. As a consequence, the total matrix representation of $L \cdot L$ can be divided in separate sub-matrices with distinct M quantum number. The possible basis states $|vXM_XM_Y\rangle$ spanning the sub-matrices with $M = M_X + 3M_Y$ can easily be recognised in the tilted weight diagrams (Figure 3.4). The diagram is tilted with respect to the angular momentum operator L_0, so that the vertical projection of every basis state immediately gives the L_0 component. As a result, all basis states, lying on the same vertical projection line form a subspace of states for which $M = M_X + 3M_Y$ holds.

An important issue with respect to actual calculations is the dimension of the matrix representations of $L \cdot L$. It is unresolved up to the present whether the rotation can be carried out in an analytic way by making use of non-commuting Clebsch-Gordan recoupling. We know from the Cartan-Weyl reduction that the set

$$\{X_0, X_+, X_-\}, \tag{3.173}$$

spans an $SU(2)$ algebra. The same is valid for the set

$$\{Y_0 - X_0, 2T_{-\frac{1}{2}\frac{1}{2}}, 2T_{\frac{1}{2}-\frac{1}{2}}\}, \tag{3.174}$$

and it can be proven that the set of angular momentum generators L_M is the only linear combination of the two mentioned $SU(2)$ algebras, able to span another $SU(2)$ in itself. However, the two algebras (3.173 & 3.174) do not commute which means that the recoupling is not feasible with the standard Clebsch-Gordan recoupling. As a consequence, we need to resort to numerical diagonalisation procedures, as e.g. the LAPACK routines [And99].

With respect to computation time, the dimensions of the representations have to be kept under control. The total number of basis states within a representation v can be determined as

$$\sum_{X=0}^{v/2} (2X+1)^2 = \frac{1}{6}(2v+3)(v+2)(v+1). \tag{3.175}$$

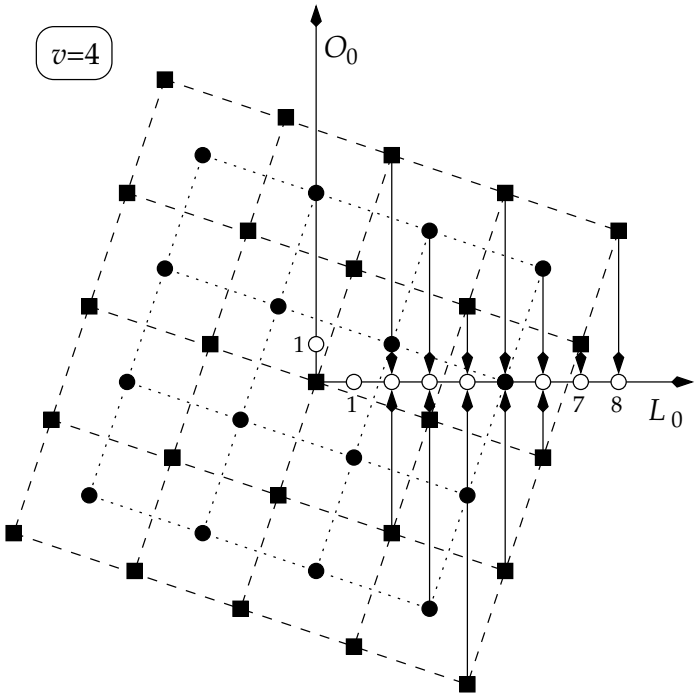

Figure 3.4: Projections of the $v = 4$ irreps on the L_0 axis, connecting all basis states for which $M = M_X + 3M_Y$ is equal. The line most on the right only projects the $M_X = v/2, M_Y = v/2$ state on the L_0 axis, resulting in an $M = 2v$ state. For $v = 4$ the maximal L_0 projection corresponds to $M = 8$

However, the dimensions of the $M = 0$ sub-blocks are lower than the total v representation space. These dimensions can be calculated according to the following formula, depending whether v is even or odd. If we define $X_m = v/2$, the number of $M = 0$ projections is then given by

$$3(X_m|3)^2 + [X_m \text{mod} 3 + 1][2(X_m|3) + 1] + 3[(X_m + 1)|3 - 1][(X_m + 1)|3] + 2[(X_m + 1)|3][(X_m + 1)\text{mod}3 + 1], \quad (3.176)$$

for even v. For odd v we obtain

$$3[(X_m + \tfrac{3}{2})|3 - 1][(X_m + \tfrac{3}{2})|3] + 2[(X_m + \tfrac{3}{2})|3][(X_m + \tfrac{3}{2})\text{mod}3 + 1] + 3[(X_m - \tfrac{1}{2})|3]^2 + [(X_m - \tfrac{1}{2})\text{mod}3 + 1][2((X_m - \tfrac{1}{2})|3) + 1]. \quad (3.177)$$

These two dimension formulas are plotted in figure 3.5. From this figure, it is

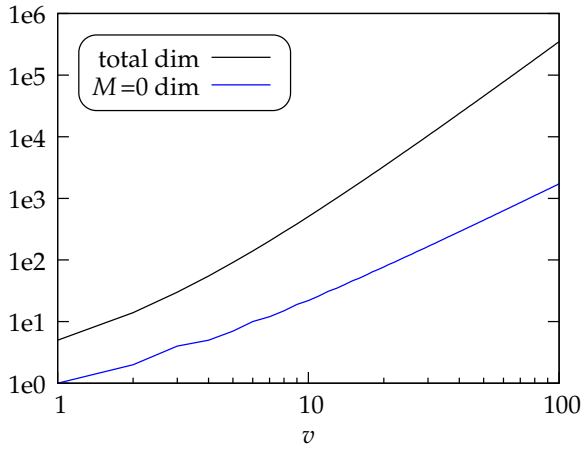

Figure 3.5: Total dimension of a representations with a given seniority v, compared to the dimension of the subspace of states with $M = 0$. It is clear that the dimension of the $M = 0$ subspace increases quadratically with increasing seniority, however it remains feasible for realistic calculations. For $v = 100$, the dimension of $M = 0$ space is 1717, while the total dimension is 348551.

clear that the dimension of the $M = 0$ subspace stays reasonable with respect to modern computation standards, as long as relatively low-order seniorities are considered. Anyhow, when performing realistic calculations, the transformation from the natural to the physical basis does not need to be repeated for every calculation, as the rotation is independent of the specific physical system (Hamiltonian) under study. In practical calculations, the rotation has to be carried out only once and stored for later use.

3.3.2 Some specific cases

Although the rotation from the natural towards the physical basis corresponds to a standard diagonalization problem, it is useful to study some specific cases. It is readily seen from figure 3.4 that the projection $M = 2v$ can only be constructed from one single basis state $|v, X = \frac{v}{2}, M_X = \frac{v}{2}, M_Y = \frac{v}{2}\rangle$, as there is only one projection state. Therefore, the matrix representation is one dimensional

$$\langle v, \tfrac{v}{2}(\tfrac{v}{2}\,\tfrac{v}{2})|L \cdot L|v, \tfrac{v}{2}(\tfrac{v}{2}\,\tfrac{v}{2})\rangle = 2v(2v+1). \tag{3.178}$$

The same is valid for $M = 2v - 1$. The only basis state with this M projection is $|v, X = \frac{v}{2}, M_X = \frac{v}{2} - 1, M_Y = \frac{v}{2}\rangle$, giving the same eigenvalue $2v(2v+1)$. For $M = 2v - 2$, there are two different states: $|v, X = \frac{v}{2}, M_X = \frac{v}{2} - 2, M_Y = \frac{v}{2}\rangle$ and $|v, X = \frac{v}{2} - \frac{1}{2}, M_X = \frac{v}{2} - \frac{1}{2}, M_Y = \frac{v}{2} - \frac{1}{2}\rangle$. which gives a 2 dimensional matrix with eigenvalues and accompanying eigenvectors

$$\lambda_+ = 2v(2v+1) \rightarrow \left(\sqrt{\tfrac{4(v-1)}{4v-1}}, \sqrt{\tfrac{3}{4v-1}} \right), \tag{3.179}$$

$$\lambda_- = (2v-2)(2v-1) \rightarrow \left(\sqrt{\tfrac{3}{4v-1}}, -\sqrt{\tfrac{4(v-1)}{4v-1}} \right). \tag{3.180}$$

So it is clear that the associated eigenvector of λ_+ belongs to the $L = 2v$ multiplet while the eigenvector of λ_- will be the heighest M state of the $L = 2v - 2$ multiplet. Basically, this procedure can be repeated up to $M = 0$ by means of a symbolic mathematical computer program or by means of numerical procedures. However, only the $M = 0$ rotation needs to be carried out, since every L state within a representation v contains an $M = 0$ projection. However, $M \neq 0$ projections are also required in the calculation of the Hamiltonian as all projections of α are present. This can be overcome by making use of the reduced matrix elements, defined by the Wigner-Eckart theorem[7]

$$\langle LM|O^l_m|L'M'\rangle = (-)^{L-M} \begin{pmatrix} L & l & L' \\ -M & m & M' \end{pmatrix} \langle L||O^l||L'\rangle. \tag{3.181}$$

Diagonalising the $L \cdot L$ matrix for $M = 0$ analytically up to $v = 3$, we can deduce the reduced matrix elements $\langle vL||\alpha||v'L'\rangle$ explicitly. These matrix elements are given in table 3.2.

Section 3.4 Building the Hamiltonian

Within the previous sections, it has been shown how the matrix elements of the collective variables, can be obtained in the physical $SU(1,1) \times O(5)$ basis. As the potential in the Hamiltonian can be expressed as an angular momentum invariant Taylor expansion in the variables, it is possible to calculate the matrix elements of all possible terms in the Hamiltonian using standard angular momentum recoupling procedures, and obtain a matrix representation of the collective Hamiltonian. Once this matrix representation is constructed, we need to rely on numerical diagonalisation procedures to compute the eigenvalues of the

[7] From now on, $\langle L||O^l||L'\rangle$ denotes the standard single reduced matrix elements.

		$v=0$	$v=1$	$v=2$		$v=3$			
v	L	$L=0$	$L=2$	$L=2$	$L=4$	$L=0$	$L=3$	$L=4$	$L=6$
0	0	.	1		.	.	.	.	.
1	2	1	.	$-\sqrt{\frac{10}{7}}$	$3\sqrt{\frac{2}{7}}$	.	.	.	.
2	2	.	$-\sqrt{\frac{10}{7}}$	.	.	$-\sqrt{\frac{1}{3}}$	$\sqrt{\frac{5}{3}}$	$-\sqrt{\frac{11}{7}}$	0
	4	.	$3\sqrt{\frac{2}{7}}$	.	.	0	$\sqrt{\frac{2}{3}}$	$\sqrt{\frac{10}{7}}$	$\sqrt{\frac{13}{3}}$
3	0	.	.	$-\sqrt{\frac{1}{3}}$	0	.	.	.	.
	3	.	.	$-\sqrt{\frac{5}{3}}$	$-\sqrt{\frac{2}{3}}$	.	.	.	.
	4	.	.	$-\sqrt{\frac{11}{7}}$	$\sqrt{\frac{10}{7}}$	.	.	.	.
	6	.	.	0	$\sqrt{\frac{13}{3}}$	.	.	.	.

Table 3.2: Reduced matrix elements $\langle vL||\alpha||v'L'\rangle$, scaled to the factor β. Reduced matrix elements are given upto $v=3$.

Schrödinger equation. Unfortunately, the Hilbert space of the collective models is infinite dimensional (which is reflected in the non-compactness of the $SU(1,1)$ group). A common way to cope with this problem is to gradually expand the Hilbert space by incorporating more basis states until convergence is reached in the lowest eigenvalues. As a consequence, we can finetune the free parameters in the basis in order to optimise the convergence. Cunning ways to do so are already available in the literature and will briefly be discussed in the present section, though we start with the construction of the matrix elements.

3.4.1 Matrix elements

We start from the collective model Hamiltonian

$$\hat{H} = \tfrac{1}{2B_2}(\pi^*\cdot\pi^*) + c_2(\alpha\cdot\alpha) + c_3([\alpha\alpha]^{(2)}\cdot\alpha) + c_4(\alpha\cdot\alpha)^2 + c_5([\alpha\alpha]^{(2)}\cdot\alpha)(\alpha\cdot\alpha) + c_6(\alpha\cdot\alpha)^3 + \ldots, \tag{3.182}$$

which we want to diagonalise

$$\hat{H}|\Psi\rangle = E|\Psi\rangle. \tag{3.183}$$

As the Hamiltonian is rotationally invariant, L and M are good quantum numbers. The eigen states $|\Psi\rangle$ of $\hat{H}$ can be expanded in the $SU(1,1)\times O(5)$ physical

basis

$$|\Psi\rangle = |L(i)M\rangle = \sum_{n v \nu} a^{L(i)M}_{nv(\nu)} |nvL(\nu)M\rangle. \tag{3.184}$$

The index (i) denotes the occurrence of the spin L in the spectrum of the Hamiltonian, whereas the Greek index (ν) differentiates between the spins L, resulting from the rotation from the Cartan to the physical basis; it may be considered as the missing quantum number (see chapter 2.2.1). Going over to the reduced matrix element framework, the diagonalisation can be written as follows

$$\sum_{n v \nu} \langle n'v'L(\nu')||\hat{H}||nvL(\nu)\rangle a^{L(i)}_{vn\nu} = \varepsilon a^{L(i)}_{n'v'\nu'}, \tag{3.185}$$

with $\varepsilon = \langle n'v'L(\nu')||\hat{1}||nvL(\nu)\rangle E$ and the index M omitted. The different terms in the Hamiltonian can all be treated using the $SU(1,1) \times O(5)$ basis.
The even powers of α or π^* can be brought back to the $SU(1,1)$ generators (3.118) and are diagonal in the $O(5)$ basis. Writing expressions (3.118) as a function of α and π^* and inverting, we obtain

$$\langle n'vL(\nu)||\alpha \cdot \alpha||nvL(\nu)\rangle = \tfrac{1}{k}\sqrt{2L+1}\langle \lambda n'|2B_0 + B_+ + B_-|\lambda n\rangle, \tag{3.186}$$

$$\langle n'vL(\nu)||\pi^* \cdot \pi^*||nvL(\nu)\rangle = k\hbar^2\sqrt{2L+1}\langle \lambda n'|2B_0 - B_+ - B_-|\lambda n\rangle. \tag{3.187}$$

Concerning the odd powers, the $O(5)$ basis is also involved. However, every odd term in the Hamiltonian can be reduced to the reduced matrix elements of α as e.g.

$$\begin{aligned}
&\langle n'v'L(\nu')|||[\alpha\alpha]^{(2)} \cdot \alpha||nvL(\nu)\rangle \\
&\quad = \tfrac{\sqrt{5}}{\sqrt{2L+1}} \sum_{n_i v_i \nu_i L_i} \begin{Bmatrix} 2 & 2 & 2 \\ L_1 & L & L_2 \end{Bmatrix} \langle n'v'L(\nu')||\alpha||n_1v_1L_1(\nu_1)\rangle \\
&\qquad \times \langle n_1v_1L_1(\nu_1)||\alpha||n_2v_2L_2(\nu_2)\rangle\langle n_2v_2L_2(\nu_2)||\alpha||nvL(\nu)\rangle,
\end{aligned} \tag{3.188}$$

where $\{n_i v_i \nu_i L_i\}$ denotes the double sum over $\{n_1 v_1 \nu_1 L_1\}$ and $\{n_2 v_2 \nu_2 L_2\}$. With respect to numerical computations, it is more convenient to consider a sidestep. The reduced matrix element can also be written as

$$\begin{aligned}
&\langle n'v'L(\nu')|||[\alpha\alpha]^{(2)} \cdot \alpha||nvL(\nu)\rangle \\
&\quad = \tfrac{1}{\sqrt{2L+1}} \sum_{n_1 v_1 \nu_1 L_1} (-)^{L+L_1} \langle n'v'L(\nu')|||[\alpha\alpha]^{(2)}||n_1v_1L_1(\nu_1)\rangle \\
&\qquad \times \langle n_1v_1L_1(\nu_1)||\alpha||nvL(\nu)\rangle,
\end{aligned} \tag{3.189}$$

where the reduced matrix element of $[\alpha\alpha]^{(2)}$ is given by

$$\begin{aligned}\langle n'v'L(\nu')||[\alpha\alpha]^{(2)}\cdot\alpha||nvL(\nu)\rangle \\ = \sqrt{5}(-)^{L+L_1}\sum_{n_2v_2\nu_2L_2}\left\{\begin{array}{ccc}2 & 2 & 2\\ L_1 & L & L_2\end{array}\right\}\langle n'v'L(\nu')||\alpha||n_2v_2L_2(\nu_2)\rangle \\ \times\langle n_2v_2L_2(\nu_2)||\alpha||nvL(\nu)\rangle. \qquad (3.190)\end{aligned}$$

From an algorithmic point of view, it is convenient to first calculate the matrix elements of $[\alpha\alpha]^{(2)}$, and then couple an extra variable α to it in order to obtain the reduced matrix elements of $[\alpha\alpha]^{(2)}\cdot\alpha$. On the one hand because it enables a transparent implementation and on the other hand since the reduced matrix elements of $[\alpha\alpha]^{(2)}$ need to be calculated anyway whenever second-order terms are included in the calculation of $T(E2)$ matrix elements. It is noteworthy that all these matrix elements can partly be calculated beforehand and recalled when a particular Hamiltonian is constructed for diagonalisation. This is particularly convenient for the part of the matrix elements, associated with the $O(5)$ substructure, since the rotation from the Cartan-Weyl basis to the physical basis cannot be done analytically[8] and demands considerable computation time. Concerning the $SU(1,1)$ substructure, it matters less whether the matrix elements have been determined beforehand or still need to be calculated at the time of constructing the Hamiltonian, since the matrix elements are known in closed form and can thus be incorporated by means of a function call.
It can be shown in general that all matrix elements can be factorised into two parts: one part depending on the $SU(1,1)$ quantum numbers, and the other part depending on the $O(5)$ quantum numbers. Indeed, the matrix element of α in the physical basis can be written as

$$\langle n'v'L'(\nu')M'|\alpha_\mu|nvL(\nu)M\rangle = \tfrac{1}{\sqrt{2k}}\langle n'v'L'(\nu')M'|(b^\dagger_\mu+\tilde{b}_\mu)|nvL(\nu)M\rangle. \quad (3.191)$$

Realising that the physical states can be developed in the Cartan-Weyl basis by means of the rotation, defined by the diagonalisation of $L\cdot L$ (see section 3.3)

$$|nvL(\nu)M\rangle = \sum_{XM_XM_Y}^{M_X+3M_Y=M} c^{nvL(\nu)M}_{vXM_XM_Y}|nvXM_XM_Y\rangle, \qquad (3.192)$$

we can rewrite the equation (3.191) as

$$\begin{aligned}\langle n'v'L'(\nu')M'|\alpha_\mu|nvL(\nu)M\rangle = \tfrac{1}{\sqrt{2k}}\sum_{XM_XM_Y}\sum_{X'M'_XM'_Y} c^{nvL(\nu)M}_{vXM_XM_Y}c^{n'v'L'(\nu')M'}_{v'X'M'_XM'_Y} \\ \times\langle n'v'X'M'_XM'_Y|(b^\dagger_\mu+\tilde{b}_\mu)|nvXM_XM_Y\rangle. \qquad (3.193)\end{aligned}$$

[8] regarding the present knowledge of the rotation (see section 3.3)

Inspecting equations (3.162) to (3.165), we realise that the matrix elements of α (and therefore also the reduced matrix elements) can be factorised in a part containing the n and λ quantum numbers of $SU(1,1)$ and a part containing the residual $O(5)$ quantum numbers

$$\langle n'v'L'(\nu')||\alpha||nvL(\nu)\rangle = \langle \lambda' n'|F_1|\lambda n\rangle \langle v'L'(\nu')||G_1||vL(\nu)\rangle, \tag{3.194}$$

where the functions $\langle n'\lambda'|F_1|n\lambda\rangle$ can be chosen as the matrix elements of β (see equations (3.168)). At this point it can be shown in a straightforward though tedious way that this factorisation persists when higher-order couplings of α are considered, i.e.

$$\langle n'v'L'(\nu')|||[\alpha\alpha]^{(2)}||nvL(\nu)\rangle = \langle \lambda' n'|F_2|\lambda n\rangle \langle v'L'(\nu')||G_2||vL(\nu)\rangle, \tag{3.195}$$

$$\langle n'v'L(\nu')|||[\alpha\alpha]^{(2)}\cdot\alpha||nvL(\nu)\rangle = \langle \lambda' n'|F_3|\lambda n\rangle \langle v'L(\nu')||G_3||vL(\nu)\rangle. \tag{3.196}$$

Here, the functions G_2 and G_3 are defined such as to meet the standard angular momentum recoupling relations

$$\begin{aligned}&\langle v'L'(\nu')||G_2||vL(\nu)\rangle \\ &\quad = \sqrt{5}(-)^{L+L_1}\sum_{v_2\nu_2L_2}\begin{Bmatrix} 2 & 2 & 2 \\ L_1 & L & L_2\end{Bmatrix}\langle v'L(\nu')||G_1||v_2L_2(\nu_2)\rangle \\ &\qquad \times \langle v_2L_2(\nu_2)||G_1||vL(\nu)\rangle,\end{aligned} \tag{3.197}$$

and

$$\begin{aligned}&\langle v'L(\nu')||G_3||vL(\nu)\rangle \\ &\quad = \tfrac{1}{\sqrt{2L+1}}\sum_{v_1\nu_1L_1}(-)^{L+L_1}\langle v'L(\nu')||G_2||v_1L_1(\nu_1)\rangle\langle v_1L_1(\nu_1)||G_1||vL(\nu)\rangle.\end{aligned} \tag{3.198}$$

As the functions G_i are well defined, we can calculate the associated factors F_i as well. The result of these calculations (upto $i = 3$) are given in appendix B.2.

3.4.2 Choice of the basis

From the results of the previous subsection, we can construct the matrix representation of the Hamiltonian as input for numerical diagonalisation procedures. As already mentioned, the Hilbert space of the collective model is infinite dimensional, which is intractable in theory. Typically, one makes use of an expansion method to circumvent this problem. The idea is to increase the dimension of the

Hilbert space until convergence is reached for the lowest eigenvalues within an acceptable error. To optimise this convergency process, we have a parameter in the $SU(1,1)$ basis at our disposal. Inspection of equations (3.186-3.187) and the functions F_i in appendix B.2 reveals that there is a dependency of the matrix representation on the $SU(1,1)$ basis parameter k, which is not determined by the dynamics of the Hamiltonian. Therefore, we can exploit this parameter in the quest towards the optimised basis with respect to convergency issues. In former calculations [Gne71, Hab74, Sei84], the dimension of the Hamiltonian was truncated upto 30 harmonic oscillator shells $(n = 15)$ to ensure convergency. In order to find the best values for the eigenvalues, the parameter k was varied to find the value which minimises the binding energy of the Hamiltonian. However, this method is a little cumbersome since one needs to scan the whole k parameter range for every different Hamiltonian, and moreover the convergency of this method is only guaranteed after close inspection and verification. To cure for the former problem, Margetan & Williams [Mar82] proposed a technique to predict a reasonable value of k, without the need of scanning the whole parameter range. This technique is based on a variational principle for the diagonal matrix elements of the Hamiltonian. The idea is to minimise the diagonal matrix elements of the lowest basis states so they lie already close to the actual eigenvalues, which will considerably enhance the convergency process. Due to limitations of computing power, the calculations were still truncated upto 30 harmonic oscillator shells, so the convergency was still to be verified a posteriori. This limitation can now be withdrawn, making use of present desktop computing power. Starting from the Margetan & Williams ansatz for the parameter k, the dimension of the Hamiltonian can be increased gradually up to the point where convergence is guaranteed. If accuracies of the order of 1eV are imposed, no more than 50 basis states need to be incorporated, which can be handled within a reasonable time (a couple of seconds) on a modern desktop computer.

It is worth mentioning that, with the development of the algebraic tractable model [Row04, Row05b, Tur05], an alternative method has been proposed to obtain a reasonable ansatz for k [Row05a]. This method is based on the physically intuitive idea that one can choose the eigenstates of an analytically solvable potential as a basis for a more complex Hamiltonian in such a way that the potential used in the basis mimics the behaviour of the potential of the Hamiltonian at the global minimum. As every analytically solvable potential can be chosen, the available bases are no longer limited to harmonic oscillators, but can be extended to e.g. Davidson type of potentials [Row05a].

As a consequence, we need to make a considerate choice about the convergence method to be used. For this purpose, a study has been undertaken to look for the most reliable method with respect to realistic Hamiltonians. The aim is to obtain a method, assuring sufficient convergence for a broad range of different potentials. Therefore, a transitional Hamiltonian covering the transitions from a spherical harmonic oscillator to a deformed γ-independent rotor has been constructed (see next section). The particular Hamiltonian can be written as follows

$$\hat{H}(\xi) = \frac{1}{2B_2}\pi \cdot \pi + (1-\xi)V_1 + \xi V_2, \tag{3.199}$$

with the potentials defined as

$$V_1 = c_2^1 \alpha \cdot \alpha, \tag{3.200}$$

$$V_2 = c_2^2 \alpha \cdot \alpha + c_4^2 (\alpha \cdot \alpha)^2, \tag{3.201}$$

where $c_2^1 = 50$ MeV, $c_2^2 = -50$ MeV and $c_4^2 = 625$ MeV. The mass parameter B_2 has been chosen so that $\hbar^2/B_2 = 1$ keV, which is a realistic value with respect to the irrotational assumption. V_1 describes a spherical harmonic oscillator, whereas V_2 describes a deformed γ-independent rotor with a global minimum at $\beta_0 = 0.2$ and depth $V(\beta_0) = -1$ MeV. It is noteworthy that for the case $\xi = 1/2$, the transitional potential becomes the critical β^4 potential.

For every value of ξ, 3 optimal guesses of the harmonic oscillator[9] basis parameter k have been calculated and for every guess, the basis was expanded until the 5 lowest eigenvalues have converged independently, within 1 eV. Once the basis has converged, the dimension of the resulting basis was plotted (see figure 3.6). It should be noted that the potential used at present has an $O(5)$ symmetry, which means that basis states with different seniority do not mix. Due to this symmetry, the diagonalisation can be handled solely within an $SU(1,1)$ framework without the need to include the $O(5)$ representations. The 3 guesses have been determined as follows

1. The first guess makes use of the technique of Margetan & Williams. In this particular case, k has been chosen such that the first 5 diagonal matrix elements are minimised. The dimension of the converged basis are given by the blue line in figure 3.6.

2. The second guess relies on the particular shape of the harmonic oscillator potential. The parameter k was adjusted such that the curvature of the basis potential becomes identical to the second derivative of the potential in

[9] In one of the cases, the basis has been extended to a Davidson-type of potential.

equation (3.199) at the global minimum. The resulting dimensions for this guess are represented by the black full line in the figure.

3. The third guess makes use of a Davidson-type of potential (see chapter 2.2.3). In this particular case, not only the curvature of the basis was adjusted, but also the position of the minimum of the basis potential was fitted to match the global minimum of the potential in equation (3.199). This is possible since the Davidson potential exhibits an extra parameter with respect to the harmonic oscillator, enabling a description of deformed structures. The results for this guess are depicted by the dashed line. It is worth mentioning that for values of $\xi \leqslant 1/2$, this guess coincides with the second guess, as the minimum of the potential is located at $\beta_0 = 0$.

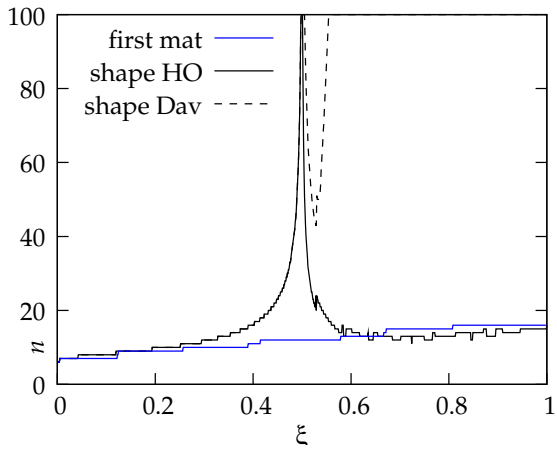

Figure 3.6: The dimensions of the bases, once convergence is reached. The number n denotes the quantum number n of the $SU(1,1)$ representations and coincides thus with half the number of harmonic oscillator shells (as $v = 0$).

Inspecting figure 3.6, one notices that the optimised harmonic oscillator bases (guesses 1 and 2, depicted by full lines) provide good convergence in the neighbourhood of the limiting cases of the transition path. For both methods, the eigenvalues have converged within $n \sim 15$ $SU(1,1)$ representations (which coincided with $N \sim 30$ harmonic oscillator shells). However, the situation is different in the vicinity of the β^4 potential ($\xi \sim 1/2$), where only the method of Margetan & Williams seems to provide reliable results. It is not surprising that the shape comparison method fails at this point, since the second derivative of β^4 iden-

tically vanishes at the minimum ($\beta = 0$). As a consequence, the curvature of the potential describing the basis is not well determined, and therefore we are confronted with divergencies. More surprising is the failure of the Davidson potential in defining a basis, since it was proposed and reported as a possible alternative basis to handle deformed potentials [Row05a]. The answer to this paradox lies in the fact that in the present study, the deformation β_0 at the global minima of the transitional Hamiltonians does not exceed the value $\beta_0 = 0.2$. Moreover the depth of the potential (order of magnitude 1 MeV) is not sufficient to localise the wavefunctions corresponding to the lowest eigenstates entirely into the well. As a result, these wavefunctions still exhibit a finite density at $\beta = 0$, something which cannot be described by a Davidson potential because of the repulsive nature of the potential at $\beta = 0$ (see figure 2.3).

Therefore and to conclude this study, we will make use of the method introduced by Margetan & Williams in all further applications since it provides robust and reliable results for a broad range of realistic Hamiltonians.

Section 3.5 Shape phase transitions

At the present point all necessary matrix elements have been constructed (section 3.4.1) and a reliable basis with good convergence properties is at hand (section 3.4.2). So we have all the ingredients to develop a computer code and study the properties of general type of collective Hamiltonians, both from a theoretical point of view as with respect to experimental data.

A first thing on the list is to study the transitional Hamiltonians, starting from spherical, going over γ-independent to end with axial deformed structures. These structures can all be described with the covering Hamiltonian (3.10)

$$\hat{H} = \tfrac{1}{2B_2}\pi\cdot\pi + c_2(\alpha\cdot\alpha) + c_3([\alpha\alpha]^2\cdot\alpha) + c_4(\alpha\cdot\alpha)^2. \tag{3.202}$$

3.5.1 Three limiting cases

Before addressing the transition paths, it is interesting to consider the three limiting cases which can be described using the Hamiltonian (3.202), i.e. the spherical-, γ-independent rotor and the axial rotor. These limits are respectively described

	$\hbar^2/B_2$	c_2	c_3	c_4
V_{spher}	4 keV	200 MeV	0 MeV	0 MeV
$V_{\gamma\text{-rot}}$	4 keV	-200 MeV	0 MeV	2500 MeV
V_{rot}	4 keV	-200 MeV	700 MeV	2500 MeV

Table 3.3: Parameters used in the potentials (3.203-3.205) of the Hamiltonian (3.202).

by the following potentials

$$V_{\text{spher}} = c_2^{\text{spher}}(\alpha \cdot \alpha), \tag{3.203}$$

$$V_{\gamma\text{-rot}} = c_2^{\gamma\text{-rot}}(\alpha \cdot \alpha) + c_4^{\gamma\text{-rot}}(\alpha \cdot \alpha)^2, \tag{3.204}$$

$$V_{\text{rot}} = c_2^{\text{rot}}(\alpha \cdot \alpha) + c_3^{\text{rot}}([\alpha\alpha]^{(2)} \cdot \alpha) + c_4^{\text{rot}}(\alpha \cdot \alpha)^2, \tag{3.205}$$

with the specific parameter choices for the different potentials as given in table 3.3. The motivation for these choices of the parameters is twofold. Within the restrictions of the given limit under study, the parameters have been chosen equal wherever possible. This allows us to relate the differences arising in the structure to the particular parameter which has been varied. On the other hand, although the sets of parameters give rise to schematic potentials, the connection with experimental observables was never totally neglected. As a consequence, the three Hamiltonians can each act as a starting point to a profound study of atomic nuclei where fingerprints of the given limiting cases have been observed.
One could argue that the parameters appear to be rather large, especially since it was demonstrated in section 3.1 that the general collective potential can be considered as a Taylor expansion in the collective quadrupole coordinate α. However, one should realise that the collective coordinates describe small deformations, which makes them small quantities by definition (typical order of magnitude $\beta_0 \sim 0.1$). Therefore, in order to contribute significantly to the structure of the potential at small deformation, the parameters of the higher-order terms need to be sufficiently large. If we consider e.g. $V_{\gamma\text{-rot}}$, we can compare the mutual effects of the parameters c_2 and c_4 around the global minimum $\beta_0 = 0.2$. Whereas c_2 lowers the potential with $200\,\text{MeV}(0.2)^2 = 8\,\text{MeV}$, c_4 gives a correction of $2500\,\text{MeV}(0.2)^4 = 4\,\text{MeV}$. As a result, the effect of c_4 is smaller than that of c_2, so we can still consider the Hamiltonian as a Taylor expansion.

We now discuss the three limiting Hamiltonians separately. For every Hamiltonian, the calculated observables have been obtained by means of the method described in the previous sections. Therefore, more than only a type-case study,

the next results serve as a genuine test for the presented technique.

The harmonic oscillator

We start with the harmonic oscillator potential V_{spher}. Contrary to the other two limiting cases, the harmonic oscillator potentials is a 'true' limit in the sense that it can be described by means of a spectrum generating algebra ($U(5)$ or $SU(1,1)$). The eigenvalues can be obtained analytically as was already profoundly discussed in chapter 2.2.2. Solving this potential numerically is therefore trivial since the basis we start from is chosen identical to the Hamiltonians eigenfunctions. We obtain a linear energy spectrum with large degeneracies, as can be seen in figure 3.7. There are two main reasons for these degeneracies. First of all, the Hamiltonian is an $O(5)$ invariant, which implies the degeneracy within a given seniority v. Secondly, the Hamiltonian can be identified with one of the generators of $SU(1,1)$, which makes $SU(1,1)$ a dynamical symmetry of the system. However,

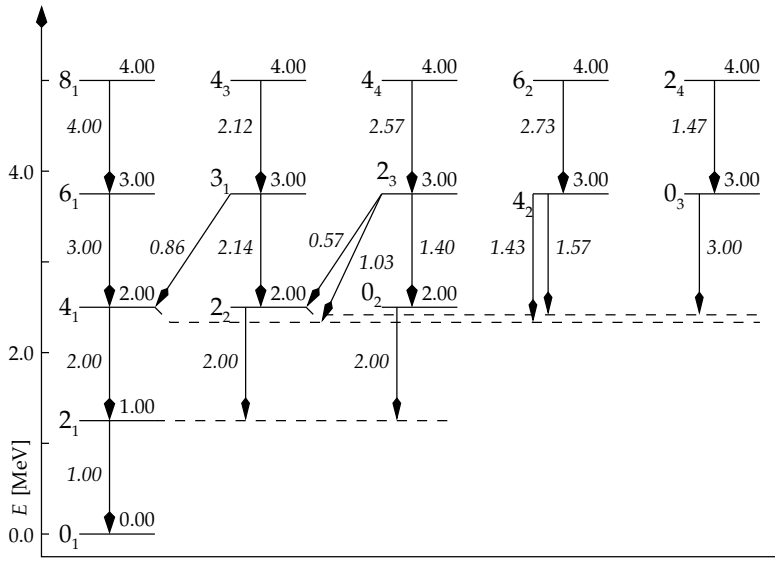

Figure 3.7: The energy spectrum and B(E2) values of a harmonic oscillator potential. Energy eigenvalues are given relative to the first $L = 2$ state and B(E2) values relative to $B(E2; 2_1 \rightarrow 0_1)$ (See the text for more details).

not every observable has the same symmetry properties as the Hamiltonian. In order to study B(E2) values or quadrupole moments, we need to know the ma-

trix elements of the collective coordinates α. It is clear from the previous sections that α is not an $O(5)$ invariant, which means that the B(E2) values distinguish between the different states within a seniority representation v. This is clearly visible in figure 3.7, where the states have been organised in bands, following the cascade of relatively large B(E2) values.
Within this figure, up to harmonic oscillator shell $N_{ho} = 3$, all eigenstates are given, together with all non-vanishing B(E2) values. For the $N_{ho} = 4$ excitation states, only the states which can be placed in one of the bands are depicted. Apart from the ground state band, one can notice that a $K = 2$ band, and two $K = 0$ bands, built on respectively the 2_2, 0_2, and 0_3 tend to develop according to the cascade of B(E2) values.
Within the figure, all eigenvalues are given relative to the excitation energy of the first excited 2_1 state, whereas the B(E2) values are given relative to the $B(E2; 2_1 \rightarrow 0_1)$ value. The absolute energy scale of the figure corresponds with the particular set of parameters for V_{spher} as given in table 3.3. The excitation energy of this 2_1 state is 1264.91 keV and the $B(E2; 2_1 \rightarrow 0_1) = 0.00158$ in units relative to $(3ZR_0^2)^2/(4\pi)^2$.

The γ-independent rotor

The second limit to be considered is the γ-independent rotor, described by the potential $V_{\gamma\text{-rot}}$. What makes this potential essentially different from the harmonic oscillator potential, is the occurrence of a global minimum at non-zero deformation β_0. Consequently, this potential is able to generate solutions which can be associated with definite deformations.
Although the Hamiltonian does not correspond to an algebraic solvable limit, still it exhibits some remarkable symmetry properties. Similar to the case of the harmonic oscillator, the Hamiltonian is an $O(5)$ invariant, leading towards degeneracies within a given representation v. This is illustrated in figure 3.8, where for all bands, except the one in the middle, the states with equal seniority v have the same eigenvalue. The main difference between $V_{\gamma\text{-rot}}$ and V_{spher} with respect to the covering group $SU(1,1)$ is that, although the Hamiltonian can be entirely written as a function of the generators of this group, it does not any longer form a dynamical symmetry for the Hamiltonian. In this particular case, it causes the $n \neq 0$ states of the harmonic oscillator to be lifted up in the spectrum. This is illustrated in figure 3.8 by the band in the middle, which lies much higher in the excitation spectrum than the corresponding band of the harmonic oscillator (figure 3.7).
Similar to figure 3.7, all eigenstates with an excitation energy, lower than or equal to the excitation energy of the 6_1 state are depicted in figure 3.8, together with

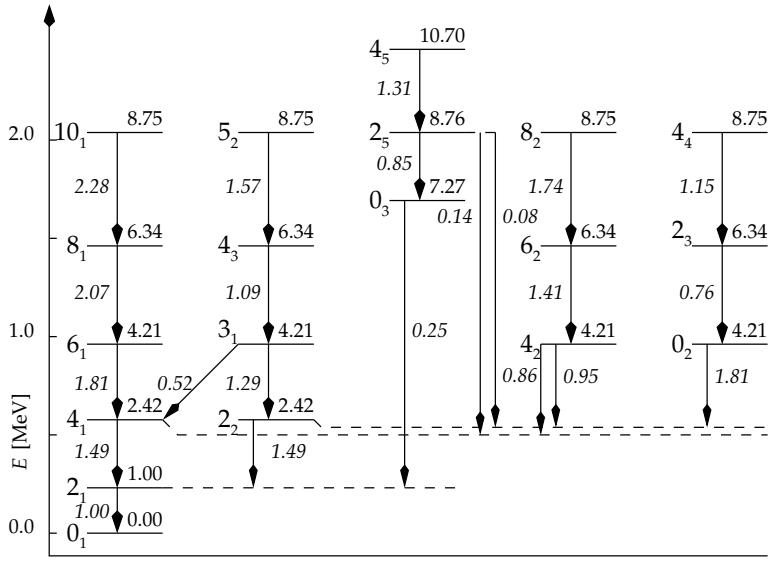

Figure 3.8: The energy spectrum and B(E2) values of a γ-independent rotor Hamiltonian. Energy eigenvalues are given relative to the first $L = 2$ state and B(E2) values relative to $B(\text{E2};2_1 \rightarrow 0_1)$ (see the text for details).

all non-vanishing B(E2) values. For the higher-lying excited states, only those states are given that fit into a given band, as well as the corresponding intraband B(E2) values to justify this classification. All eigenvalues are again given relative to the 2_1 state, which has an absolute excitation energy of 233.8 keV and the $B(E2; 2_1 \rightarrow 0_1)$=0.00759, measured in units $(3ZR_0^2)^2/(4\pi)^2$.

The axial deformed rotor

The third limit describes axial deformed rotational structures. In this particular case, we insert the term $[\alpha\alpha]^{(2)} \cdot \alpha$ in the potential, breaking all the remaining degeneracies from the γ-independent rotor case. Moreover, the classification into bands by following cascades of B(E2) values is even more pronounced as the bands all occur at different energy scales in the spectrum. Whereas the bands built on top of the 2_2 state in the harmonic oscillator and γ-independent rotor limit, had energy scales comparable with respect to the ground-state band energy scale, in this particular case, they are now observed at much higher excitation energies. This has been illustrated in figure 3.9 by the dashed box, pointing out that

the $K = 2$ and $K = 0$ band, built on top of respectively the 2_2 and 0_2 state, result in the spectrum above the 12_1 state of the groundband.
From an experimental point of view, this might be an unsatisfactory situation, as it can occur that the excitation bands, built on the 2_2 and 0_2 states, can descend low into the excitation spectrum, to side the rotational groundband (see e.g. ^{180}Hf [Wu03]). However, the chosen potential (3.205) does not contain many free parameters to tune the excitation energy of the associated bands while keeping the minimum at a physical deformation $\beta_0 \sim 0.1$. We can as well adjust the mass parameter B_2 of the kinetic energy. A decrease of the mass parameter would lead to an overall lowering of the excitation energy of the excited bands, but this would also affect the ground state band, which would lose its rotational character. To cope with this issue, a modified kinetic energy term was proposed in the GCM (3.8) in order to lower the excited bands without affecting the rotational structure of the bands.

In the figure 3.9, only the three lowest bands are depicted, with energies relative to the 2_1 state and B(E2) values relative to $B(E2; 2_1 \rightarrow 0_1)$. The excitation energy of the 2_1 state is 71.29 keV and $B(E2; 2_1 \rightarrow 0_1) = 0.01245$ in units of $(3ZR_0^2)^2/(4\pi)^2$.

We can compare the outcome of this calculation with the results obtained in the Rotation-Vibration model (RVM) [Fae62, Eis87]. The latter model starts from the assumption that an axially deformed nucleus can be described by means of a harmonic oscillator potential, both in γ and β around the minimum in the potential. Then the Bohr Hamiltonian can be analytically solved up to some approximations regarding the decoupling of the γ-rotational degrees of freedom. Now it would be interesting to treat the potential $V_{\gamma\text{-rot}}$ in the framework of the RVM and compare the approximate solutions with the full diagonalisation. The solutions of the RVM model can be written as [Eis87]

$$E_{LKn_2n_0} = [L(L+1) - K^2]\tfrac{1}{2}\varepsilon + [\tfrac{1}{2}|K| + 1 + 2n_2]E_\gamma + [n_0 + \tfrac{1}{2}]E_\beta, \qquad (3.206)$$

with K the angular momentum projection quantum number along the intrinsic axis and (n_2,n_0) the vibrational quantum numbers associated with respectively the vibrations in the γ- and β-direction. E_γ, E_β and ε are parameters, determined by the shape and localisation of the RVM potential. Rewriting the potential $V_{\gamma\text{-rot}}$ around the minimum $\beta_0 = 0.264$ as a Taylor expansion in β and γ, gives rise to the following parameters of the RVM: $E_\gamma = 1885.22$ keV, $E_\beta = 2093.96$ keV and $\epsilon = 19.15$ keV. Substituting these parameters in equation (3.206) gives some remarkable results, compared to the solutions of $V_{\gamma\text{-rot}}$ (see figure 3.9). First, the

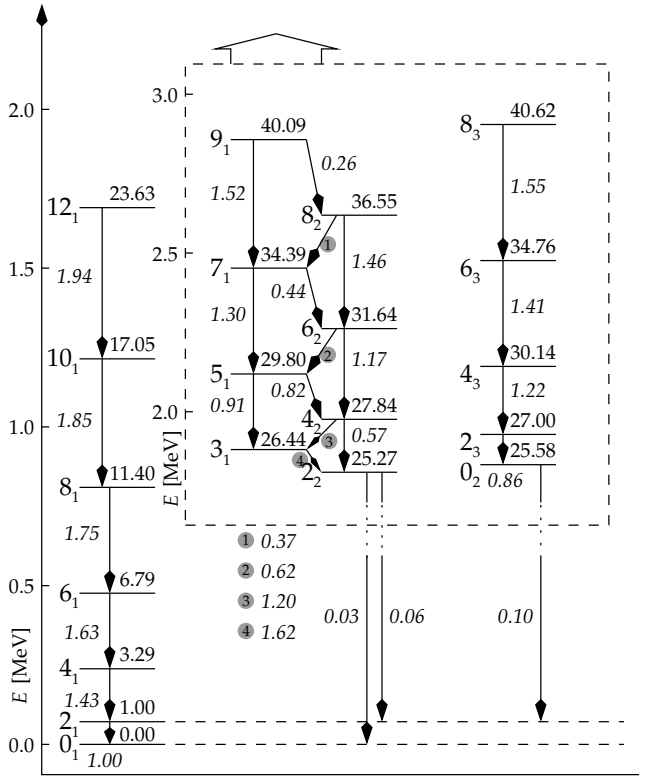

Figure 3.9: The energy spectrum and B(E2) values of an axial deformed rotor. Energy eigenvalues are given relative to the first $L = 2$ state and B(E2) values relative to $B(\mathrm{E2};2_1 \rightarrow 0_1)$. Details are described in the text.

spacing of the different levels within a given band are well reproduced by the parameter ε. Second, the position of the first $K = 2$ band is to be expected at $E_\gamma = 1888.22$ keV according to the RVM, something which is very well fulfilled as can be seen from figure 3.9. More interesting is the classification of the first excited $K = 0$-band, built on top of the 0_2 state. Within the language of the RVM model, we can either associate this band with a β- vibrational ($n_0 = 1, n_2 = 0$) or γ-vibrational ($n_0 = 0, n_2 = 1$). Substituting the corresponding quantum numbers (n_0, n_2) into equation (3.206) gives us the following predictions: the excitation energy of the 0_γ bandhead of the γ-vibrational band is to be expected at $2E_\gamma = 3770.44$ keV, whereas the 0_β bandhead of the β-vibrational band can be

found at $E_\beta = 2093.96$ keV. Comparison of these values with the excitation energies from the diagonalisation of the axial deformed Hamiltonian leads towards the conclusion that the lowest excited $K = 0$ band can best be associated with the β-band of the RVM.

To conclude, we can state that we are able to cover typical cases of collective potentials within the framework, developed in the present chapter. Therefore, we can start a study on transitional classes of Hamiltonians, for which the potentials discussed in the present section can serve as limiting benchmark potentials.

3.5.2 Along the transition paths

From the previous discussion, we know the specific structure of the Hamiltonian (3.202) in three limiting cases (spherical, γ-rotational and axial rotational). In the present section, we explore how these structures evolve when going over from one limit to another. We consider the three transitional Hamiltonians

$$\hat{H}_{12} = \frac{\hbar^2}{2B_2}\pi\cdot\pi + (1-\xi)V_{\text{spher}} + \xi V_{\gamma-\text{rot}}, \tag{3.207}$$

$$\hat{H}_{23} = \frac{\hbar^2}{2B_2}\pi\cdot\pi + (1-\xi)V_{\gamma-\text{rot}} + \xi V_{\text{rot}}, \tag{3.208}$$

$$\hat{H}_{31} = \frac{\hbar^2}{2B_2}\pi\cdot\pi + (1-\xi)V_{\text{rot}} + \xi V_{\text{spher}}, \tag{3.209}$$

for which we calculate the excitation energy and electric quadrupole observables along the transition path. The results are presented in the following figures. For easy comparison, the three different transition paths (respectively $\hat{H}_{12}$, $\hat{H}_{23}$ and $\hat{H}_{31}$) are plotted next to each other using the same scaling.

We start with the discussion of the energy spectra. In figure 3.10, the energy spectra are plotted as a function of ξ. In the left panel, the transition from the spherical to the γ-independent rotor is presented. Since $O(5)$ is a symmetry of both limits of the transition, it is also a symmetry for every intermediate Hamiltonian $\hat{H}_{12}$, which makes the seniority quantum number v a good quantum number along the whole path. As a consequence, together with the ground band, the bands, built on top of the 0_3 and 2_2 state in figure 3.7, are lowered in the energy spectrum as long as the associated states exhibit the same seniority quantum number v as the ground band states. The only band in the low-energy region which does not follow the trend of the ground band is the band, built on top of the 0_2 state of figure 3.7. Following the transition path from vibrational to γ-independent rotor limit, we notice that the 0_3 state of the γ independent rotor (figure 3.8) originates from the 0_2 state in the vibrational limit (figure 3.7), so these two states undergo a pure

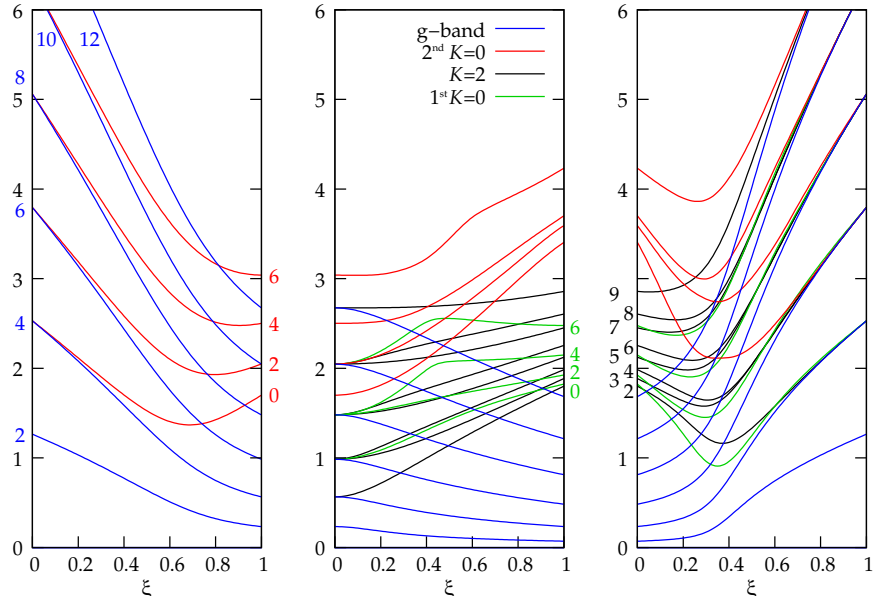

Figure 3.10: The energy spectra for the transitional Hamiltonians (3.207, 3.208 & 3.209) as a function of ξ.

crossing at $\xi = 0.75$. From the B(E2) values (see figure 3.11), one can also see that the band on top of the 0_2 (up to $\xi = 0.75$) state behaves differently from the lower-lying excited bands, as the $B(E2; 0_2 \rightarrow 2_1)/B(E2; 2_1 \rightarrow 0_1)$ value decreases faster than the values $B(E2; L_1 \rightarrow (L-2)_1)/B(E2; 2_1 \rightarrow 0_1)$ of the ground-band members or even the $B(E2; 3_1 \rightarrow 2_2)/B(E2; 2_1 \rightarrow 0_1)$. In order to simplify the notation, it is convenient to introduce the following quantity

$$R(E2, L_i \rightarrow L_f) = \frac{B(E2; L_i \rightarrow L_f)}{B(E2; 2_1 \rightarrow 0_1)}, \tag{3.210}$$

for the B(E2) values, relative to $B(E2; 2_1 \rightarrow 0_1)$ as plotted in figure 3.11.

In the middle panel of figure 3.10, the transition from the γ-independent to axial deformed rotor is plotted (see equation 3.208). By introducing the seniority breaking term $[\alpha\alpha] \cdot \alpha$ in the Hamiltonian, the remaining $O(5)$ symmetry of the γ-independent rotor is lifted. This happens in a rather prompt way for small values of ξ, so the development into separate bands rapidly appears into the spectrum. At the right-end of the transition path ($\xi = 1$), a clear picture arises with

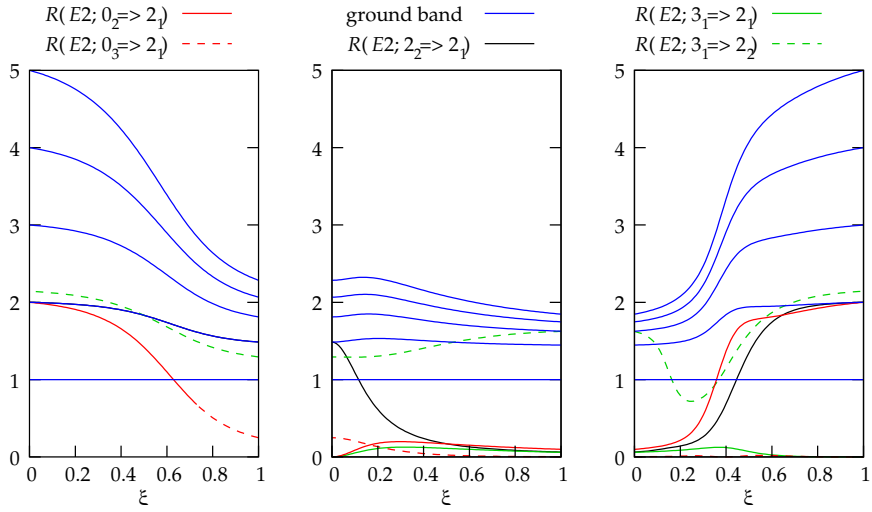

Figure 3.11: Selected B(E2) values along the transition lines, relative to the $B(E2; 2_1 \rightarrow 0_1$ transition (see equation (3.210)).

separate rotational and vibrational-like bands at different energy scales. The fact that the states can now unambiguously be organised into bands is also reflected in the $R(E2, L_i \rightarrow L_f)$ values in the middle panel of figure 3.11. There it can be seen that the value $R(E2, 2_2 \rightarrow 2_1)$ quickly drops while $R(E2, 3_1 \rightarrow 2_2)$ stays reasonable unaffected along the transition line, which clearly points out that 2_2 and 3_1 can be positioned into the same ($K = 2$) band. This band is depicted in the dashed box of figure 3.9.

In the right panel of figure 3.10, we close the circle by studying the transition from the axial deformed limit to the vibrational limit. It can be seen from that figure that this transition is less gradual, compared to the harmonic oscillator to γ-independent rotor transition. In the latter case, only the $U(5)$ (or $SU(1,1)$) symmetry was broken, whereas in the present case, also the $O(5)$ symmetry is immediately broken by adding the $[\alpha\alpha]^{(2)} \cdot \alpha$ term in the Hamiltonian.

There is something peculiar to be noted about the total of the three panels of figure 3.10, concerning the identification of the $K = 0$ bands as γ- or β-vibrational band. From the comparison of the axial deformed limit with the predictions made by RVM, we could unambiguously identify the lowest $K = 0$ (built on the 0_2 state)

as the β-vibrational band. This can further be justified if we follow the transition path towards the harmonic oscillator, as depicted in the right panel of figure 3.10. We notice that this β-vibrational band (green lines) evolves towards the states with $SU(1,1)$ quantum number $n = 1$. As an example, the 0_2 state of the axial deformed rotor develops into the $(n = 1, v = 0)$ state of the vibrational limit. From the discussion of the harmonic oscillator (chapter 2.2.2), we know that the quantum number n can be associated to the number of β-phonons. Consequently, the β-vibrational character of the lowest $K = 0$ band of the axial deformed rotor is further justified, as it evolves from the significant β-vibrational quantum number ($n = 1$) of the harmonic oscillator limit. However, this is not the only path to reach the harmonic oscillator. One could go the opposite way in figure 3.10, and follow the transition from axial deformed rotor to harmonic oscillator limit via the γ-independent rotor limit. Following e.g. the 0_2 state along each transition (middle and left panel) , we find that in this case, we end up in the $(n = 0, v = 3)$ state, which cannot be associated with β-vibrations as the $SU(1,1)$ quantum number n is equal to zero. The solution to this paradox lies in the middle panel of figure 3.10. From this panel, it is clear that all states in the γ-independent to axial rotor limit are subject to considerable mixing and 'no-crossing' effects, due to the large admixture of states with different seniority quantum numbers. Moreover, as the 0_3 of the γ-independent rotor limit clearly evolves from the 0_2, $(n = 1, v = 0)$ state of the harmonic oscillator, we can state that the 0_2 and 0_3 state must have switched nature along the transition path from γ-independent to axial deformed rotor. As a conclusion, caution is necessary when associating $K = 0$ bands with β- or γ vibrational structures, as considerable mixing effects can arise along the transition paths, perturbing the clear picture of vibrational motion along the β- or γ direction.

Apart from the relative B(E2) values, it is also interesting to calculate the absolute B(E2) values, as they give an indication of the collective deformation of an atomic nucleus [Eis87]. In figure 3.12, the $B(E2; 2_1 \rightarrow 0_1)$ values are presented along the different transition paths. One can clearly see that, going from the harmonic oscillator to the γ-rotational limit, the $B(E2; 2_1 \rightarrow 0_1)$ value rises steadily, due to the manifestation of a deformed minimum in the potential. This rise persists in the transition from the γ-independent rotor to the rotational limit, as the onset of the terrm $[\alpha\alpha] \cdot \alpha$ in the potential breaks the symmetry in the γ-direction, driving the minimum in the potential towards prolate structures. Finally, along the rotational to vibrational transition path, the $B(E2; 2_1 \rightarrow 0_1)$ drops back to the originally value of the spherical harmonic oscillator.

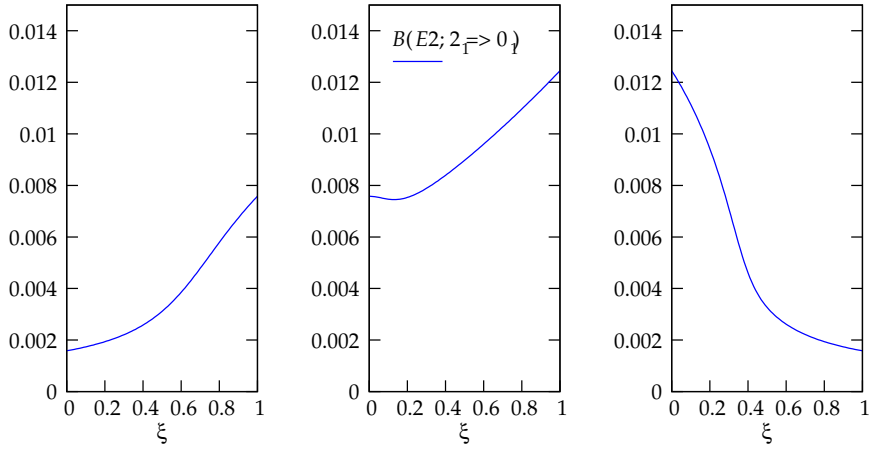

Figure 3.12: $B(E2; 2_1 \rightarrow 0_1)$ values along the different transition paths, given in units $(3ZR_0^2)^2/(4\pi)^2$.

Similar conclusions can be drawn from a study of the spectroscopic quadrupole moment of the first excited 2_1 state, defined by (if the same linear approximation of $\hat{T}(E2)$ is used when calculating the B(E2) values [Eis87])

$$Q = \sqrt{\frac{16\pi}{5}}\langle 2_1 M = 2|\hat{T}(E2)|2_1 M = 2\rangle, \tag{3.211}$$

$$= \sqrt{\frac{16\pi}{5}}\frac{3ZR_0^2}{4\pi}\begin{pmatrix} 2 & 2 & 2 \\ -2 & 0 & 2 \end{pmatrix}\langle 2_1||\alpha||2_1\rangle. \tag{3.212}$$

The results for Q are presented in figure 3.13. Contrary to the other figures, the transition from the harmonic oscillator to the γ-independent rotor is not depicted since, within the linear approximation of $\hat{T}(E2)$, the selection rules for α ($\Delta v = \pm 1$) render the quadrupole moments identically zero along the whole transition path. Here again, we can see that, as soon as the seniority-breaking term in the potential is turned on (along both transition paths), the quadrupole moment sharply rises (in absolute value) to reach a maximum at the rotational limit. It can be noticed that this rise is more pronounced in the transition from the γ-independent rotor to rotational limit as compared with the transition from the spherical to rotational limit. The explanation for this difference stems from the fact that in the former transition the potential already exhibits a deformed minimum in the β direction, while in the latter transition the minimum in the

β direction is steadily developing from the spherical minimum towards a minimum at a distinct deformation β_0.

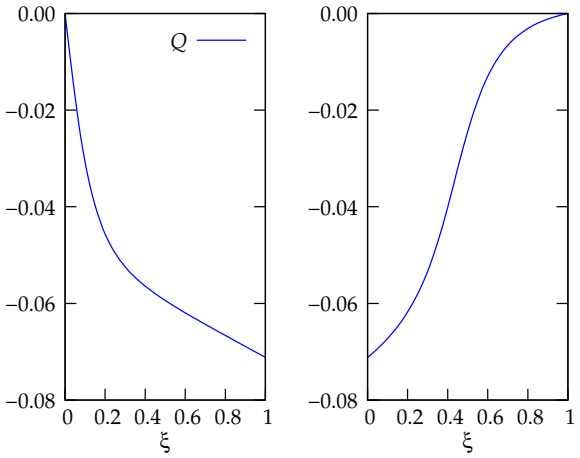

Figure 3.13: The quadrupole moments of the first excited 2_1 state, given in units $\sqrt{16\pi/5}(3ZR_0^2)/(4\pi)$. The transition from harmonic oscillator to the γ-independent rotor is not depicted as the quadrupole moments are identically zero.

As a conclusion, we have studied the schematic transitions from spherical over γ-independent towards axial deformed rotational structures in the collective model. For this purpose, we made use of the Cartan-Weyl framework, as presented in this thesis. This schematic study can be considered as a thorough test for the formalism, as the obtained results can be confronted with the already available knowledge on this subject. We have now come to a crossroad with multiple open tracks. Supported by the results of the present study, one can extend the Hamiltonian to more complex and realistic structures, such as e.g. triaxiality or shape coexistence. For this purpose, we need to include higher-order terms in the Taylor expansion, as it is impossible to describe these structures using the tractable and schematic collective Hamiltonian (3.202), studied in the present section. From a theoretical point of view, it will be interesting to see how this enlargement of the phase space will affect the structure of this Hamiltonian. Later on, these insights might be exploited, once this collective Hamiltonian is confronted with experimental data, specially in the light of the recent developments in exotic beam

facilities, (such as e.g. SPIRAL 2).

It's tough to make predictions,
especially about the future

Yogi Berra

4

CONCLUSIONS AND OUTLOOK

Section 4.1 The geometrical collective model, ...

The atomic nucleus is a fairly complex system. Although the number of constituent particles is relatively small (up to a couple of hundred), it is a tremendous, if not overwhelming task to perform ab-initio nuclear structure calculations starting but from the free nucleon-nucleon interaction. In order to grasp an understanding of the large variety of phenomena observed in nuclear structure physics through experiments, physicists are obliged to resort to theoretical models. One major benchmark is the *Collective model* developed by Aage Bohr and Ben Mottelson [Boh52, Boh53], which interpretes the atomic nucleus as a macroscopic charged liquid drop, disregarding the internal structure of the droplet. The physical motivation for this assumption is that the constituent particles cooperate in a collective coherent way to form the excitation modes of the atomic nucleus, giving rise to deformations of the surface. It soon became clear that this model could account for vibrational or rotational modes of motion, observed in the low-energy excitation spectra of atomic nuclei away from closed shells.

Apart from some schematic cases, solving the Schrödinger equation of the Bohr Hamiltonian can become quite involved. A major milestone was set by the General Collective Model [Gne71], which enabled the numerical construction of a matrix representation of the Hamiltonian within a $SU(1,1) \times O(5)$ Lie-algebraic framework. However, as $SU(1,1)$ is a *non-compact* group, the Hilbert space is infinite dimensional, leading towards numerical complexities with respect to the convergence in the model space. This might be the reason why the GCM was eclipsed during the previous decades by the Interacting Boson Model [Iac87], which was conceived as a unifying model to cover both vibrational ($U(5)$) and rotational ($SU(3)$) structures. Based on representations of the *compact* enveloping $U(6)$ group, the IBM Hilbert space could be truncated to finite dimensions, de-

pending on the number of valence particles outside the closed shells. As a result, numerically tractable calculations could be performed within the IBM, resulting in realistic descriptions of collective nuclear structure with a firm connection to microscopic (shell) models by means of mapping procedures.

With the dawn of quantum *shape* transitions in the Interacting Boson Model, the collective model reclaimed considerable attention. It was pointed out that transition points from the vibrational limit to rotational limits of the IBM can quite adequately be described with an infinite well potential in the collective model, the so-called $E(5)$ and $X(5)$ solutions [Iac00, Iac01]. This result reopened the doorway to the collective model, its special solutions, algebraic properties and potential applications to experimental data.

The present thesis focuses on several aspects of the collective model. In a first chapter (chapter 2), analytically solvable potentials in the intrinsic framework are discussed. In the maiden paper on the collective Hamiltonian, Bohr already introduced the harmonic oscillator potential in 5D as an analytically solvable potential. More than just an academic curiosity, this potential has proven to be a significant benchmark of collectivity in vibrational-like atomic nuclei not far from the closed shells. Subsequently, a variety of potentials have been proposed with the aim of describing different facets of collective motion. One particularly interesting facet covers the topic of *triaxiality*, which is the phenomenon were spheroidal atomic nuclei exhibit three intrinsic main axes with different lengths. In section 2.3, a schematic potential of the Wilets & Jean type is studied, where a Davidson potential is chosen for the β-part, whereas the γ-part is modeled by means of a harmonic oscillator potential confining the triaxiality to the vicinity of a free parameter γ_0. This potential can be approximately solved, making use of a $SU(1,1)_\beta \times SU(1,1)_\gamma$ scheme. It was applied to the chain of Os isotopes, for which evidence of triaxiality has been previously reported both by experimental as well as theoretical studies. The conclusions from the present study are, that this type of schematic potential can render a reasonably well description of soft-triaxial nuclei within the limitations of the approximations. (see section 2.3.3)

One of these approximations causes the violation of γ-periodicity, emerging naturally from the collective model. Therefore, in chapter 2.4, an analytic solvable Pöschl-Teller potential has been constructed, preserving the periodicity in γ. This potential has the remarkable property that its minimum occurs at maximal triaxiality $\gamma = \pi/6$. Although the geometry of the associated ellipsoid is maximally asymmetric at $\gamma = \pi/6$, the rotational part of the Bohr Hamiltonian can be diag-

onalised exactly using an $O(3)$ algebra with projection quantum number along the intrinsic x-axis. However, there is a cost involved: the symmetry is only valid at the absolute minimum $\gamma = \pi/6$. So to exploit the symmetry, we need to freeze out the γ-dependence to the average value at the minimum of the potential. To check the validity of this approximation, the potential has been diagonalize exactly. The general conclusion of this diagonalisation is that the freeze-out approximation inserts minor deviations from the exact description, which justifies the approximation a posteriori. The main asset of the Pöschl-Teller potential with respect to the solvability is also the major drawback concerning applicability: the restriction to $\gamma = \pi/6$ structures. Nevertheless, some remarkable cases of maximal triaxiality were previously marked in the Pt isotopes, so they formed the ideal testcase for the potential. A single-parameter fit (apart from a scaling factor) on this chain of isotopes demonstrated that the schematic Pöschl-Teller potential is able to rather adequately describe the energy spectrum of ^{196}Pt as a γ-soft rotor in the vicinity of maximal triaxiality.

In chapter 3, the field of schematic potentials is abandoned, resorting to more general polynomial potentials. These potential are considered general within the assumption that every potential can be developed as a Taylor expansion in the collective variables, with the constraint that they describe small deviations from a spherical shape. As a result, with respect to numerical matrix representations of the collective Hamiltonian, we need the matrix elements of the collective variables in a suitable basis. It turns out that the natural Cartan-Weyl reduction scheme of the $SU(1,1) \times O(5)$ algebra provides an eligible framework to construct the matrix elements. Starting from the commutation relations and explicit expressions of the generators of $SU(1,1)$ as well as $O(5)$, an intermediate state method can be exploited to derive closed expressions for the matrix elements of the collective variables (section 3.2.4) , the canonic conjugate momenta (section 3.2.5) and the associated spin-2 phonon creation and annihilation operators (section 3.2.6). It is noteworthy that this technique is utterly algebraic in the sense that no explicit representation in terms of γ and β nor heighest weight states have to be constructed. However, working in the Cartan-Weyl basis of $SU(1,1) \times O(5)$ has the drawback that the $O(5) \supset O(4) \cong SU(2) \times SU(2)$ reduction is not compatible with the $O(3)$ rotational symmetry, observed in experimental spectra. To construct basis states with good angular momentum L (and M), the rotation of the Cartan-Weyl basis to the $O(3)$ basis has to be carried out explicitly, as discussed in section 3.3. Once the collective variables have been determined, calculating the necessary matrix elements in the Hamiltonian corresponds to standard angular momentum recoupling, so the matrix representations of all (even and odd) terms

in the Hamiltonian can be constructed.

From a numerical point of view, the use of the Cartan-Weyl framework provides an estimable platform with respect to precision and computer time. Concerning computer time, the bottleneck of the calculation is the rotation of the Cartan-Weyl basis to the angular momentum basis. However, the dimensions of the matrix representations of the $O(3)$ Casimir operator $L \cdot L$ stay reasonably small with respect to present desktop computing standards as long as low seniority quantum numbers are used. In any case, the rotation is independent of the matrix representation of the Hamiltonian, and can thus be extracted once and stored for later use. Since the matrix elements of the collective variables are analytically in the Cartan-Weyl basis, any precision loss is due to the rotation of the natural to the physical basis. Sufficiently accurate numerical procedures are available (e.g the lapack routines) for this purpose.

Currently, a computer code is under development in the nuclear structure theory group of Ghent to diagonalise general collective Hamiltonians within the Cartan-Weyl scheme, for which the theoretical framework is presented in the present thesis.

Section 4.2 ... an ongoing story.

Therefore, the story is not finished with this thesis. Once the computer code, based on the Cartan-Weyl scheme, is compiled and sufficiently tested, it can be deployed in the study of collectivity accross the nuclear chart. It will be interesting to investigate e.g. to what extent general Hamiltonians can improve on the description of triaxiality in the Os and Pt isotopes with respect to the schematic potentials (chapter 2) and how they position to other theoretical studies in this region, such as PES (potential energy surface) [Ben87] and IBM calculations [Har97, McC05]. For this purpose, a systematic study of the physical meaning of the different parameters used in the potential is needed. Along a similar line, it would be interesting to investigate the effect of a density-dependent nucleon-nucleon interaction on the parameters of the potential in a semi-classical framework (chapter 3.1) and a profound study of the mass parameter in the kinetic energy must be undertaken to validate the irrotational hypothesis and how to correct for it. It is clear that these questions and remarks can and will be addressed making use of the code, resulting from the theoretical framework described in this thesis.

From a more theoretical perspective, we can extend the study on shape phase transitions. In the present manuscript, the transitions from vibrational over γ-independent to axial deformed structures have been investigated. This partly as a complementary view to the widely used Interacting Boson Model based studies on the topic, and partly as a thorough (and successful) test of the Cartan-Weyl based formalism. At the present point, it will be very interesting to see how more involved structures, such as triaxiality or shape coexistence, can arise when the Hamiltonian is extended to higher-order terms in the Taylor expansion.
Another line of research would be to what extent the current Cartan-Weyl scheme can be widened to higher-order multipole excitation modes as e.g. considerable B(E4) hexadecupole strengths have been observed in the Pt isotopes (chapter 2.4.4), admixing with the quadrupole degrees of freedom. The $L = 4$ hexadecupole collective variable has 9 angular momentum projections, which means that the Cartan-Weyl basis involves the reduction of $O(9)$. As the reduction of $O(5)$ is already quite knotty and lengthy, it is not clear at present whether the hexadecupole phonon is still manageable within the framework we have developed in chapter 3.
Not only from a theoretical point of view, but also with the aim at numerical improvements, an extension of the standard Clebsch-Gordan recoupling towards non-commuting $SU(2)$ coupling might shed light on the problem of the missing quantum number in the reduction of the $O(5)$ group to the physical $O(3)$ group with respect to the natural $SU(2) \times SU(2)$ subgroup. If the non-commuting Clebsch-Gordan coefficients would be known, the bottleneck in the calculation of the quadrupole variable matrix elements could be withdrawn, opening a pathway to even more sophisticated potentials which require larger Hilbert spaces.

To conclude the conclusions, I feel tempted to address these topics right away, though, to quote one of the songs of the late Johnny Cash who was vividly alive in my .mp3 playlist during the months of the thesis writing:

> *If there's a light up ahead, well brother I don't know.*
> *But I got this fever burnin' in my soul.*

What is the matrix?

Neo – *The Matrix*

A

MATRIX ELEMENTS OF THE TRIAXIAL DEFORMED DAVIDSON MODEL

ABSTRACT

This appendix contains the matrix elements, needed in the diagonalisation of the rigid triaxial Davydov model and the triaxial deformed Davidson potential (section 2.3). Also the matrix elements for the exact treatment of the Pöschl-Teller potential of the second kind are discussed (section 2.4).

Section A.1 Angular momentum generators.

In order to diagonalise the Davydov Hamiltonian (2.53) or the rotational part of the triaxial deformed Davidson potential (2.57), we need a good basis in which both the intrinsic ($\hat{L}'_i$) and lab-frame angular momenta ($\hat{L}_i$) can be diagonalized. According to Racah [Rac42], the complex conjugate Wigner-D functions [Ros57] have a good $O(3)$ tensorial character. Acting with the angular momentum raising and lowering operators

$$\hat{L}_\pm = L_1 \pm i\hat{L}_2, \tag{A.1}$$

on the Wigner-D functions gives (with $\hat{L}_0 = \hat{L}_3$)

$$\hat{L}_+ D^{l*}_{mm'} = \sqrt{(l-m)(l+m+1)}\, D^{l*}_{m+1,m'}, \tag{A.2}$$

$$\hat{L}_- D^{l*}_{mm'} = \sqrt{(l+m)(l-m+1)}\, D^{l*}_{m-1,m'}, \tag{A.3}$$

$$\hat{L}_0 D^{l*}_{mm'} = m D^{l*}_{mm'}, \tag{A.4}$$

for the lab frame, and

$$\hat{L}'_{+} D^{l*}_{mm'} = \sqrt{(l+m')(l-m'+1)} D^{l*}_{m,m'-1}, \tag{A.5}$$

$$\hat{L}'_{-} D^{l*}_{mm'} = \sqrt{(l-m')(l+m'+1)} D^{l*}_{m,m'+1}, \tag{A.6}$$

$$\hat{L}'_{0} D^{l*}_{mm'} = m' D^{l*}_{mm'}, \tag{A.7}$$

for the intrinsic frame. Therefore,the complex conjugate Wigner-D functions are suitable to construct a basis. Because of symmetry considerations [Boh52, Eis87] of the ellipsoid, only a subset of all Wigner-D functions are contained in the basis. The wavefunctions, symmetric under all transformations leaving an ellipsoid invariant, are given by

$$|LMK\rangle = \sqrt{\frac{2L+1}{16\pi^2(1+\delta_{K0})}} (D^{L*}_{MK} + (-1)^L D^{L*}_{M-K}), \tag{A.8}$$

with K even. Now we have the ingredients to calculate the matrix elements $\langle LMK'|\hat{L}'^2_i|LMK\rangle$, needed for the matrix representation of rotational Hamiltonians. The special structure of the $K = 0$ states demands a special treatment. Since

$$|LM0\rangle = \sqrt{\frac{2L+1}{8\pi^2}} D^{L*}_{M0}, \tag{A.9}$$

we obtain

$$\langle LM0|\hat{L}'^2_1|LM0\rangle = \tfrac{1}{2} L(L+1), \tag{A.10}$$

$$\langle LM0|\hat{L}'^2_2|LM0\rangle = \tfrac{1}{2} L(L+1), \tag{A.11}$$

$$\langle LM0|\hat{L}'^2_3|LM0\rangle = 0. \tag{A.12}$$

For the same reason, the matrix elements $\langle LM0|\hat{L}'_i|LM2\rangle$ also require a special treatment

$$\langle LM0|\hat{L}'^2_1|LM2\rangle = \tfrac{1}{2\sqrt{2}} \sqrt{(L-1)L(L+1)(L+2)}, \tag{A.13}$$

$$\langle LM0|\hat{L}'^2_2|LM2\rangle = -\tfrac{1}{2\sqrt{2}} \sqrt{(L-1)L(L+1)(L+2)}, \tag{A.14}$$

$$\langle LM0|\hat{L}'^2_3|LM2\rangle = 0. \tag{A.15}$$

The general case is given by

$$\begin{aligned}
\langle LMK'|\hat{L}_1^2|LMK\rangle &= \tfrac{1}{2}(L(L+1)-K^2)\delta_{K'K} \\
&\quad + \tfrac{1}{4}\sqrt{(L-K)(L-K-1)(L+K+1)(L+K+2)}\delta_{K'K+2} \\
&\quad + \tfrac{1}{4}\sqrt{(L+K)(L+K-1)(L-K+1)(L-K+2)}\delta_{K'K-2}, \\
\langle LMK'|\hat{L}_2^2|LMK\rangle &= \tfrac{1}{2}(L(L+1)-K^2)\delta_{K'K} \\
&\quad - \tfrac{1}{4}\sqrt{(L-K)(L-K-1)(L+K+1)(L+K+2)}\delta_{K'K+2} \\
&\quad - \tfrac{1}{4}\sqrt{(L+K)(L+K-1)(L-K+1)(L-K+2)}\delta_{K'K-2}, \\
\langle LMK'|\hat{L}_3^2|LMK\rangle &= K^2\delta_{K'K}.
\end{aligned} \tag{A.16}$$

Now we are in the position to construct the matrix representation of rotational Hamiltonians of the form

$$\hat{H} = \sum_i A_i \hat{L}_i'^2. \tag{A.17}$$

A typical example is given by the $L = 2$ states. Since the only allowed K states are $K = 0$ and $K = 2$, we have a two dimensional matrix

$$\hat{H}_{(L=2)} = \begin{pmatrix} 3A_1 + 3A_2 & \sqrt{3}(A_1 - A_2) \\ \sqrt{3}(A_1 - A_2) & A_1 + A_2 + 4A_3 \end{pmatrix}. \tag{A.18}$$

The eigenvalues of this matrix are given by

$$\omega_\pm = 2\sum_i A_i \pm 2\sqrt{\sum_i A_i^2 - \sum_{i<j} A_i A_j}, \tag{A.19}$$

with associated eigenstates

$$|2M\rangle = a_0^2|2M0\rangle + a_2^2|2M2\rangle. \tag{A.20}$$

The coefficients in the wavefunction are given by

$$a_0^2 = -\frac{V}{\sqrt{V^2 + (B \mp W)^2}}, \qquad a_2^2 = \frac{B \mp W}{\sqrt{V^2 + (B \mp W)^2}}, \tag{A.21}$$

with

$$B = A_1 + A_2 - 2A_3, \quad W = 2\sqrt{\sum A_i^2 - \sum A_i A_j}, \quad V = \sqrt{3}(A_1 - A_2). \tag{A.22}$$

Section A.2 Quadrupole moments

The quadrupole moment of a state with angular momentum L_i^+ is defined by [Eis87]

$$Q = \sqrt{\frac{16\pi}{5}} \begin{pmatrix} L & 2 & L \\ -L & 0 & L \end{pmatrix} \langle n_\beta n_\gamma L_i || \hat{T}(E2) || n_\beta n_\gamma L_i \rangle. \tag{A.23}$$

Up to first order in α_μ, the quadrupole transition operator $\hat{T}(E2)$ is given by

$$\hat{T}(E2)_\mu = \frac{3ZR_0^2}{4\pi} \alpha_\mu^*. \tag{A.24}$$

Since the wavefunction of the triaxial deformed Davidson Hamiltonian can be factorised into a β and a γ-rotational part and the collective coordinate can be written as (equation (2.5))

$$\alpha_\mu = \beta[\cos\gamma D^{2*}_{\mu 0} + \tfrac{1}{\sqrt{2}} \sin\gamma (D^{2*}_{\mu 2} + D^{2*}_{\mu -2})], \tag{A.25}$$

the calculation of the quadrupole moment falls apart in a β- and a γ-rotational part. The β-part is relatively simple as the first 2_1^+ state is a $n_\beta = 0$ excitation. The wavefunction reads (with $\tilde{v}(\tilde{v}+3) = \omega + B_D$ and ω defined by 2.62)

$$\xi_{(n_\beta=0)}(\beta) = \sqrt{\tfrac{2}{\Gamma(\tilde{v})}} A_D^{\tilde{v}/4} \beta^{\tilde{v}-5/2} e^{-\frac{\sqrt{A_D}}{2}\beta^2}. \tag{A.26}$$

The β-part is then

$$\langle n_\beta = 0 | \beta | n_\beta = 0 \rangle = \int_0^\infty |\xi_{(n_\beta=0)}(\beta)|^2 \beta^5 d\beta = \tfrac{\Gamma(\tilde{v}+1/2)}{A_D^{1/4}\Gamma(\tilde{v})}. \tag{A.27}$$

The γ-rotational part is a little more cumbersome, as we need to calculate them in the same approximative scheme as the energy spectrum calculations. Defining the following operator

$$O^2_{mk} = \sqrt{\tfrac{1}{2(1+\delta_{k0})}} \left(D^2_{mk} + D^2_{m-k} \right), \tag{A.28}$$

we can rewrite the complex conjugate quadrupole coordinate α_m^*

$$\alpha_m^* = \beta \left[O^2_{m0} \cos\gamma + O^2_{m2} \sin\gamma \right]. \tag{A.29}$$

The reduced matrix elements with respect to the lab frame magnetic quantum number M in the rotational basis (A.8) are then[1]

$$\begin{aligned}\langle L'K'||O^2_k||LK\rangle = &\sqrt{\tfrac{(2L'+1)(2L+1)}{(16\pi^2)^2(1+\delta_{K'0})(1+\delta_{K0})}}\sqrt{\tfrac{2}{1+\delta_{k0}}}\langle L'||D^2||L\rangle \\ &\left[(-)^{L'}\begin{pmatrix} L' & L & 2\\ K' & -K & k\end{pmatrix} + (-)^{L'+L}\begin{pmatrix} L' & L & 2\\ K' & K & k\end{pmatrix}\right. \\ &\left. +(-)^{L}\begin{pmatrix} L' & L & 2\\ -K' & K & k\end{pmatrix} + \begin{pmatrix} L' & L & 2\\ -K' & -K & k\end{pmatrix}\right].\end{aligned} \tag{A.30}$$

The γ-degree of freedom is contained in the goniometric part ($\cos\gamma$,$\sin\gamma$) of the quadrupole coordinate. Within the freeze-out approximation ($\gamma = \gamma_0 + x$), we can rewrite them as

$$\begin{aligned}\cos(\gamma_0 + x) &= \cos\gamma_0\cos x - \sin\gamma_0\sin x \approx \cos\gamma_0(1-\tfrac{x^2}{2}) - \sin\gamma_0 x,\\ \sin(\gamma_0 + x) &= \sin\gamma_0\cos x + \cos\gamma_0\sin x \approx \sin\gamma_0(1-\tfrac{x^2}{2}) + \cos\gamma_0 x.\end{aligned} \tag{A.31}$$

Let us define the following boson operators

$$b^\dagger = \tfrac{1}{\sqrt{2\sqrt{C}}}\left(\sqrt{C}x - ip\right), \qquad b = \tfrac{1}{\sqrt{2\sqrt{C}}}\left(\sqrt{C}x + ip\right), \tag{A.32}$$

that close under boson commutation relations $[b, b^\dagger] = 1$. If we construct the following operators

$$\hat{B}_+ = \tfrac{1}{2}b^\dagger b^\dagger, \tag{A.33}$$
$$\hat{B}_- = \tfrac{1}{2}bb, \tag{A.34}$$
$$\hat{B}_0 = \tfrac{1}{2}(b^\dagger b + \tfrac{1}{2}), \tag{A.35}$$

we can see that they span an $SU(1,1)$ algebra with representations $|\lambda n\rangle$, defined by [Row98]

$$\hat{\mathcal{C}}_{SU(1,1)}|\lambda n\rangle = \tfrac{1}{4}\lambda(\lambda-2)|\lambda n\rangle, \tag{A.36}$$
$$\hat{B}_0|\lambda n\rangle = \tfrac{1}{2}(\lambda+2n)|\lambda n\rangle, \tag{A.37}$$
$$\hat{B}_+|\lambda n\rangle = \sqrt{(\lambda+n)(n+1)}|\lambda, n+1\rangle, \tag{A.38}$$
$$\hat{B}_-|\lambda n\rangle = \sqrt{(\lambda+n-1)n}|\lambda, n-1\rangle. \tag{A.39}$$

[1] Care has to be taken as the operator O^2_{mk} has $O(3)$ tensorial character 2 with projection $-m$.

The Casimir operator of the present 1D realisation of the $SU(1,1)$ algebra is a plain constant

$$\hat{C}_{SU(1,1)} = -\tfrac{3}{16}. \tag{A.40}$$

Thus, the Casimir quantum numbers λ can take the two values $\lambda = 1/2$ or $\lambda = 3/2$. We can associate a physical interpretation to the quantum numbers n and λ. Acting with $\hat{B}_0$ on the lowest-weight state $|\lambda 0\rangle$ gives

$$\hat{B}_0|\lambda 0\rangle = \tfrac{\lambda}{2}|\lambda 0\rangle, \tag{A.41}$$

$$b^\dagger b|\lambda 0\rangle = (\lambda - \tfrac{1}{2})|\lambda 0\rangle. \tag{A.42}$$

Because the operator $b^\dagger b$ counts the number of b-bosons in a given state, we can conclude that the $\lambda = 1/2$ lowest-weight state corresponds to the boson vacuum $|\theta\rangle$ and the $\lambda = 3/2$ lowest-weight state contains precisely one boson. Acting with $\hat{B}_+$ on the lowest-weight states increases the boson number with an amount of 2, which means that we can label the even number of boson states with $\lambda = 1/2$ and the odd number of bosons with $\lambda = 3/2$. Since

$$|\lambda n\rangle = \frac{(\hat{B}_+)^n}{\sqrt{(\lambda+n-1)(\lambda+n-2)...(\lambda+1)\lambda}\sqrt{n!}}|\lambda 0\rangle, \tag{A.43}$$

we obtain

$$|\tfrac{1}{2}n\rangle = \frac{(b^\dagger)^{2n}}{\sqrt{2n!}}|\theta\rangle, \qquad |\tfrac{3}{2}n\rangle = \frac{(b^\dagger)^{2n+1}}{\sqrt{(2n+1)!}}|\theta\rangle \tag{A.44}$$

The connection of n with the γ-vibration quantum number n_γ of equation (2.62) is clear from the explicit (x) realisation of $\hat{B}_0$,

$$4\sqrt{C}\hat{B}_0 = -\frac{\partial^2}{\partial x^2} + Cx^2. \tag{A.45}$$

As a result, we obtain the relation $2n_\gamma + 1 = 4n + 2\lambda$. For the lowest 2_1^+ state holds $n_\gamma = 0$, which corresponds to the $SU(1,1)$ representation $|1/2, 0\rangle$. To obtain the (approximative) matrix elements of $\cos\gamma$ and $\sin\gamma$ for this state, we need the matrix elements of the linear and quadratic term in x (A.31). The linear term $x = 1/\sqrt{2\sqrt{C}}$ can only mix even ($\lambda = 1/2$) with odd ($\lambda = 3/2$) states and is therefore irrelevant for the calculation of quadrupole moments. The quadratic term can be rewritten in terms of the $SU(1,1)$ generators

$$x^2 = \tfrac{1}{\sqrt{C}}(2\hat{B}_0 - \hat{B}_+ - \hat{B}_-). \tag{A.46}$$

As a result, we obtain the matrix elements

$$\begin{aligned}\langle n_\gamma = 0|\cos\gamma|n_\gamma = 0\rangle &\approx \cos\gamma_0(1-\tfrac{1}{4\sqrt{C}}),\\ \langle n_\gamma = 0|\sin\gamma|n_\gamma = 0\rangle &\approx \sin\gamma_0(1-\tfrac{1}{4\sqrt{C}}).\end{aligned} \tag{A.47}$$

Recalling that the rotational eigenstate can be written as (A.20),

$$|2M\rangle = a_0^2|2M0\rangle + a_2^2|2M2\rangle, \tag{A.48}$$

we can combine all results (A.27, A.30 and A.47) to obtain the expression of the quadrupole moment of the first 2_1^+ state

$$Q_{2_1^+} = \sqrt{\frac{16\pi}{5}}\begin{pmatrix}2 & 2 & 2\\ 2 & 0 & -2\end{pmatrix}\frac{3ZR_0^2}{4\pi}\langle 2_1^+||\alpha_2^*||2_1^+\rangle \tag{A.49}$$

$$= \sqrt{\tfrac{1}{5\pi}}\tfrac{6}{7}ZR_0^2\frac{\Gamma(\tilde{v}+1/2)}{A_D^{1/4}\Gamma(\tilde{v})}(1-\tfrac{1}{4\sqrt{C}})[\cos\gamma_0(a_2^2-a_0^2)+2a_2a_0\sin\gamma_0]. \tag{A.50}$$

Section A.3 — Matrix elements in the Legendre basis

In this appendix, we summarise the techniques to calculate the necessary matrix elements for section 2.4 in the basis of the associated Legendre functions using recursion relations, which largely reduces the computational effort.
The orthonormal form of the Associated Legendre functions, with weight function $\sin(3\gamma)$ over the interval $\gamma \in [0, \pi/3]$, is

$$\overline{P}_q^m(\cos(3\gamma)) = \sqrt{\frac{3}{2}(2q+1)\frac{(q-m)!}{(q+m)!}}P_q^m(\cos(3\gamma)), \tag{A.51}$$

where we distinguish the normalised functions $\overline{P}_q^m(\cos(3\gamma))$ from the unnormalised $P_q^m(\cos(3\gamma))$, defined in [Arf01]. The aim is to calculate matrix elements of a given function $f(\gamma)$

$$F_{qp}^m := \int_0^{\pi/3}\overline{P}_q^m(\cos(3\gamma))f(\gamma)\overline{P}_p^m(\cos(3\gamma))\sin(3\gamma)d\gamma. \tag{A.52}$$

Note that $q, p = m, m+1, ...$ for a specific basis and that F_{qp}^m is symmetric under exchange of q and p.
Making use of recursion relations for the Associated Legendre functions [Arf01],

we can deduce two recursion relations for the matrix elements

$$\sqrt{\tfrac{(q-m)(q+m)}{(2q+1)(2q-1)}}F^m_{qp} = \sqrt{\tfrac{(p-m)(p+m)}{(2p+1)(2p-1)}}F^m_{q-1,p-1} + \sqrt{\tfrac{(p+1-m)(p+m+1)}{(2p+1)(2p+3)}}F^m_{q-1,p+1} - \sqrt{\tfrac{(q+m-1)(q-m-1)}{(2q-1)(2q-3)}}F^m_{q-2,p}, \tag{A.53}$$

$$\sqrt{\tfrac{(p+m)(p+m-1)}{(2p+1)(2p-1)}}F^m_{qp} = \sqrt{\tfrac{(q+m)(q+m+1)}{(2q+1)(2q-1)}}F^{m-1}_{q-1,p-1} - \sqrt{\tfrac{(q-m+1)(q-m+2)}{(2q+1)(2q+3)}}F^{m-1}_{q+1,p-1} + \sqrt{\tfrac{(p-m)(p+m-1)}{(2p-1)(2p-3)}}F^m_{q,p-2}. \tag{A.54}$$

Rule (A.54) connects matrix elements from different basis functions that differ in $\Delta m = \pm 1$. We choose $m = 1$ because of the relevance for the present study. Now, rule (A.53) reduces a great amount of the computational work. Matrix elements with fixed q can easily be obtained as long as the matrixelements with $q-1$ and $q-2$ are known (see figure A.1). This rule is still valid when $q = m+1$, but fails for $q = m$. Thus, this still leaves the matrix elements F^m_{mp} to be calculated, or taking our choice into account, F^1_{1p}.

A.3.1 $\cos\gamma$ and $\sin\gamma$ transition matrix elements

In order to calculate $E2$-transition rates, the matrix elements of $\cos\gamma$ and $\sin\gamma$ need to be evaluated. We denote them by

$${}^sM^m_{qp} = \int_0^{\pi/3} \overline{P}^m_q(\cos(3\gamma))\sin\gamma\overline{P}^m_p(\cos(3\gamma))\sin(3\gamma)d\gamma, \tag{A.55}$$

$${}^cM^m_{qp} = \int_0^{\pi/3} \overline{P}^m_q(\cos(3\gamma))\cos\gamma\overline{P}^m_p(\cos(3\gamma))\sin(3\gamma)d\gamma. \tag{A.56}$$

Using rule (A.53), leaves us to calculate

$${}^sM^1_{1p} = \int_0^{\pi/3} \overline{P}^1_1(\cos(3\gamma))\sin\gamma\overline{P}^1_p(\cos(3\gamma))\sin(3\gamma)d\gamma, \tag{A.57}$$

$${}^cM^1_{1p} = \int_0^{\pi/3} \overline{P}^1_1(\cos(3\gamma))\cos\gamma\overline{P}^1_p(\cos(3\gamma))\sin(3\gamma)d\gamma. \tag{A.58}$$

Inserting the specific forms of the Associated Legendre functions

$$P^1_1(\cos(3\gamma)) = \sin(3\gamma), \qquad P^1_p(\cos(3\gamma)) = -\frac{1}{3}\frac{\partial}{\partial\gamma}P_p(\cos(3\gamma)), \tag{A.59}$$

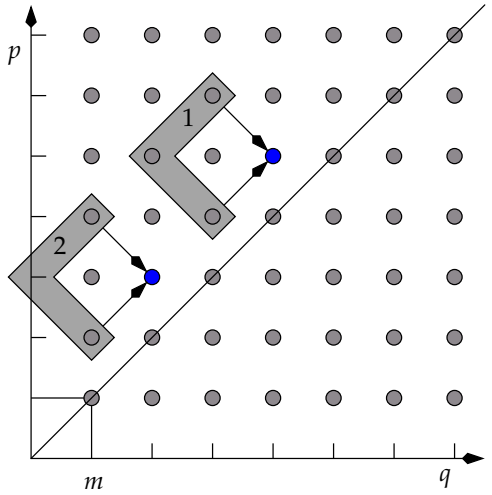

Figure A.1: Visual representation of rule (A.53). An unknown matrix element can be expressed in terms of the known elements inside the boomerang (1). Boomerang (2) points out that F^m_{mp} cannot be obtained by rule (A.53) and are still to be calculated. (Taken from [DB06])

and performing a partial integration, we obtain the result

$$ {}^{s}M^1_{1p} = \tfrac{1}{2}\sqrt{\tfrac{3}{2}\tfrac{2p+1}{p(p+1)}}\int_0^{\pi/3}\frac{\partial}{\partial\gamma}\left[\sin\gamma\sin^2(3\gamma)\right]P_p(\cos(3\gamma))d\gamma, \tag{A.60} $$

$$ {}^{c}M^1_{1p} = \tfrac{1}{2}\sqrt{\tfrac{3}{2}\tfrac{2p+1}{p(p+1)}}\int_0^{\pi/3}\frac{\partial}{\partial\gamma}\left[\cos\gamma\sin^2(3\gamma)\right]P_p(\cos(3\gamma))d\gamma. \tag{A.61} $$

The derivatives can be worked out

$$ \frac{\partial}{\partial\gamma}\left[\sin\gamma\sin^2(3\gamma)\right] = \tfrac{1}{2}\sin(3\gamma)\left[7\sin(4\gamma)-5\sin(2\gamma)\right], \tag{A.62} $$

$$ \frac{\partial}{\partial\gamma}\left[\cos\gamma\sin^2(3\gamma)\right] = \tfrac{1}{2}\sin(3\gamma)\left[7\cos(4\gamma)+5\cos(2\gamma)\right]. \tag{A.63} $$

So, the calculation of the matrix elements (A.60) and (A.61), essentially reduces to calculating integrals of the general form

$$ \begin{aligned} {}^{s}U^m_p &= \int_0^{\pi/3}\sin(m\gamma)P_p(\cos(3\gamma))\sin(3\gamma)d\gamma, \\ {}^{c}U^m_p &= \int_0^{\pi/3}\cos(m\gamma)P_p(\cos(3\gamma))\sin(3\gamma)d\gamma. \end{aligned} \tag{A.64} $$

After two partial integrations and, applying recursion relations for Legendre polynomials along the way, we obtain for the integrals

$$\begin{aligned} {}^sU_p^m &= \tfrac{3}{[m^2-(3(p+1))^2]}\left(\left[\sin(m\gamma)P_p(\cos(3\gamma))\cos(3\gamma)\right]_0^{\pi/3} + 3{}^sV_{p-1}^m\right), \\ &= \tfrac{3}{[m^2-(3(p+1))^2]}\left((-1)^{p+1}\sin(\tfrac{m\pi}{3}) + 3{}^sV_{p-1}^m\right), \end{aligned} \tag{A.65}$$

$$\begin{aligned} {}^cU_p^m &= \tfrac{3}{[m^2-(3(p+1))^2]}\left(\left[\cos(m\gamma)P_p(\cos(3\gamma))\cos(3\gamma)\right]_0^{\pi/3} + 3{}^cV_{p-1}^m\right), \\ &= \tfrac{3}{[m^2-(3(p+1))^2]}\left((-1)^{p+1}\cos(\tfrac{m\pi}{3}) - 1 + 3{}^sV_{p-1}^m\right), \end{aligned} \tag{A.66}$$

with

$$\begin{aligned} {}^sV_p^m &= \int_0^{\pi/3}\sin(m\gamma)\frac{\partial P_p(\cos(3\gamma))}{\partial\cos(3\gamma)}\sin(3\gamma)d\gamma, \\ &= {}^sV_{p-2}^m + (2q-1){}^sU_{p-1}^m, \end{aligned} \tag{A.67}$$

$$\begin{aligned} {}^cV_p^m &= \int_0^{\pi/3}\cos(m\gamma)\frac{\partial P_p(\cos(3\gamma))}{\partial\cos(3\gamma)}\sin(3\gamma)d\gamma, \\ &= {}^cV_{p-2}^m + (2p-1){}^cU_{p-1}^m, \end{aligned} \tag{A.68}$$

where the relationship

$$\frac{d}{dx}P_p(x) = \frac{d}{dx}P_{p-2}(x) + (2p-1)P_{p-1}(x), \tag{A.69}$$

has been used in the last step.
Finally, we have obtained a coupled recursion relations between the U and V integrals. The only integrations that need to be carried out are ${}^sV_0^m$, ${}^cV_0^m$ and ${}^sV_1^m$, ${}^cV_1^m$. The former are identically zero ($P_0 = 1$) while the latter can be calculated exactly

$${}^sV_1^m = \frac{3\sin\left(\frac{m\pi}{3}\right)}{9-m^2}, \tag{A.70}$$

$${}^cV_1^m = \frac{3\left(1+\cos\left(\frac{m\pi}{3}\right)\right)}{9-m^2}. \tag{A.71}$$

A.3.2 Moments of inertia

To diagonalise the Hamiltonian with the $1/\sin^2 3\gamma$ potential (2.4.3), we have to calculate the matrix elements of the soft moments of inertia $\mathcal{J}_i$, appearing in the denominator.

$$\frac{1}{\mathcal{J}_i} = \frac{1}{\sin^2(\gamma - \frac{2\pi i}{3})}. \tag{A.72}$$

We use the notation

$$ {}^{i}A^{m}_{qp} := \int_0^{\pi/3} \frac{\overline{P}^{m}_{q}(\cos(3\gamma))\overline{P}^{m}_{p}(\cos(3\gamma))}{\sin^2(\gamma - \frac{2\pi i}{3})} \sin(3\gamma) d\gamma. \tag{A.73} $$

Again, using rule (A.53), combined with the specific form of the Associated Legendre functions (A.59), the computational effort is largely reduced, and we obtain

$$ {}^{i}A^{1}_{1p} = -\frac{1}{2}\sqrt{\frac{3}{2}\frac{2p+1}{p(p+1)}} \int_0^{\pi/3} \frac{\frac{\partial}{\partial\gamma}P_p(\cos(3\gamma))}{\sin^2(\gamma - \frac{2\pi i}{3})} \sin^2(3\gamma) d\gamma. \tag{A.74} $$

We multiply nominator and denominator with the factor $\prod_{k\neq i}\sin^2(\gamma - \frac{2\pi k}{3})$, and take the property $\sin(\gamma - \frac{2\pi}{3})\sin(\gamma - \frac{4\pi}{3})\sin(\gamma - \frac{6\pi}{3}) = -\frac{1}{4}\sin(3\gamma)$ into account. Then we obtain

$$ {}^{i}A^{1}_{1p} = -8\sqrt{\frac{3}{2}\frac{2p+1}{p(p+1)}} \int_0^{\pi/3} \prod_{k\neq i}\sin^2(\gamma - \tfrac{2\pi k}{3}) \frac{\partial}{\partial\gamma}P_p(\cos(3\gamma)) d\gamma. \tag{A.75} $$

Performing a partial integration gives

$$ \begin{aligned} {}^{i}A^{1}_{1p} = 8\sqrt{\frac{3}{2}\frac{2p+1}{p(p+1)}} \Bigg[& \int_0^{\pi/3} \frac{\partial}{\partial\gamma}\left(\prod_{k\neq i}\sin^2(\gamma - \tfrac{2\pi k}{3})\right) P_p(\cos(3\gamma)) d\gamma \\ & + \frac{9}{16}(\delta_{i3} - (-1)^q\delta_{i2})\Bigg]. \end{aligned} \tag{A.76} $$

Substituting

$$ \frac{\partial}{\partial\gamma}\left(\prod_{k\neq i}\sin^2(\gamma - \tfrac{2\pi k}{3})\right) = -\sin(3\gamma)\cos(\gamma - \tfrac{2\pi i}{3}), \tag{A.77} $$

in equation (A.76), we obtain as a final result

$$ {}^{i}A^{1}_{1p} = 8\sqrt{\frac{3}{2}\frac{2p+1}{p(p+1)}} \left[\frac{9}{16}(\delta_{i3} - (-1)^p\delta_{i2}) - {}^{i}B_p\right], \tag{A.78} $$

with

$$ {}^{i}B_p = \int_0^{\pi/3} \cos(\gamma - \tfrac{2\pi i}{3}) P_p(\cos(3\gamma)) \sin(3\gamma) d\gamma. \tag{A.79} $$

Making use of the property $\cos(\gamma - \frac{2\pi i}{3}) = \cos\gamma\cos(\frac{2\pi i}{3}) + \sin\gamma\sin(\frac{2\pi i}{3})$, the integral ${}^{i}B_p$ can be rewritten in terms of the ${}^{c}U_p^1$ and ${}^{s}U_p^1$ integrals (A.64), thus reducing the original problem of evaluating the necessary matrix elements of the rotational part of the Hamiltonian, to the integrals involved in the study of E2 transition probabilities (appendix A.3.1)

$$ {}^{i}B_p = \cos(\tfrac{2\pi i}{3}){}^{c}U_p^1 + \sin(\tfrac{2\pi i}{3}){}^{s}U_p^1. \tag{A.80} $$

I'm the operator,
with my pocket calculator

Kraftwerk

B

OPERATORS AND MATRIX ELEMENTS IN THE CARTAN-WEYL BASIS

Section B.1 Operators

The generators L_M and O_M can explicitly be expressed in terms of the collective variables and their canonic conjugate momenta according to the definition (3.13)

$$L_M = -\frac{i\sqrt{10}}{\hbar}[\alpha\pi^*]^1_M = -\frac{i\sqrt{10}}{\hbar}\sum_{\mu\mu'}\langle 2\mu 2\mu'|1M\rangle\alpha_\mu\pi^*_{\mu'}, \tag{B.1}$$

$$O_M = -\frac{i\sqrt{10}}{\hbar}[\alpha\pi^*]^3_M = -\frac{i\sqrt{10}}{\hbar}\sum_{\mu\mu'}\langle 2\mu 2\mu'|3M\rangle\alpha_\mu\pi^*_{\mu'}, \tag{B.2}$$

where $\langle j_1 m_1 j_2 m_2|j_3 m_3\rangle$ are the commonly known Clebsch-Gordan coefficients. Taking the rotation to the Cartan representation into account (3.17), explicit and relatively simple expressions for the generators can be obtained

$$X_+ = \tfrac{i}{\hbar}(\alpha_2\pi^*_{-1} - \alpha_{-1}\pi^*_2), \qquad Y_+ = \tfrac{i}{\hbar}(\alpha_2\pi^*_1 - \alpha_1\pi^*_2), \tag{B.3}$$

$$X_- = \tfrac{-i}{\hbar}(\alpha_1\pi^*_{-2} - \alpha_{-2}\pi^*_1), \qquad Y_- = \tfrac{-i}{\hbar}(\alpha_{-1}\pi^*_{-2} - \alpha_{-2}\pi^*_{-1}), \tag{B.4}$$

$$X_0 = \tfrac{-i}{2\hbar}(\alpha_2\pi^*_{-2} + \alpha_1\pi^*_{-1} - \alpha_{-1}\pi^*_1 - \alpha_{-2}\pi^*_2), \tag{B.5}$$

$$Y_0 = \tfrac{-i}{2\hbar}(\alpha_2\pi^*_{-2} - \alpha_1\pi^*_{-1} + \alpha_{-1}\pi^*_1 - \alpha_{-2}\pi^*_2), \tag{B.6}$$

$$T_{\frac{1}{2}\frac{1}{2}} = \tfrac{-i}{\hbar\sqrt{2}}(\alpha_2\pi^*_0 - \alpha_0\pi^*_2), \qquad T_{-\frac{1}{2}\frac{1}{2}} = \tfrac{-i}{\hbar\sqrt{2}}(\alpha_1\pi^*_0 - \alpha_0\pi^*_1), \tag{B.7}$$

$$T_{\frac{1}{2}-\frac{1}{2}} = \tfrac{-i}{\hbar\sqrt{2}}(\alpha_{-1}\pi^*_0 - \alpha_0\pi^*_{-1}), \qquad T_{-\frac{1}{2}-\frac{1}{2}} = \tfrac{-i}{\hbar\sqrt{2}}(\alpha_{-2}\pi^*_0 - \alpha_0\pi^*_{-2}). \tag{B.8}$$

Section B.2 Matrix elements

The matrix elements of α, $[\alpha\alpha]^{(2)}$ and $[\alpha\alpha]^{(2)} \cdot \alpha$ can be factorised in a part containing the quantum numbers n and $\lambda = v + \frac{5}{2}$ of $SU(1,1)$ and a part containing the residual quantum numbers of $O(5)$ (see chapter 3.4)

$$\langle n'v'L'(\nu')||\alpha||nvL(\nu)\rangle = \langle \lambda' n'|F_1|\lambda n\rangle \langle v'L'(\nu')||G_1||vL(\nu)\rangle, \tag{B.9}$$

$$\langle n'v'L'(\nu')||[\alpha\alpha]^{(2)}||nvL(\nu)\rangle = \langle \lambda' n'|F_2|\lambda n\rangle \langle v'L'(\nu')||G_2||vL(\nu)\rangle, \tag{B.10}$$

$$\langle n'v'L(\nu')||[\alpha\alpha]^{(2)} \cdot \alpha||nvL(\nu)\rangle = \langle \lambda' n'|F_3|\lambda n\rangle \langle v'L(\nu')||G_3||vL(\nu)\rangle. \tag{B.11}$$

Due to selection rules, only a limited number of these matrix elements differ from zero. The functions G_i are determined by means of standard angular momentum recoupling relations (see chapter 3.4), which govern the selection rules for the angular momentum quantum numbers $L \to L'$ in G_i. The functions F_i are built from the matrix elements $\langle \lambda' n'|\beta|\lambda n\rangle$, which means that the selection rules for the quantum numbers n and λ are built from the selection rules for the matrix elements of β. The non-vanishing functions F_i are depicted in figure B.1 and are given as following.

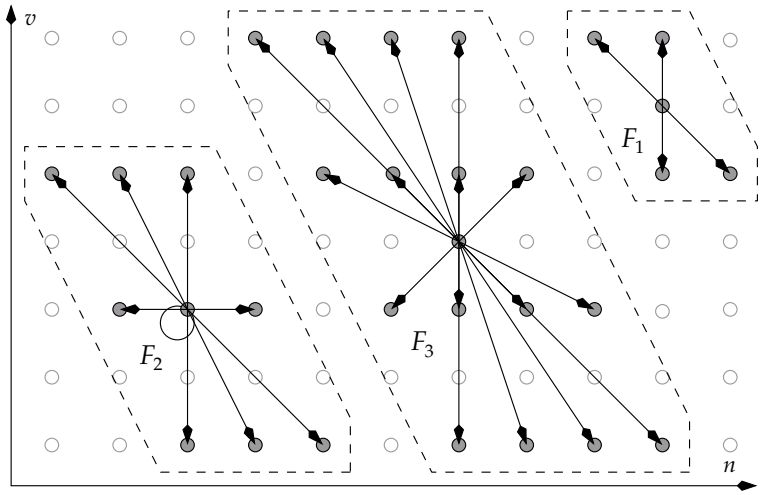

Figure B.1: Graphical representation of the non-vanishing functions $\langle n'\lambda'|F_i|\lambda n\rangle$ for $i = 1, 2, 3$.

1. The functions F_1 are chosen identical to the matrix elements $\langle n'\lambda'|\beta|\lambda n\rangle$, so they can only relate seniority quantum numbers that differ one unit $v' = v \pm 1$

   - $v' = v + 1$

$$\begin{aligned}\langle \lambda+1, n|F_1|\lambda n\rangle &= \tfrac{1}{\sqrt{k}}\sqrt{\lambda+n},\\ \langle \lambda+1, n-1|F_1|\lambda n\rangle &= \tfrac{1}{\sqrt{k}}\sqrt{n},\end{aligned} \tag{B.12}$$

   - $v' = v - 1$

$$\begin{aligned}\langle \lambda-1, n+1|F_1|\lambda n\rangle &= \tfrac{1}{\sqrt{k}}\sqrt{n+1},\\ \langle \lambda-1, n|F_1|\lambda n\rangle &= \tfrac{1}{\sqrt{k}}\sqrt{\lambda+n-1}.\end{aligned} \tag{B.13}$$

2. The functions F_2 are built from the product from two F_1 functions, therefore they connect seniority quantum number differing 2, 0 or -2 in units.

   - $v' = v + 2$

$$\begin{aligned}\langle \lambda+2, n|F_2|\lambda n\rangle &= \tfrac{1}{k}\sqrt{(\lambda+n)(\lambda+n+1)},\\ \langle \lambda+2, n-1|F_2|\lambda n\rangle &= \tfrac{2}{k}\sqrt{n(\lambda+n)},\\ \langle \lambda+2, n-2|F_2|\lambda n\rangle &= \tfrac{1}{k}\sqrt{n(n-1)},\end{aligned} \tag{B.14}$$

   - $v' = v$

$$\begin{aligned}\langle \lambda, n+1|F_2|\lambda n\rangle &= \tfrac{1}{k}\sqrt{(n+1)(\lambda+n)},\\ \langle \lambda, n|F_2|\lambda n\rangle &= \tfrac{1}{k}(\lambda+2n),\\ \langle \lambda, n-1|F_2|\lambda n\rangle &= \tfrac{1}{k}\sqrt{n(\lambda+n-1)},\end{aligned} \tag{B.15}$$

   - $v' = v - 2$

$$\begin{aligned}\langle \lambda-2, n+1|F_2|\lambda n\rangle &= \tfrac{1}{k}\sqrt{(n+1)(\lambda+n)},\\ \langle \lambda-2, n|F_2|\lambda n\rangle &= \tfrac{1}{k}(\lambda+2n),\\ \langle \lambda-2, n-1|F_2|\lambda n\rangle &= \tfrac{1}{k}\sqrt{n(\lambda+n-1)}.\end{aligned} \tag{B.16}$$

3. The functions F_3 are constructed from the product of 3 β matrix elements, so the seniority selection rules are $v' = v \pm 1, v \pm 3$.

- $v' = v + 3$

$$\begin{aligned}
\langle \lambda+3, n|F_3|\lambda n\rangle &= \tfrac{1}{k^{3/2}}\sqrt{(\lambda+n)(\lambda+n+1)(\lambda+n+2)},\\
\langle \lambda+3, n-1|F_3|\lambda n\rangle &= \tfrac{3}{k^{3/2}}\sqrt{n(\lambda+n)(\lambda+n+1)},\\
\langle \lambda+3, n-2|F_3|\lambda n\rangle &= \tfrac{3}{k^{3/2}}\sqrt{n(n-1)(\lambda+n)},\\
\langle \lambda+3, n-3|F_3|\lambda n\rangle &= \tfrac{1}{k^{3/2}}\sqrt{n(n-1)(n-2)},
\end{aligned} \tag{B.17}$$

- $v' = v + 1$

$$\begin{aligned}
\langle \lambda+1, n+1|F_3|\lambda n\rangle &= \tfrac{1}{k^{3/2}}\sqrt{(n+1)(\lambda+n)(\lambda+n+1)},\\
\langle \lambda+1, n|F_3|\lambda n\rangle &= \tfrac{1}{k^{3/2}}\sqrt{\lambda+n}(\lambda+3n+1),\\
\langle \lambda+1, n-1|F_3|\lambda n\rangle &= \tfrac{1}{k^{3/2}}\sqrt{n}(2\lambda+3n-1),\\
\langle \lambda+1, n-2|F_3|\lambda n\rangle &= \tfrac{1}{k^{3/2}}\sqrt{n(n-1)(\lambda+n-1)},
\end{aligned} \tag{B.18}$$

- $v' = v - 1$

$$\begin{aligned}
\langle \lambda-1, n+2|F_3|\lambda n\rangle &= \tfrac{1}{k^{3/2}}\sqrt{(n+1)(n+2)(\lambda+n)},\\
\langle \lambda-1, n+1|F_3|\lambda n\rangle &= \tfrac{1}{k^{3/2}}\sqrt{n+1}(2\lambda+3n),\\
\langle \lambda-1, n|F_3|\lambda n\rangle &= \tfrac{1}{k^{3/2}}\sqrt{\lambda+n-1}(\lambda+3n),\\
\langle \lambda-1, n-1|F_3|\lambda n\rangle &= \tfrac{1}{k^{3/2}}\sqrt{n(\lambda+n-1)(\lambda+n-2)},
\end{aligned} \tag{B.19}$$

- $v' = v - 3$

$$\begin{aligned}
\langle \lambda-3, n+3|F_3|\lambda n\rangle &= \tfrac{1}{k^{3/2}}\sqrt{(n+1)(n+2)(n+3)},\\
\langle \lambda-3, n+2|F_3|\lambda n\rangle &= \tfrac{3}{k^{3/2}}\sqrt{(n+1)(n+2)(\lambda+n-1)},\\
\langle \lambda-3, n+1|F_3|\lambda n\rangle &= \tfrac{3}{k^{3/2}}\sqrt{(n+1)(\lambda+n-1)(\lambda+n-2)},\\
\langle \lambda-3, n|F_3|\lambda n\rangle &= \tfrac{1}{k^{3/2}}\sqrt{(\lambda+n-1)(\lambda+n-2)(\lambda+n-3)}.
\end{aligned} \tag{B.20}$$

NEDERLANDSTALIGE SAMENVATTING

Het collectief model

De thesis opent met een metafoor: 'De atoomkern is zoals een enorme voetbalploeg, alhoewel het spel bepaald wordt door individuele acties, het is de ploeg die de wedstrijd wint'. Met deze metafoor wordt bedoeld dat de atoomkern bestaat uit een aantal individuele nucleonen (protonen en neutronen), maar het is de samenwerking van alle mogelijke interacties tussen deze nucleonen die de uiteindelijke kernstructuur zullen bepalen. Helaas, we mogen deze metafoor niet over de volledige lijn trekken. Zo zijn de 'spelregels' op het atomaire terrein ver weg van gekend, gezien de protonen en neutronen geen elementaire deeltjes zijn, maar op hun beurt nog eens opgebouwd zijn uit quarks. In principe zou het mogelijk moeten zijn om testinteracties te gebruiken in kernstructuur berekeningen, en die testinteracties dan a posteriori zuiver te stemmen door middel van de confrontatie van de berekeningen met de experimentele data. Realiteit is echter een stuk minder eenvoudig. Vermits de atoomkern een type voorbeeld is van een *veeldeeltjes systeem*, kunnen *ab initio* berekeningen, startend van de vrije nucleon-nucleon interactie, vrij ingewikkeld om niet te zeggen onmogelijk worden met toenemend deeltjesaantal[1] [Car98]. Men zou een statistische methode kunnen overwegen om dit probleem te omzeilen, maar deze technieken eisen enorme deeltjes aantallen omwille van statistische relevantie, en hiervoor heeft de atoomkern dan weer veel te weinig deeltjes. We kunnen dus enkel maar besluiten dat een beschrijving van kernstructuur noodgedwongen zal moeten gebeuren aan de hand van *modellen*. Ruwweg is het ruime spectrum aan modellen opdeelbaar in twee grote groepen, de *microscopische*- en *macroscopische* modellen.

Een schoolvoorbeeld van microscopische modellen is het *kernschillen model* [Hey94]. Dit model werd ontwikkeld als antwoord op de vraag waarom sommige kernen

[1] Huidige ab initio berekeningen kunnen atoomkernen aan met massagetal $A \sim 10$.

met zogenaamde *magische* deeltjes aantallen (8, 20, 50,etc) opmerkelijk sterker gebonden zijn dan voorspeld aan de hand van eerdere macroscopische modellen. Naar analogie met de electronen schillen van het atoom, werd verondersteld dat de protonen en neutronen op orbitalen bewegen, waardoor de extra bindings energie te danken is aan het sluiten van een bezette schil. In tegenstelling tot het atoom, is er echter geen extern centraal kracht veld aanwezig die een dergelijke schillen structuur kan verklaren. De fysische verantwoording voor een effectieve centrale kracht wordt gehaald uit *gemiddeld veld* of *Hartree-Fock* berekeningen, die aantonen dat een enkel nucleon benaderend onafhankelijk kan bewegen in een gemiddeld veld, opgewekt door de andere nucleonen in de atoomkern [Fet71]. Dit gemiddeld veld wordt gegenereerd op een iteratieve diagrammatische manier. Vaak worden echter fenomenologische en oplosbare potentialen gebruikt in plaats van Hartree-Fock gebaseerde gemiddelde velden, waarop gecorrigeerd wordt met residuele interacties die niet in de potentiaal vervat zijn.

Vanuit historisch oogpunt was het eerste kernmodel macroscopisch van aard, het zogenaamde *vloeistofdruppel model* [Wei35, Bet36]. Het wordt gecatalogeerd onder macroscopische modellen vermits het de atoomkern als een macroscopisch object behandelt met een welgedefinieerd oppervlak. De vergelijking met water druppels is afkomstig vanuit de inwendige structuur. Beide types objecten zijn samengesteld uit enkelvoudige deeltjes die, ten gevolge van de aantrekkende wisselwerking, zullen wedijveren naar een minimalisatie van het volume en de oppervlakte van het totale object. Dit idee werd toegepast door Bethe en Weizsäcker om de toenmalig gemeten bindings energieën met succes te verklaren. Fijnere metingen brachten echter systematische afwijkingen van de Bethe-Weizsäcker formule aan het licht rond de magische getallen, zodat de macroscopische interpretatie van atoomkernen overschaduwd werd door het schillenmodel. Maar dit model was evenmin almachtig, gezien het de experimenteel geobserveerde grote kwadrupool momenten niet kon verklaren. Rainwater suggereerde dat dit te wijten kon zijn aan het onafhankelijk karakter van de nucleonen in de toenmalige schillenmodel berekeningen en dat *collectieve* bewegingsmodes, waarin alle deeltjes coherent deelnemen aan de vervorming van de kern, onuitdenkbaar zijn [Rai50]. Dit bracht Bohr en Mottelson ertoe om het vloeistof druppel model te heroverwegen, maar ditmaal in een kwantum mechanisch kader [Boh52, Boh53]. Dit formalisme leidde tot een dynamische beschrijving van het oppervlak waaraan enkelvoudige deeltjes konden gekoppeld worden, verantwoordelijk voor de polarisatie van de kern.

Eén van de basis ingrediënten voor dit dynamisch collectief model is de potenti-

aal in de Hamiltoniaan. Deze potentiaal kan geconstrueerd worden op grond van microscopische nucleon-nucleon interacties, maar men kan ook toevlucht zoeken tot meer schematische potentialen, vertrekkende vanuit fenomenologische overwegingen. Zich baserend op het klassieke argument van oppervlaktespanning, voorzag Aage Bohr reeds in het allereerste artikel de analytisch oplosbare 5D harmonische oscillator als potentiaal voor kwadrupoolvormige (of ellipsoidale) vibrationele kernen. Andere collectieve structuren, zoals bijvoorbeeld rotaties konden later verklaard worden in het rotatie-vibratie model waarbij een axiaal vervormde potentiaal aanleiding gaf tot rotatiebanden die benaderend analytisch konden worden bepaald. Vanuit experimenteel oogpunt is het weinig waarschijnlijk dat de structuur van collectieve atoomkernen accuraat kan beschreven worden met deze archetypes van potentialen. Daarom was er nood voor een omvattende methode waarin algemenere potentialen kunnen opgelost worden. Deze werd aangereikt door het *algemeen collectief model* (ACM), ontwikkeld door de Frankfurt groep [Gne71]. Het ACM is gebaseerd op de veronderstelling dat de collectieve variabelen kleine afwijkingen beschrijven ten opzichte van de sferische vorm, zodat iedere potentiaal kan ontwikkeld worden als een baanimpulsmoment invariante Taylor ontwikkeling in de variabelen. Deze Taylor ontwikkeling is niet langer analytisch oplosbaar zodat men moet overgaan op een matrix representatie van de Hamiltoniaan als input voor numerieke diagonalisatie procedures. Gebruik makend van een Lie algebraisch $SU(1,1) \times O(5)$ structuur, kan men expliciete basis representaties opbouwen en aanwenden voor de berekening van de matrix elementen. Echter, vermits $SU(1,1)$ een *niet-compacte* Lie groep is, is de Hilbert ruimte oneindig dimensionaal, hetgeen voor numerieke kwesties kan zorgen inzake de convergentie in de model ruimte. Dit kan een reden zijn waarom het ACM de voorbije decennia vrijwel overschaduwd geweest is door the *interagerend boson model* (IBM).

Het IBM is voortgesproten uit de wens naar een unificatie van vibrationele $U(5)$ en rotationele $SU(3)$ structuren [Iac87]. Steunend op de representaties van de omvattende *compacte* $U(6)$ groep, is het mogelijk om een eindig dimensionale Hilbert ruimte te construeren waarbij de dimensie fysisch vastgelegd wordt aan de hand van het aantal valentie deeltjes buiten de afgesloten schillen. Dit zorgde ervoor dat collectiviteit in atoomkernen kon bestudeerd worden met computervriendelijke codes, met de surplus dat de connectie met microscopische modellen gegarandeerd was via afbeelding of *mapping* procedures.

De rijke algebraische structuur van het IBM zorgde ervoor dat het ideaal terrein werd voor de studie van *kwantum (vorm)fasetransities*. In dit vakgebied worden

overgangen bestudeerd tussen systemen met een verschillende onderliggende fysische structuur, zoals bijvoorbeeld de overgang van vibrationele kernen naar rotationele kernen. Opmerkelijk genoeg bleek dat de transitiepunten van de vibrationele limit naar rotationele limieten in het IBM vrij adequaat beschreven worden door middel van oneindige put potentialen in het geometrisch model, de zogeheten $E(5)$ en $X(5)$ kritische punt oplossingen [Iac00, Iac01]. Het is dankzij deze oplossingen, dat het geometrisch model de laatste jaren opnieuw in de schijnwerpers kwam te staan. Naast de beschrijving van kritische punten, werd eveneens onderzoek verricht naar andere oplosbare potentialen, de onderliggende algebraische structuur, en de potentiële toepasbaarheid van het geometrisch model in het kader van moderne theoretische en computer technische middelen.

Ook deze thesis tracht een steentje bij te dragen aan de kennis over het geometrisch model. In een eerste deel werd onderzocht in welke mate schematische en analytisch oplosbare potentialen een bijdrage kunnen leveren aan het begrijpen van *triaxialiteit*. Een tweede gedeelte behandelt een algemeen theoretisch kader voor het oplossen van algemenere potentialen zoals voorgesteld in het ACM.

Triaxialiteit

Het begrip triaxialiteit wordt gekaderd in de geometrie van ellipsoiden. De familie van ellipsoidale objecten kan opgedeeld worden in drie verschillende klassen naar gelang de symmetrie. De hoogst symmetrische ellips is de bol, vermits hij invariant blijft onder willekeurige rotaties in de volledige 3D ruimte. De volledige $O(3)$ symmetrie kan gebroken worden door één van de 3 hoofdassen van de bol te verkorten of verlengen. Op die manier wordt de symmetrie verlaagd van $O(3)$ naar $O(2)$, hetgeen willekeurige rotaties in het 2D vlak beschrijft, loodrecht ten opzichte van de symmetrie brekende hoofdas. We spreken in dit geval van respectievelijk *oblate* (of discusvormige) en *prolate* (of sigaarvormige) ellipsoiden. Uiteindelijk kan de rotationele symmetry volledig gebroken worden door de lengtes van de 3 hoofdassen verschillend van mekaar te kiezen. Ellipsoiden waarvan de lengtes van de hoofdassen allen verschillend zijn, worden *non-axiale* of *triaxiale* objecten genoemd. Het is vermeldenswaardig dat de symmetrie niet volledig gebroken is in het geval van triaxialiteit. Het is immers mogelijk aan de hand van projecties en rotaties over 90°, de ellipsoide in zichzelf om te zetten, hetgeen er voor zorgt dat er een discrete symmetrie overleeft die zodoende aanleiding geeft tot periodieke randvoorwaarden voor de collectieve variabele γ in het intrinsiek assenstelsel.

In hoofdstuk 2.3 wordt een schematische potentiaal geïntroduceerd die in staat

is om triaxiaal gedeformeerde atoomkernen te beschrijven. De potentiaal is een voorbeeld van de klasse van Wilets & Jean $\beta - \gamma$ ontkoppelbare potentialen. Voor het β-gedeelte werd een analytische oplosbare Davidson potentiaal geopteerd, terwijl een harmonische oscillator potentiaal gekozen werd voor het gedeelte in γ. Deze harmonische oscillator wordt geconstrueerd opdat hij minimaal is in het punt $\gamma = \gamma_0$ waarbij γ_0 als vrije parameter gekozen wordt. Gecombineerd met de Davidson potentiaal in β, zorgt dit ervoor dat de totale potentiaal één enkel duidelijk gedeformeerd triaxiaal minimum vertoont. Deze potentiaal kan analytisch worden opgelost door gebruik te maken van een $SU(1,1)_\beta \times SU(1,1)_\gamma$ schema, indien enkele fysisch verantwoorde benaderingen worden doorgevoerd.
Gezien de Os isotopen reeds als triaxiale rotors geïdentificeerd waren in tal van voorafgaande theoretische studies, is het interessant te onderzoeken in welke mate deze reeks van isotopen kan beschreven worden met de huidige schematische potentiaal in het geometrisch model, met een algemeen vrij positief antwoord als resultaat (hoofdstuk 2.3.3).

Het dient opgemerkt te worden dat de harmonische oscillator potentiaal in γ niet voldoet aan de periodieke randvoorwaarden in γ, zoals die opgelegd zijn door het geometrisch model. Daarom werd er in onze onderzoeksgroep een zoektocht gestart naar schematische en analytisch oplosbare potentialen die deze symmetrie wel respecteert. Een goede kandidaat werd gevonden onder de vorm van de Pöschl-Teller potentiaal van de 2e soort. Deze potentiaal heeft de opmerkelijke eigenschap dat het een minimum vertoont bij maximale triaxialiteit $\gamma = \pi/6$. Alhoewel de rotationele symmetrie van het geometrisch object maximaal verbroken is, is het toch mogelijk om deze potentiaal op te lossen aan de hand van een $O(3)$ algebra als gevolg van een toevallige symmetrie in de traagheidsmomenten. Vermits deze symmetrie enkel geldig is voor exact maximale triaxialiteit, moeten we de γ-afhankelijkheid van de traagheids momenten vastvriezen in het minimum van de potentiaal, willen we de oplosbaarheid van de potentiaal garanderen. Dit zorgt ervoor dat de gekoppelde γ-rotationele differentiaal vergelijking approximatief kan ontkoppeld worden in een afzonderlijk γ- en rotationeel gedeelte. Gebruik makend van de theorie over speciale functies en elementaire baanimpulsmoment theorie, kan men analytische oplossingen bekomen van deze Pöschl-Teller potentiaal. Om de geldigheid van de aangewende benadering a posteriori te verifiëren, werd een volledige diagonalisatie doorgevoerd in een complete basis. De algemene conclusie van deze diagonalisatie is dat het vastvriezen van de traagheidsmomenten slechts kleine afwijkingen veroorzaakt ten opzichte van de exacte oplossing.
De localisatie van het minimum van de Pöschl-Teller potentiaal rond $\gamma = \pi/6$,

begunstigt enerzijds de oplosbaarheid van de potentiaal, maar anderzijds bemoeilijkt dit aanzienlijk de toepasbaarheid ervan, gezien het heel onwaarschijnlijk is om atoomkernen op te sporen die kunnen beschreven worden als maximaal triaxiale rotors. Desalniettemin heeft men aan de hand van starre rotor studies reeds enkele gevallen kunnen indentificeren in de Pt isotopen. Met dit opzicht was het interessant om de toepasbaarheid van de Pöschl-Teller te testen in deze reeks isotopen. In hoofdstuk 2.4.4 wordt aangetoond met behulp van een fit procedure met één enkele parameter (met uitzondering van een algemene schaalfactor) dat het energy spectrum van ^{196}Pt vrij goed kan beschreven worden aan de hand van deze potentiaal, zodat deze atoomkern effectief kan beschouwd worden als een γ-rotor rond maximale triaxialiteit.

Een Cartan-Weyl perspectief

In een tweede deel wordt het domein van schematische en analytisch oplosbare potentialen verlaten voor meer algemenere vormen van potentialen. Vermits de collectieve variabelen klein verondersteld worden, is het mogelijk om elke potentiaal te schrijven als een Taylor ontwikkeling in deze variabelen. Dit heeft als gevolg dat we enkel de matrix elementen nodig hebben van de collectieve variabelen (en canonisch toegevoegde momenta) in een vooropgestelde basis om de volledige matrix representatie van de Hamiltoniaan op te bouwen. Het blijkt dat de Cartan-Weyl groep reductie van de overkoepelende $SU(1,1) \times O(5)$ een zeer geschikte basis aanreikt voor deze opdracht. Startend van de commutatie relaties en de expliciete uitdrukkingen voor de $SU(1,1)$ and $O(5)$ generatoren, mits gebruik makend van een intermediaire toestand methode, is het mogelijk om expliciete uitdrukkingen te bekomen voor de matrix elementen van zowel de collectieve variabele als de canonisch toegevoegde momenta (en als gevolg eveneens de spin-2 fonon creatie- en annihilatie operatoren). Deze methode is volledig algebraisch in de zin dat alle matrix elementen bekomen zijn zonder gebruik te maken van expliciete basisrepresentaties, noch hoogste gewicht toestanden. Het enige minpunt van deze techniek is dat de natuurlijke Cartan-Weyl reductie van $O(5) \supset O(4) \cong SU(2) \times SU(2)$ niet verenigbaar is met de $O(3)$ rotationele symmetrie die waargenomen is in experimentele spectra. Indien men toch basis toestanden wil met goed $O(3)$ kwantum getal L (en M), moet de rotatie van de natuurlijke naar de fysische basis expliciet doorgevoerd worden. Eens dit gedaan is, heeft men de matrix elementen van de collectieve variabelen ter beschikking in de fysische basis. Hogere orde impulsmoment invariante veeltermen kunnen nu eenvoudig bepaald worden aan de hand van standaard Clebsch-Gordan herkoppeling schema's, zodat de volledige Hamiltoniaan kan opgebouwd worden.

De Cartan-Weyl reductie levert niet enkel een elegant theoretisch kader, ook vanuit numeriek perspectief is het een rechtlijnige en handelbare techniek. Met betrekking tot computertijd, kunnen alle matrix elementen binnen redelijke tijd berekend worden, zolang de dimensies van de representaties van $O(5)$ betrekkelijk klein blijven[2]. De rotatie van de natuurlijke naar de fysische basis fungeert daarbij als de voornamelijke tijdsopslorper, gezien dit intrinsiek inhoudt dat een diagonalisatie van de Casimir operator $L \cdot L$ van $O(3)$ moet worden doorgevoerd. Gezien de matrix representatie van de Hamiltoniaan enkel afhankelijk is van de matrix elementen van de variabelen in de fysische basis, dient de rotatie slechts eenmaal uitgevoerd te worden waarna men de bekomen matrix elementen kan opslaan in een extern bestand voor later gebruik. Voor wat betreft de numerieke precisie van de methode, is het zo dat de matrix elementen analytisch zijn in de Cartan-Weyl basis zodat enige verlies van precisie eveneens te wijten is aan de rotatie. Er zijn echter voldoende accurate algoritmes op de markt (zoals bijvoorbeeld de Lapack routines) om dit naar tevredenheid te behandelen.

Rest ons nog te vermelden dat een numeriek algoritme algemene potentialen binnen het kader van de natuurlijke Cartan-Weyl reductie op het eigenste moment in volle ontwikkeling is in de kernstructuur groep te Gent, met het oog op verder onderzoek in het geometrisch model. Verschillende onderzoekslijnen zullen daarbij aan bod komen. Zo is er bijvoorbeeld de vraag over de toepasbaarheid van het ACM doorheen de nuclidekaart, zowel voor de reeds gekende- als de toekomstig ontdekte atoomkernen in het licht van de huidige exotische bundel faciliteiten. Hierbij zal een degelijke studie inzake de fysische betekenis en relevantie van de gebruikte parameters zeker inzicht brengen in de structuur van de aangewende potentialen en de bekomen oplossingen. Langs een gelijklopend pad, bevindt zich de vraag of het niet mogelijk is deze potentialen op te bouwen vanuit een semi-klassiek formalisme, vertrekkende van een microscopische dichtheidsafhankelijke interactie (zie hoofdstuk 3.1) en tot welke hoogte de veronderstelling van irrotationele beweging stand houdt in de bepaling van de massa parameter. Het is duidelijk dat al deze vragen kunnen en zullen beantwoord worden aan de hand van deze code, gebaseerd op het theoretisch formalisme beschreven in deze thesis.

Vanuit een eerder theoretisch perspectief, openen zich andere onderzoekspaden. De kwantum vormfasetransities kunnen perfect behandeld worden, waarbij de mogelijkheid bestaat om complexere structuren te incorporeren, zoals triaxialiteit

[2] senioriteiten v tot aan 100 kunnen makkelijk verwerkt worden binnen enkele minuten op een huidige commerciëel verkrijgbare desktop computer

en vorm coexistentie. Een ander pad beklimt de weg naar hogere multipolariteiten in het geometrisch model. Het is interessant om te onderzoeken of dit Cartan-Weyl schema kan toegepast worden op bijvoorbeeld de hexadecupool vrijheidsgraden, vermits aanzienlijke B(E4) waarden zijn waargenomen in de Pt isotopen, die het zuivere kwadrupool beeld grondig verstoren in de $L = 4$ toestanden. Aangezien de $L = 4$ hexadecupool variabele 9 intrinsieke impulsmoment projecties bevat, dient de overkoepelende groepsstructuur de $O(9)$ groep te bevatten. Het is niet duidelijk tot op welke hoogte een Cartan-Weyl reductie van deze 36 parameter Lie groep nog handelbaar is met een intermediaire toestand method hoofdstuk 3.
Niet enkel vanuit theoretisch, maar ook vanuit numeriek oogpunt is een studie van een mogelijke extensie van de standaard Clebsch-Gordan herkoppeling schema's naar niet-commuterende $SU(2)$ groepen interessant te noemen. Indien de niet-commuterende Clebsch-Gordan coefficiënten gekend zouden zijn, houdt dit een aanzienlijke vereenvoudiging in voor de rotatie van de natuurlijke naar fysische basis, met een gevoelige tijdswinst als gevolg. Hierdoor zouden hogere senioriteit representatie kunnen geconstrueerd worden, waardoor nog complexere potentialen kunnen worden behandeld.

Het verhaal is dus duidelijk nog niet ten einde...

List of publications

Part of the work presented in the present manuscript has been published in the literature

- **Soft triaxial rotor in the vicinity of $\gamma = \pi/6$ and its extensions**
  L. Fortunato, S. De Baerdemacker and K. Heyde,
  Eur. Phys. J. A25, 439 (2005).
- **Solution of the Bohr Hamiltonian for a periodic potential with minimum at $\gamma = \pi/6$**
  S. De Baerdemacker, L. Fortunato, V. Hellemans, and K. Heyde,
  Nucl. Phys. A769, 16 (2006).
- **Solution of the Bohr hamiltonian for soft triaxial nuclei.**
  L. Fortunato, S. De Baerdemacker and K. Heyde,
  Phys. Rev. C74, 014310 (2006).
- **Quadrupole collective variables in the natural Cartan-Weyl basis**,
  S. De Baerdemacker, V. Hellemans and K. Heyde,
  J. Phys. A40, 2733 (2007)

BIBLIOGRAPHY

[And99] Anderson E, Bai Z, Bischof C, Blackford S, Demmel J, Dongarra J, Du Croz J, Greenbaum A, Hammarling S, McKenney A & Sorensen D. *LAPACK Users' Guide* (Society for Industrial and Applied Mathematics, Philadelphia, 1999), third edition.

[Ans86] Ansari A. *Shape transition in Os and Pt isotopes*. *Phys. Rev. C* **33** p. 321 (1986).

[Ans88] Ansari A. *Structure of Os and Pt isotopes*. *Phys. Rev. C* **38** p. 953 (1988).

[Arf01] Arfken G B & Weber H J. *Mathematical methods for physicists* (Harcourt Academic Press, San Diego, 2001).

[Ari76] Arima A & Iachello F. *Interacting boson model of collective states I. the vibrational limit*. *Ann. Phys. NY* **99** p. 253 (1976).

[Ari79] Arima A & Iachello F. *Interacting boson model of collective nuclear states IV. the $o(6)$ limit*. *Ann. Phys. NY* **123** p. 468 (1979).

[Bag98] Baglin C M. *Nuclear data sheets for $A = 192$*. *Nucl. Data Sheets* **84** p. 717 (1998).

[Bag03] Baglin C M. *Nuclear data sheets for $A = 186$*. *Nucl. Data Sheets* **99** p. 1 (2003).

[Bas06] Basunia M S. *Nuclear data sheets for $A = 176$*. *Nucl. Data Sheets* **107** p. 791 (2006).

[Ben87] Bengtsson R, Bentsson T, Dudek J, Leander G, Nazarewicz W & Zhang J y. *Shape coexistence and shape transitions in even-even pt and hg isotopes*. *Phys. Lett. B* **183** p. 1 (1987).

[Bès59] Bès D. *The gamma dependent part of the wave functions representing gamma unstable surface vibrations*. *Nucl. Phys.* **10** p. 373 (1959).

[Bet36] Bethe H & Bacher R F. *Nuclear physics a. stationary states of nuclei*. *Rev. Mod. Phys.* **8** p. 82 (1936).

[Bij80] Bijker R, Dieperink A E L, Scholten O & Spanhoff R. *Description of the Pt and Os isotopes in the interacting boson model*. *Nucl. Phys. A* **344** p. 207 (1980).

[Boh52] Bohr A. *The coupling of nuclear surface oscillations to the motion of individual nucleons*. *Mat. Fys. Medd. Dan. Vid. Selsk* **26** p. 14 (1952).

[Boh53] Bohr A & Mottelson B R. *Collective and individual-particle aspects of nuclear structure*. *Mat. Fys. Medd. Dan. Vid. Selsk* **27** p. 1 (1953).

[Boh80] Bohr A & Mottelson B R. *Features of nuclear deformations produced by the alignment of individual particles or pairs*. *Phys. Scripta* **22** p. 468 (1980).

[Boh98] Bohr A & Mottelson B. *Nuclear Structure, Vol.2* (World Scientific, Singapore, 1998).

[Bon04] Bonatsos D, Lenis D, Minkov N, Petrellis D, Raychev P & Terziev P. *E(5) and X(5) critical point symmetries obtained from Davidson potentials through a variational procedure*. *Phys. Rev. C* **70** p. 024305 (2004).

[Bon05] Bonatsos D, Lenis D, Petrellis D, Terziev P A & Yigitoglu I. *γ-rigid solution of the Bohr hamiltonian for $\gamma = 30^\circ$ compared to the E(5) critical point symmetry*. *Phys. Lett. B* **621** p. 102 (2005).

[Bri05] Brink D & Broglia R. *Nuclear superfluidity, pairing in finite systems* (Cambridge University Press, Cambridge, 2005).

[Bro94] Browne E. *Nuclear data sheets for $A = 178$*. *Nucl. Data Sheets* **72** p. 221 (1994).

[Bro99] Browne E & Junde H. *Nuclear data sheets for $A = 174$*. *Nucl. Data Sheets* **87** p. 15 (1999).

[Bru77] Brussaard P & Glaudemans P. *Shell-model applications in nuclear spectroscopy* (North Holland, Amsterdam, 1977).

[Cap03] Caprio M A. *Simplified approach to the application of the geometric collective model*. *Phys. Rev. C* **68** p. 054303 (2003).

[Cap04] Caprio M A. *Phase structure of a two-fluid bosonic system*. *Phys. Rev. Lett.* **93** p. 242502 (2004).

[Cap05] Caprio M A & Iachello F. *Phase structure of a two-fluid bosonic system*. *Annals of Phys.* **318** p. 454 (2005).

[Car94] Cartan E. *Sur la structure des Groupes de Transformation Finis et continus*. Ph.D. thesis, Ecole normale supérieure de Paris (1894).

[Car98] Carlson J & Sciavilla R. *Structure and dynamics of few-nucleon systems*. *Rev. Mod. Phys.* **70** p. 743 (1998).

[Cas31] Casimir H. *Rotation of a rigid body in quantum mechanics*. Ph.D. thesis, Rijksuniversiteit Leiden (1931).

[Cas93] Casten R, Lipas P, Warner D, Otsuka T, Heyde K & Draayer J. *Algebraic Approaches to Nuclear Structure* (Harwood academic, Chur, 1993).

[Cas07] Casten R F & McCutchan E A. *Quantum phase transitions and structural evolution in nuclei*. *J. Phys. G* **34** p. R256 (2007).

[Cej03] Cejnar P, Heinze S & Jolie J. *Ground-state shape phase transitions in nuclei: Thermodynamic analogy and finite-N effects*. *Phys. Rev. C* **68** p. 034326 (2003).

[Cha76] Chacón E, Moshinsky M & Sharp R T. *Group theory of the collective model*. *Jour. Math. Phys* **17** p. 668 (1976).

[Cha77] Chacón E & Moshinsky M. *Group theory of the collective model*. *Jour. Math. Phys* **18** p. 870 (1977).

[Chu98] Chunmei Z, Wang G & Tao Z. *Nuclea data sheets for A=101*. *Nucl. Data Sheets* **83** p. 145 (1998).

[Cor76] Corrigan T M, Margetan F J & Williams S A. *Exact solution of the quadrupole surface vibration Hamiltonian in body-fixed coordinates*. *Phys. Rev. C* **14**(6) p. 2279 (1976).

[Dav32] Davidson P M. *Eigenfunctions for calculating electronic vibrational intensities*. *Proc. Roy. Soc. A* **135** p. 459 (1932).

[Dav58] Davydov A S & Filippov G F. *Rotational states in even atomic nuclei*. *Nucl. Phys.* **8** p. 237 (1958).

[Dav59] Davydov A S & Rostowsky V. *Relative transition probabilities between rotational levels of non-axial nuclei*. *Nucl. Phys.* **12** p. 58 (1959).

[Dav60] Davydov A S & Chaban A A. *Rotation-vibration interaction in non-axial even nuclei*. *Nucl. Phys.* **20** p. 499 (1960).

[Dav61] Davydov A S. *Collective excitations corresponding to quadruple nuclear surface vibrations*. *Nucl. Phys.* **24** p. 682 (1961).

[DB06] De Baerdemacker S, Fortunato L, Hellemans V & Heyde K. *Solution of the Bohr Hamiltonian for a periodic potential with minimum at* $\gamma = \pi/6$. *Nucl. Phys. A* **769** p. 16 (2006).

[DB07] De Baerdemacker S, Heyde K & Hellemans V. *Quadrupole collective variables in the natural Cartan-Weyl basis*. *J. Phys. A* **40** p. 2733 (2007).

[Die80] Dieperink A E L, Scholten O & Iachello F. *Classical limit of the interacting-boson model*. *Phys. Rev. Lett.* **44** p. 1747 (1980).

[Eis87] Eisenberg J M & Greiner W. *Nuclear Models; Vol.2* (North Holland, Amsterdam, 1987).

[Ell86] Elliott J P, Evans J A & Park P. *A soluble* γ*-unstable Hamiltonian*. *Phys. Lett. B* **169** p. 309 (1986).

[Ess97] Esser L, Neuneyer U, Casten R F & von Brentano P. *Correlations of the deformation variables* β *and* γ *in even-even Hf, W, Os, Pt and Hg nuclei*. *Phys. Rev. C* **55** p. 206 (1997).

[Fae62] Faessler A & Greiner W. *Die Rotations-Vibrations-Wechselwirkung in deformierten gg-Kernen*. *Z. Phys. A* **168** p. 425 (1962).

[Fet71] Fetter L & Walecka J D. *Quantum theory of many-particle systems* (McGraw-Hill, New York, 1971).

[Fir89] Firestone R B. *Nuclear data sheets for* $A = 184$. *Nucl. Data Sheets* **58** p. 243 (1989).

[Flü41] Flügge S. *Die Eigenschwingungen eines Flüssigkeitstropfens und ihre Anwendung auf die Kernphysik*. *Ann. Physik* **39** p. 373 (1941).

[For03] Fortunato L & Vitturi A. *Analytically solvable potentials for* γ*-unstable potentials*. *J. Phys. G* **29** p. 1341 (2003).

[For04] Fortunato L. *Soft triaxial rotovibrational motion in the vicinity of* $\gamma = \pi/6$. *Phys. Rev. C* **70** p. 011302 (2004).

[For05a] Fortunato L. *Solutions of the Bohr Hamiltonian, a compendium*. *Eur. Phys. J. A* **26** p. 1 (2005).

[For05b] Fortunato L, De Baerdemacker S & Heyde K. *Soft triaxial rotor in the vicinity of* $\gamma = \pi/6$ *and its extensions*. *Eur. Phys. J. A* **25** p. 439 (2005).

[For06] Fortunato L, De Baerdemacker S & Heyde K. *Solution of the Bohr Hamiltonian for soft triaxial nuclei*. *Phys. Rev. C* **74** p. 014310 (2006).

[Fra94] Frank A & Van Isacker P. *Algebraic methods in molecular and nuclear structure physics* (J. Wiley and Sons, New York, 1994).

[Gar05] García-Ramos J E, Dukelsky J & Arias J M. β^4 *potential at the* $U(5) - O(6)$ *critical pont of the interacting boson model*. *Phys. Rev. C* **72** p. 037301 (2005).

[Ghe78] Gheorghe A, Raduta A A & Ceausescu V. *On the exact solution of the harmonic quadrupole collective Hamiltonian*. *Nucl. Phys. A* **296** p. 228 (1978).

[Gil81] Gilmore R. *Catastrophe theory for scientists and engineers* (J. Wiley and Sons, New York, 1981).

[Gin80] Ginocchio J N & Kirson M W. *Relationship between the Bohr Collective Hamiltonian and the Interacting-Boson Model*. *Phys. Rev. Lett.* **44** p. 1744 (1980).

[Gne71] Gneuss G & Greiner W. *Collective potential energy surfaces and nuclear structure*. *Nucl. Phys. A* **171** p. 449 (1971).

[Góź80] Góźdź A & Spikowski S. *Complete and orthonormal solution of the five-dimensional spherical harmonic oscillator in Bohr-Mottelson collective internal coordinates*. *Nucl. Phys. A* **349** p. 359 (1980).

[Hab74] Habs D, Klewe-Nebenius H, Wisshak K, Löhken R, Nowicki G & Rebel H. *The spherical to asymmetric shape transition in the mass region with* $50 < (n, z) < 82$. *Z. Phys. A* **267** p. 149 (1974).

[Ham64] Hamermesh M. *Group theory and its applications to physical problems* (Addison-Wesley, Reading, Massachusetts, 1964).

[Har97] Harder M K, Tang K T & Van Isacker P. *An IBM description of coexistence in the platinum isotopes*. *Phys. Lett. B* **405** p. 25 (1997).

[Hec65] Hecht K T. *Some simple R_5 Wigner coefficients and their applications*. *Nucl. Phys.* **63** p. 177 (1965).

[Hei06] Heinze S, Cejnar P, Jolie J & Macek M. *Evolution of spectral properties along the $O(6) - U(5)$ transition in the interacting boson model. I. Level dynamics*. *Phys. Rev. C* **73** p. 014306 (2006).

[Hey94] Heyde K. *The nuclear shell model* (Springer-Verlag, Berlin, 1994).

[Hey99] Heyde K. *Basic ideas and concepts in nuclear physics* (Institute of Physics Publishing, Bristol, 1999).

[Iac87] Iachello F & Arima A. *The interacting boson model* (Cambridge University Press, Cambridge, 1987).

[Iac93] Iachello F. *Dynamic symmetries and supersymmetries in nuclear physics*. *Rev. Mod. Phys.* **65** p. 569 (1993).

[Iac99] Iachello F. *Dynamic symmetries in nuclei*. *J. Phys. G* **25** p. 655 (1999).

[Iac00] Iachello F. *Dynamic symmetries at the critical point*. *Phys. Rev. Lett.* **85** p. 3580 (2000).

[Iac01] Iachello F. *Analytic description of critical point nuclei in a spherical-axially deformed shape phase transition*. *Phys. Rev. Lett.* **87** p. 052502 (2001).

[Iac06] Iachello F. *Lie algebras and applications, Lecture notes in physics* (Springer-Verlag, Berlin, 2006).

[Inf51] Infeld L & Hull T E. *The factorization method*. *Rev. Mod. Phys.* **23** p. 21 (1951).

[Jön96] Jönsson L. *Instabilities in folded Yukawa-plus-exponential liquid drop models*. *Nucl. Phys. A* **608** p. 1 (1996).

[Kra79] Krapp H J, Nix J R & Sierck A J. *Unified nuclear potential for heavy-ion elastic scattering, fusion, fission and ground-state masses and deformations*. *Phys. Rev. C* **20** p. 992 (1979).

[Kum68] Kumar K & Barranger M. *Nuclear deformation in the pairing+quadrupole model (V). energy levels and electromagnetic moments of the W, Os and Pt nuclei.*. *Nucl. Phys. A* **122** p. 273 (1968).

[Kum74] Kumar K. *Collective hamiltonian derived from the pairing-plus-quadrupole model: Modification and application to the transitional nuclei $^{150,152}Sm$*. *Nucl. Phys. A* **231** p. 189 (1974).

[Lóp95] López-Moreno E & Castaños O. *Shapes and stability within the interacting boson model: dynamical symmetries*. *Phys. Rev. C* **54** p. 2374 (1995).

[Mar82] Margetan F J & Williams S A. *Optimization of finite expansion bases for nuclear collective-model calculations*. *Phys. Rev. C* **25** p. 1602 (1982).

[McC05] McCutchan E M & Zamfir N V. *Simple description of light W, Os, and Pt nuclei in the interacting boson model*. *Phys. Rev. C* **71** p. 054306 (2005).

[McW02] McWeeny R. *An introduction to group theory and its applications* (Dover publications, Mineola, New York, 2002).

[Mey75] Meyer-Ter-Vehn J. *Collective model description of transitional odd-A nuclei*. *Nucl. Phys. A* **249** p. 111 (1975).

[Pod28] Podolsky B. *Quantum mechanically correct form of Hamiltonian function for conservative systems*. *Phys. Rev.* **32** p. 812 (1928).

[Rac42] Racah G. *Theory of complex spectra. I*. *Phys. Rev.* **61**(3-4) pp. 186 (1942).

[Rag89] Raghavan P. *Table of nuclear moments*. *At. Nucl. Data Tables* **42** p. 189 (1989).

[Rai50] Rainwater J. *Nuclear energy level argument for a spheroidal nuclear model*. *Phys. Rev.* **79**(3) p. 432 (1950).

[Rak57] Rakavy G. *The classification of states of surface vibrations*. *Nucl. Phys.* **4** p. 289 (1957).

[Ros57] Rose M E. *Elementary theory of angular momentum* (J. Wiley and Sons, New York, 1957).

[Row94a] Rowe D J. *Representations of the five- and six-dimensional harmonic oscillators in a $u(5) \supset so(5) \supset so(3)$ basis*. *Jour. Math. Phys* **35** p. 3178 (1994).

[Row94b] Rowe D J. *Vector-coherent-state representations of $so(5)$ in and $so(3)$ basis*. *Jour. Math. Phys* **35** p. 3163 (1994).

[Row95] Rowe D J & Hecht K T. *Representation of the five-dimensional harmonic oscillator with scalar-valued $U(5) \supset SO(5) \subset SO(3)$-coupled vcs wave functions*. *Jour. Math. Phys* **36** p. 4711 (1995).

[Row96] Rowe D J. *Dynamical symmetries of collective nuclear models*. *Prog. Part. Nucl Phys.* **37** p. 265 (1996).

[Row98] Rowe D J & Bahri C. *Rotation-vibrational spectra of diatomic molecules and nuclei with Davidson interactions*. *J. Phys. A* **31** p. 4947 (1998).

[Row04] Rowe D J. *A computationally tractable version of the collective model*. *Nucl. Phys. A* **735** p. 372 (2004).

[Row05a] Rowe D J. *An algebraic approach to problems with polynomial Hamiltonians on Euclidean spaces*. *J. Phys. A* **38** p. 10181 (2005).

[Row05b] Rowe D J & Turner P. *The algebraic collective model*. *Nucl. Phys. A* **753** p. 94 (2005).

[Sei84] Seiwert M, Maruhn J A & Hess P O. *Comparison of different collective models describing the low spin structure of* ^{168}Er. *Phys. Rev. C* **30** p. 1779 (1984).

[Set91] Sethi A, Hintz N M, Mihailidis D N, Mack A M, Gazzaly M, Jones K W, Pauletta G, Santi L & Goutte D. *Inelastic proton scattering from Pt isotopes and the interacting boson model*. *Phys. Rev. C* **44** p. 700 (1991).

[Sin95a] Singh B. *Nuclear data sheets for* $A = 172$. *Nucl. Data Sheets* **75** p. 199 (1995).

[Sin95b] Singh B & Firestone R B. *Nuclear data sheets for* $A = 182$. *Nucl. Data Sheets* **74** p. 383 (1995).

[Sin02] Singh B. *Nuclear data sheets for* $A = 188$. *Nucl. Data Sheets* **95** p. 387 (2002).

[Sin03] Singh B. *Nuclear data sheets for* $A = 190$. *Nucl. Data Sheets* **99** p. 275 (2003).

[Spi80] Spikowski S & Góźdź A. *The orthonormal basis for symmetric irreducible representations of* $O(5) \times SU(1,1)$ *and its application to the interacting boson model*. *Nucl. Phys. A* **340** p. 76 (1980).

[Tal93] Talmi I. *Simple models of complex nuclei* (Harwood academic, Chur, 1993).

[Tur05] Turner P. *The algebraic collective nuclear model and SO(5)*. Ph.D. thesis, University of Toronto (2005).

[Tur06] Turner P, Rowe D J & Repka J. *Vector coherent state theory of the generic representations of so(5) in an so(3) basis*. *Jour. Math. Phys* **47** p. 023507 (2006).

[Ui68] Ui H. *$su(1,1)$ quasi-spin formalism of the many-boson system in a spherical field*. *Ann. Phys. NY* **49** p. 69 (1968).

[War82] Warner D & Casten R. *Revised formulation of the phenomenological interacting boson model*. *Phys. Rev. Lett.* **48** p. 1385 (1982).

[Wei35] Weizsäcker. *Zur theorie der kernmassen*. *Z. Phys.* **96** p. 431 (1935).

[Wer05] Werner V, Scholl C & von Brentano P. *Triaxiality and the determination of the cubic shape parameter K_3 from five observables*. *Phys. Rev. C* **71** p. 054314 (2005).

[Wil56] Wilets L & Jean M. *Surface oscillations in even-even nuclei*. *Phys Rev.* **102** p. 788 (1956).

[Woo04] Wood J L, Oros-Peusquens A M, Zabballa R, Allmond J M & Kulp W D. *Triaxial rotor model for nuclei with independent inertia and electric quadrupole tensors*. *Phys. Rev. C* **70** p. 024308 (2004).

[Wu03] Wu S & Niu H. *Nuclear data sheets for $A = 180$*. *Nucl. Data Sheets* **100** p. 483 (2003).

[Wyb74] Wybourne B G. *Classical groups for Physicists* (J. Wiley and Sons, New York, 1974).